Investigating Vagus Nerve Modulation During Temporal Lobe Seizures in a Kainic Acid Rat Model

Elena Acedo Reina

Thesis submitted in fulfillment of the requirements for the degree of Ph.D. Degree in Biomedical and Pharmaceutical Science

Thèse présentée en vue de l'obtention du grade de Docteur en Sciences Biomédicales et Pharmaceutiques

27 AUGUST 2025

Promotor : Prof. Dr. Riëm El Tahry

Institute of Neuroscience, Université Catholique de Louvain, Belgium

Cliniques Universitaires Saint Luc, Center for Refractory Epilepsy, Belgium

Co-promotor : Prof. Antoine Nonclercq

BEAMS Department, Université Libre de Bruxelles, Belgium

Examination board :

President

Prof. Emmanuel Hermans

Institute of Neuroscience, Université Catholique de Louvain, Belgium

Secretary

Prof. André Mouraux

Institute of Neuroscience, Université Catholique de Louvain, Belgium

Prof. Robrecht Raedt

University of Gent, Faculty of Medicine and Health Science, Department of Head and Skin, Belgium

Prof. Dominique Durand

Case Western Reserve University, Department of Biomedical Engineering, United States

Prof. Estelle Rikir

Centre Hospitalier Neurologique William Lennox, Belgium

Table of contents

Abbreviations

ABVN - Auricular branch of the vagus nerve

AUC – Area under the curve

ANT – Anterior nucleus of the thalamus

ANS – Autonomic nervous system

ASMs – Antiseizure medications

Bpm – beats per minute

BP – Blood pressure

CAE – Childhood absence epilepsy

CAN – Central autonomic network

CAPs – Compound Action Potentials

CCK-8 – Cholecystokinin-8

CNT – Carbon nanotube

crVENG – Cardiac-related vagus nerve electroneurogram

DBS – Deep Brain Stimulation

DG – Dentate gyrus

DVN – Dorsal vagal nucleus

ECG – Electrocardiography

EEG – Electroencephalography

EMG – Electromyography

GAERS – Genetic absence epilepsy rats from Strasbourg

GCP – Granule cell dispersion

GI – Gastrointestinal

GSA – General somatic afferent

GVA – General visceral afferent

GVE – General visceral efferent

HS – Hippocampal sclerosis

IBED – Intrabeat Energy Difference

ICA – Ictal central apnea

IGE – Idiopathic generalized epilepsy

IGLEs – Intraganglionic laminar endings

IMAs – Intramuscular arrays

KARs – Kainate receptors

KA – Kainic acid

ILAE – International League Against Epilepsy

MAP – Mean arterial pressure

MES – Maximal electroshock

MFS – Mossy fiber sprouting

NMDA – N-methyl-D-aspartate

NP – Nitroprusside

NREM – Non-Rapid Eye Movement

NA – Nucleus ambiguus

NTS – Nucleus tractus solitarius

OR – odds ratios

PE – Phenylephrine

PPV – Positive predictive value

PTZ – Pentylenetetrazol

PVN – Paraventricular nucleus

RARs – Rapidly adapting receptors

RMS – Root mean square

RNS – Responsive Neurostimulation

ROC – Receiver Operating Characteristic

ROS – Reactive oxygen species

RSNA – Renal sympathetic nerve activity

RVLM – Rostral ventrolateral medulla

SARs – Slowly adapting receptors

SE – Status epilepticus

SNR – Signal-to-noise ratio

SRS – Spontaneous recurrent seizure

SUDEP – Sudden Unexpected Death in Epilepsy

SUA – Single Unit Activity

SV – Stroke volume

SVA – Special visceral afferent

SVE – Special visceral efferent

SWDs – Spike-and-wave discharges

TLE – Temporal lobe epilepsy

TPS – Total Peripheral Resistance

tVNS - Transcutaneous vagus nerve stimulation

VENG – Vagus nerve electroneurogram

VLM – Ventrolateral medulla

VNA – Vagus nerve activity

VNS – Vagus nerve stimulation

WAR – Wistar Audiogenic Rat

Remerciements - Acknowledgments

Alors que j'avais déjà tenté deux fois d'obtenir le FRIA avec le Professeur Frédéric Clotman, plus déterminée que jamais à poursuivre ma formation de jeune scientifique, et après deux belles années passées à l'Institut Jules Bordet, un soir d'insomnie, je suis tombée sur l'annonce d'un doctorat au sein du laboratoire de Riëm. Les neurosciences m'ayant toujours fascinée, j'ai tout de suite été attirée par ce projet sur l'épilepsie, même si je connaissais encore peu cette maladie.

Merci, merci à **Riëm** de m'avoir offert l'opportunité d'effectuer cette thèse, de m'avoir permis d'aller au bout de ce cheminement et de cette envie. Tu m'as ouvert les portes de ton laboratoire et m'as offert une bourse, mais plus encore, tu m'as permis de grandir en tant que chercheuse et en tant que personne. En effet, cette thèse n'a pas été de tout repos et j'ai beaucoup apprécié ton soutien, ta disponibilité et ta confiance.

J'aimerais également remercier **Antoine**, mon co-promoteur, qui m'a aussi ouvert les portes du BEAMS. Ton accompagnement en tant que scientifique ainsi que ta gentillesse et ta bienveillance m'ont guidée tout au long de ce chemin. Tous deux, par votre optimisme parfois déconcertant, vous m'avez aidée à persévérer quand je me sentais perdue dans ce projet si ambitieux et à tirer le positif de chaque situation.

Je voudrais également remercier les membres de mon comité d'accompagnement : **Emmanuel Hermans** comme président, **André Mouraux** ainsi que **Robrecht Raedt**. Votre soutien lors de mes comités m'a réellement aidée dans ce chemin sinueux.

Enfin, j'aimerais remercier les membres externes, le Professeur **Dominique Durand** ainsi que le Dr **Estelle Rikir** pour votre présence lors de ma défense de thèse, ainsi que pour vos visions très pertinentes, vos remarques constructives et votre bienveillance.

À présent, je voudrais remercier toutes les personnes qui m'ont accompagnée au quotidien. À commencer par mes collègues : je ne pensais pas qu'en entrant dans le labo de Riëm, je rencontrerais autant de personnes incroyables.

Vénéthia et Alex, mes "zozos" préférés, je me souviens encore de notre première rencontre, mais je chéris surtout tous les souvenirs incroyables que

nous avons construits ensemble : les dîners, les soirées, les congrès, le voyage en Floride… tant de moments gravés à jamais. Et le meilleur reste à venir.

Inci et Elise, votre rencontre a été une véritable bénédiction, cette thèse n'aurait pas été la même sans vous. Nos discussions sur la "terrasse" du 52+5 me manqueront beaucoup.

Javier, mon binôme de labo, je suis heureuse d'avoir partagé tous ces moments avec toi, notamment nos longues discussions pendant les expériences PTZ. Et attention : si tu travailles trop, j'appellerai toujours la police !

Merci également à mes collègues **Auriane, Enrique, Ayse, Roberto, Vincent et Simone**, ainsi qu'à mes **collègues du BEAMS**, pour les défenses de thèse partagées, les congrès et tous les moments simples vécus au laboratoire. Un clin d'œil spécial aux **amis de NEUR** : nos midis au Luculus, les raclettes, les gâteaux d'anniversaire, les discussions interminables dans la cuisine… autant de moments qui resteront gravés. **Emi et Claire**, merci pour votre écoute, votre soutien : vous êtes des personnes formidables ! Et bien sûr, merci à la team des "gens biens", **Vlad, Amélie, MH, Solenn**, je suis heureuse de vous avoir rencontrés et d'avoir partagé tant de bons repas ensemble. Ainsi que **mes copines de CEMO**, qui m'ont accueillie à mon arrivée. **Pauline**, avec qui j'ai partagé de nombreux commérages et conversations mariage.

Merci aussi à **mes amis** de longue date, ceux que j'ai rencontrés bien avant cette thèse et qui continuent de partager ma vie aujourd'hui. Ces amitiés nées à l'université ou en dehors et qu'on espère garder toute une vie.

Et finalement, **ma famille**. **Ma famille, ma belle-famille, ma marraine, ma cousine**. Vous m'avez toujours soutenue, acceptée avec mes forces et mes faiblesses. Vous êtes mon roc, mon refuge, ceux auprès de qui je me sens à ma place. **Plus particulièrement mes frères et sœurs**, qui trouvent toujours les mots pour me faire rire. **Et mes parents**, qui m'ont donné la force, la résilience et l'envie d'aller toujours au bout de ce que j'entreprends.

Enfin, à toi, **Rémy**. Mon fiancé, mon futur mari. Au moment où j'écris ces quelques lignes, nous sommes à moins d'un mois de notre mariage. Tu m'as soutenue depuis le premier jour, tu as cru en moi, tu m'as encouragée à poursuivre mes ambitions. Je n'aurais jamais pu rêver d'un partenaire comme toi à mes côtés. J'ai hâte de continuer cette aventure main dans la main, avec notre petite famille : toi, moi et Bébert.

Abstract

Epilepsy is one of the most prevalent neurological disorders, affecting over 50 million people worldwide. Approximately one-third of patients exhibit drug-resistant forms for which resective surgery is not always indicated. Neuromodulation, particularly vagus nerve stimulation (VNS), represents a less invasive therapeutic alternative. Closed-loop VNS systems, which rely on ictal tachycardia detection, have improved clinical efficacy; however, their specificity remains limited due to variability in cardiac responses, highlighting the need for more reliable biomarkers for seizure detection and the optimization of stimulation strategies.

This thesis focuses on the characterization of vagus nerve activity during seizures in the kainic acid rat model, a relevant model of human temporal lobe epilepsy. Temporal lobe seizures are frequently associated with pronounced autonomic alterations, including changes in cardiac, respiratory, and gastrointestinal function. The vagus nerve, as the main parasympathetic relay, provides access to these multi-organ signals, offering an integrative approach for seizure assessment. The work investigates VNA both in acute anesthetized conditions and in chronic awake recordings to evaluate its potential as a biomarker for the development of closed-loop stimulation strategies.

Résumé

L'épilepsie est l'une des maladies neurologiques les plus fréquentes, touchant plus de 50 millions de personnes dans le monde. Environ un tiers des patients présentent une forme pharmaco-résistante, pour laquelle la chirurgie resective n'est pas toujours indiquée. La neuromodulation, en particulier la stimulation du nerf vague (VNS), constitue une alternative thérapeutique moins invasive. Les systèmes VNS en boucle fermée, basés sur la détection de tachycardie ictale, ont amélioré l'efficacité clinique, mais leur spécificité reste limitée en raison de la variabilité des réponses cardiaques, soulignant le besoin de biomarqueurs plus fiables pour la détection des crises et l'optimisation des stratégies de stimulation.

Cette thèse se concentre sur la caractérisation de la modulation du nerf vague pendant les crises d'épilepsie dans le modèle acide kainique chez le rat, un modèle pertinent de l'épilepsie temporale humaine. Les crises du lobe temporal s'accompagnent fréquemment de fortes altérations autonomes, incluant des modifications cardiaques, respiratoires et gastro-intestinales. Le nerf vague, principal relais parasympathique, permet d'accéder à ces informations multi-organes, offrant une approche intégrative pour l'évaluation des crises. Les travaux explorent la VNA à la fois en conditions aiguës sous anesthésie et en enregistrements chroniques à l'état éveillé, afin d'évaluer son potentiel comme biomarqueur pour le développement de stratégies de stimulation en boucle fermée.

CHAPTER 1 : Introduction

1. Epilepsy

Epilepsy is a chronic neurological disorder characterized by stigma, psychiatric comorbidities, and significant economic costs (1). It affects over 50 million people globally, with a prevalence of 7.6 per 1,000 individuals.

In 2014, the International League Against Epilepsy (ILAE) formally redefined epilepsy in an official report. The report characterized epilepsy as a brain disease defined by at least one of the following criteria: [1] At least two unprovoked (or reflex) seizures occurring >24 h apart; [2] one unprovoked (or reflex) seizure and a probability of further seizures similar to the general recurrence risk (at least 60%) after two unprovoked seizures, occurring over the next 10 years; [3] diagnosis of an epilepsy syndrome (2).

1.1. Seizures: Definition and classification

A seizure is defined as a transient event characterized by signs and/or symptoms resulting from abnormal, excessive, or synchronous neuronal activity in the brain. While previous classifications of seizures were based on anatomical considerations, modern research has changed our understanding of the pathophysiological mechanisms involved. It has been shown that epilepsy is a network disease and not only a symptom of local brain abnormalities (3, 4). In 2017, the ILAE introduced a modern classification of seizures based on the initial onset, establishing a clinically practical and biologically meaningful framework. This classification was refined in the 2024 operational update, which maintains the core structure while incorporating new evidence and implementation feedback. Seizures are now classified into four main categories: focal, generalized, unknown (whether focal or generalized), and unclassified (3, 5). When the onset of a seizure cannot be determined, it is categorized as unknown or unclassified. These categories are further subdivided using classifiers, which reflect biologically meaningful distinctions that impact clinical care, and descriptors, which convey additional clinical features, such as motor or non-motor symptoms (5).

In focal seizures, awareness is a key classifier, assessed operationally based on the patient's ability to respond and recall during the event. If the patient maintains awareness throughout, the seizure is termed focal aware; if awareness is impaired, it is termed focal impaired awareness.

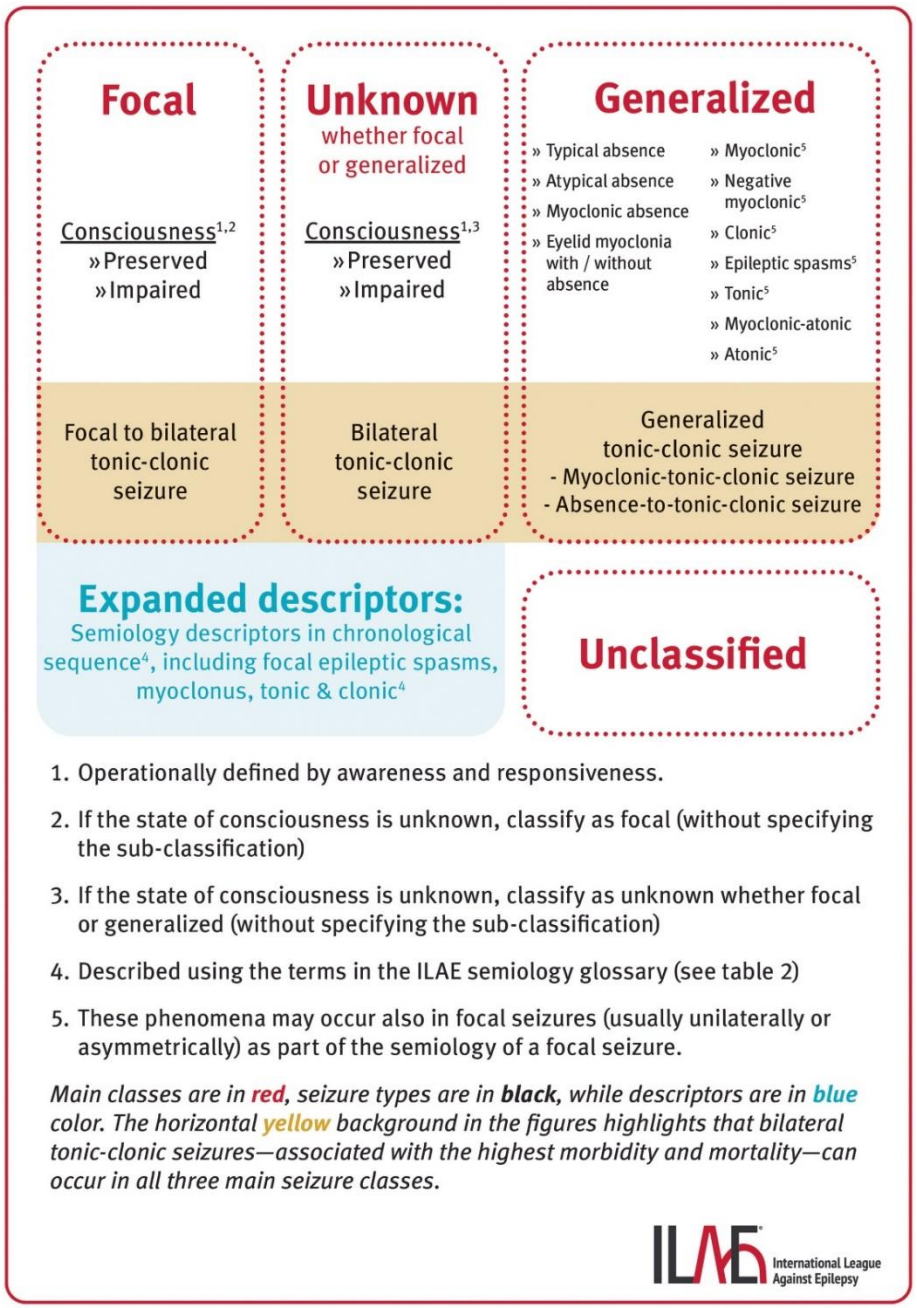

Figure 1: Expanded version of the ILAE 2024 operational classification of seizure types. Figure extracted from: Beniczky, S., et al. (2025). Updated classification of epileptic seizures: Position paper of the International League Against Epilepsy. Epilepsia (6).

If awareness cannot be assessed, the seizure remains classified under the parent focal category. Additionally, focal seizures can evolve to involve both hemispheres, resulting in a focal to bilateral tonic–clonic seizure, corresponding to the 1981 terminology "partial onset with secondary generalization" (3, 5).

Generalized seizures involve both hemispheres from the onset and are categorized into absence seizures, generalized tonic–clonic seizures, and other generalized seizures. Within generalized motor seizures, classification is based on observable patterns such as tonic, clonic, or tonic–clonic activity. Tonic seizures are characterized by sudden, sustained muscle contractions, often affecting limb or axial muscles. In contrast, clonic seizures consist of sustained rhythmic jerking or twitching movements, generated by repeated short contractions of a group of muscles. These clonic jerks occur at a regular frequency, typically ranging from 0.2 to 5 times per second (7). Tonic–clonic seizures, also known as “grand mal seizures” or “convulsions,” combine both tonic and clonic phases within a single episode (7). Seizure classification can follow a basic version, identifying the presence or absence of observable signs, or an expanded version that describes the chronological sequence of semiology. A complete diagram of the updated classification framework is presented in *Figure 1*.

1.2. Drug-resistant epilepsy

Despite the availability of over 30 antiseizure medications (ASMs), 30% to 40% of the 50 million people worldwide living with epilepsy remain pharmacoresistant, failing to achieve sustained seizure freedom (8, 9). In 2010, the ILAE defined drug-resistant epilepsy as “failure of adequate trials of two tolerated, appropriately chosen and used antiepileptic drug schedules (whether as monotherapies or in combination) to achieve sustained seizure freedom” (10).

The underlying mechanisms of drug resistance remain elusive. Several hypotheses supported by both human and animal data have been proposed (10-13), each explaining resistance to specific ASMs but failing to account for multidrug resistance, which highlights the complexity of the condition and underscores the need for continued investigation (11).

In case of inappropriate seizure control with ASMs, the first treatment option is resective brain surgery. Surgery remains a key therapeutic strategy for drug-resistant epilepsy (12). Long-term seizure freedom rates vary by resection site, ranging from 66% for temporal lobe resections to 27% for frontal lobe

surgeries (13). Advances in presurgical evaluation, including structural MRI, SPECT, PET, intracranial Electroencephalography (EEG), and cortical stimulation, have enhanced surgical precision and safety, but emerging techniques such as resting-state fMRI, connectivity analysis, tractography, and task-specific fMRI further promise improved surgical outcomes (14). Nevertheless, adverse events remain significant, including visual field deficits, memory decline (especially with dominant resections), wound infections, and severe complications such as stroke or death (15, 16).

However, surgery is not a viable option for patients with multifocal seizure onset zones, generalized epilepsy, seizure foci located in eloquent cortex regions (involved in critical functions such as language, motor control, or higher-order cognition), or those with prior unsuccessful surgical interventions. Therefore, alternative therapeutic approaches are required for these patients.

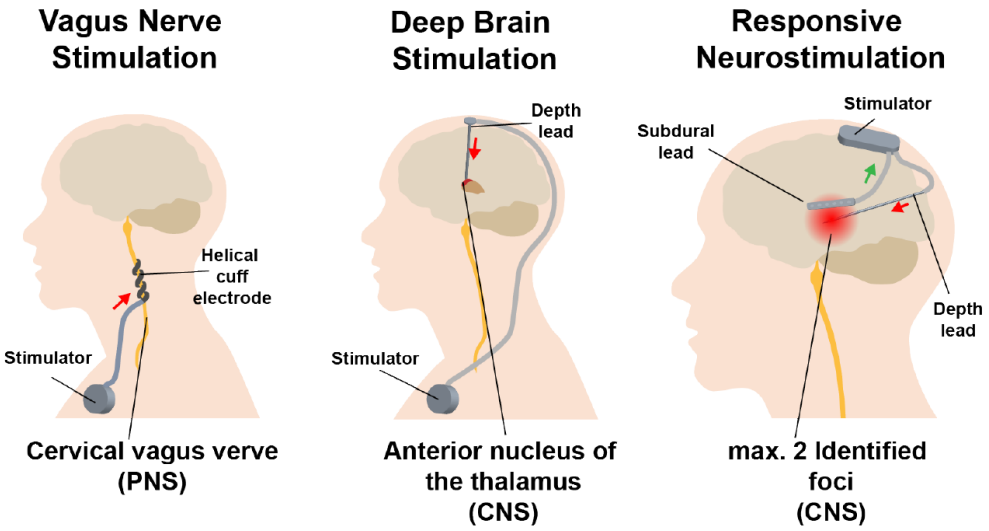

Figure 2 provides a schematic representation of the diverse invasive neurostimulation techniques utilized in the treatment of drug-resistant epilepsy. It delineates approaches targeting both the Peripheral Nervous System (PNS) and Central Nervous System (CNS), with red arrows indicating the stimulation pathways and green arrows representing the sensing of neural activity. This figure has been reproduced from Lars Stumpp's thesis (2020).

Neuromodulation emerged as a therapeutic strategy for neurological disorders during the mid-20th century, particularly through ablative procedures in stereotactic and functional neurosurgery. In 1954, during intraoperative brain recordings in epilepsy patients, Wilder Penfield and Herbert Jasper demonstrated that brief counter-stimulation could interrupt seizure-like activity (17). Such discoveries led to the development of modern neurostimulation therapy, encompassing both invasive and non-invasive approaches that utilize electrical stimulation to modulate neural circuit function. Implantable systems specifically target deep subcortical, cortical, spinal, cranial, or peripheral nerve structures to regulate neuronal activity. Deep Brain Stimulation (DBS) and Responsive Neurostimulation (RNS), illustrated in *Figure 2*, are advanced invasive neuromodulation techniques that target the epileptogenic zone or deep cortical structures, such as the anterior nucleus of the thalamus (ANT). DBS operates in an open-loop configuration, delivering continuous stimulation regardless of neuronal activity, whereas RNS employs a closed-loop system, activating stimulation upon detection of seizure onset. EEG remains the gold standard for seizure detection, with RNS achieving a 75% median reduction in seizure frequency after nine years (18). However, the high invasiveness of this therapy and its limited approval worldwide underscore the necessity for alternative, less invasive detection methods.

Vagus Nerve Stimulation (VNS), a less invasive neuromodulation therapy for drug-resistant epilepsy, is illustrated in the left panel of Figure 2. Introduced in 1988, it has since been widely adopted, with over 125,000 implantations globally (19). Traditionally, patient outcomes were summarized by the "rule of thirds," with one-third experiencing a ≥50% reduction in seizure burden, one-third showing limited benefit, and one-third deriving little to no benefit after 6 months of treatment (20, 21). However, large retrospective studies by Elliott Robert et al (2011) have nuanced this perspective, reporting that approximately 8% of patients become seizure-free, around 20% achieve >90% seizure reduction, and nearly 70% reach a ≥50% reduction in seizure frequency (21, 22).

Initially, VNS operated in an open-loop mode, delivering intermittent stimulation at preset intervals. Patients could also initiate on-demand stimulation using a handheld magnet, which has been shown to reduce seizure severity, duration, or abort seizures entirely (23, 24). A retrospective analysis of the E03 and E04 clinical trials indicated that magnet use was associated with clinically significant benefit: 22% of patients reported seizure termination and 31% noted seizure diminution. Approximately half of those using the magnet

experienced some degree of seizure improvement, regardless of their response to programmed stimulation, highlighting its utility as a complementary intervention (24, 25).

A major advancement occurred with the introduction of the AspireSR device in 2014, which marked the transition to closed-loop stimulation. This system includes an AutoStim mode, which detects ictal tachycardia, defined as a rapid increase in heart rate, and delivers stimulation accordingly (26). The efficacy of this approach was demonstrated in both pediatric and adult patients across various epilepsy etiologies (21, 27, 28). In a retrospective study, Hamilton et al. reported that among patients receiving a new AspireSR implant, 59% achieved a seizure reduction of 50% or greater. Furthermore, in patients whose VNS battery was upgraded from a previous model to AspireSR, 71% experienced an additional ≥50% seizure burden reduction, with 98% reporting a benefit equal to or greater than that obtained from their initial VNS implant. While direct head-to-head comparisons between open-loop and closed-loop VNS systems are lacking, current findings suggest that cardiac-based seizure detection coupled with responsive stimulation may confer additional therapeutic benefits, even in patients previously responsive to conventional open-loop VNS (21).

Nevertheless, challenges remain. Multicentric clinical studies referred to in the literature as “E-36” (29) and “E-37” (30) highlighted limitations in the specificity of ictal tachycardia detection, with only about 50% of seizures associated with a significant heart rate increase (>20%). This interindividual variability in autonomic seizure expression, along with instances of false-positive detections unrelated to seizures, underscores the need for enhanced biomarker sensitivity and specificity in future VNS systems (31).

In addition to invasive modalities, a fully non-invasive alternative, transcutaneous vagus nerve stimulation (tVNS), has been developed to stimulate the auricular branch of the vagus nerve (ABVN) via cutaneous electrodes placed on the left ear, most commonly on the cymba conchae and tragus. This technique aims to replicate the therapeutic effects of invasive VNS without the need for surgical implantation. Clinical trials have demonstrated favorable safety profiles and moderate efficacy, with seizure frequency reductions of up to 34% after 20 weeks of stimulation in some patients with drug-resistant epilepsy (32).

Nevertheless, the heterogeneity of clinical outcomes may be partly attributed to anatomical and neurophysiological factors. The ABVN contains substantially

fewer myelinated Aβ fibers, the primary mediators of the antiepileptic effects of cervical VNS, compared to the cervical vagus nerve (33). In addition, cadaveric studies have shown marked interindividual variability in the fiber composition and trajectory of the ABVN, which may impact the consistency of neural recruitment. As well as the precise positioning of the electrodes which may likely further modulate stimulation efficacy by influencing the extent of activation within the brainstem and central autonomic structures (33).

Although tVNS represents a promising and accessible alternative to invasive stimulation, further efforts are needed. Future trials should aim to directly compare tVNS and iVNS, ideally incorporating prolonged video-EEG monitoring to objectively assess treatment efficacy (32).

1.3. Autonomic dysregulation associated with seizures

Focal and generalized epilepsies disrupt autonomic regulation across ictal, postictal, and interictal states, impacting the parasympathetic, sympathetic, and adrenal medullary systems. Seizures originating from or propagating to regions within the central autonomic network (CAN) can modulate autonomic responses or mimic autonomic afferent activation. The CAN includes cortical and limbic structures such as the amygdala, anterior insula, anterior cingulate cortex, and posterior orbitofrontal cortex, which establish direct connections with subcortical regions such as the hypothalamus, periaqueductal gray, parabrachial nucleus, nucleus tractus solitarius (NTS), and ventrolateral medulla (VLM) (34-36). Together, these interconnected regions regulate sympathetic and parasympathetic outputs by influencing premotor and preganglionic autonomic neurons located in the brainstem and spinal cord (36, 37). Both electrical stimulation and spontaneous epileptiform activity involving cortical and limbic regions can profoundly alter autonomic functions and evoke visceral or affective responses. Ictal autonomic disturbances encompass cardiovascular, respiratory, gastrointestinal, cutaneous, pupillary, urinary, and genital manifestations, with potential implications for homeostatic stability (34).

Sympathetic responses predominate during most seizures, causing tachycardia, tachypnea, increased blood pressure (BP), pupillary dilatation, diaphoresis, and facial flushing. Tonic-clonic seizures and focal to bilateral tonic-clonic seizures, whether of temporal or extratemporal origin, frequently induce these sympathetic responses from infancy through adulthood. However, in some cases, ictal parasympathetic activity or sympathetic inhibition can predominate, causing increased salivation, gastric acid secretion, peristalsis, miosis, reduced heart and respiratory rates, and decreased BP. Complex

patterns involving simultaneous or sequential activation and inhibition of sympathetic and parasympathetic pathways can also occur during individual seizures, reflecting the intricate autonomic dynamics associated with epilepsy (34).

The role of cerebral hemispheric lateralization in cardiovascular autonomic regulation remains a subject of ongoing investigation and debate. A central question concerns the differential representation of parasympathetic and sympathetic functions between the dominant and nondominant hemispheres (34, 38). Emerging evidence suggests that at least some lateralization of cardiovascular representation may exist in humans, with sympathetic predominance of cardiovascular regulation being a proper insular function and parasympathetic cardiac neural regulation relating to the left insula (34, 38, 39). This hypothesis is further supported by findings from Oppenheimer et al., who demonstrated that electrical stimulation of the human insular cortex induces distinct cardiovascular responses: stimulation of the right insula frequently results in tachycardia, while stimulation of the left insula more commonly evokes bradycardia (40). Additional evidence from patients with TLE suggests that hippocampal sclerosis lateralization may influence interictal autonomic tone. Clinical studies have reported a tendency toward bradycardia and increased parasympathetic activity in patients with left-sided TLE, whereas right-sided TLE is more often associated with tachycardia and enhanced sympathetic drive (41-43). These findings should nevertheless be interpreted with caution, as they are often based on indirect autonomic markers such as heart rate variability, and the notion of strict hemispheric lateralization remains debated. Given this, a better understanding of this hemispheric specialization is crucial for elucidating the neural mechanisms underlying autonomic disturbances in epilepsy and their potential clinical implications.

In the following subsection, the main autonomic dysfunction during seizures will be summarized.

1.3.1. Respiratory changes

The relationship between epilepsy and respiratory function is intricate and bidirectional, with seizures significantly altering respiratory patterns, while disruptions in breathing can, in turn, increase seizure susceptibility and severity. Ictal respiratory disturbances have increasingly been reported in both generalized and focal seizures, especially those originating from the temporal lobe, which are strongly associated with autonomic disturbances (34, 44). These disturbances encompass a range of abnormalities, including central or obstructive apnea, tachypnea, bradypnea, hypoventilation, and hypoxemia (45-

47). When prolonged, such respiratory impairments may constitute a significant risk factor for Sudden Unexpected Death in Epilepsy (SUDEP). Notably, postictal central apnea has been identified as a critical contributor to SUDEP pathophysiology (48-50)

1.3.1.1. Obstructive apnea

While obstructive apnea occurs in both generalized and focal epilepsy, several studies indicate a higher prevalence in patients with generalized epilepsy (51, 52). Animal models have provided valuable insights into the pathophysiology of seizure-induced obstructive apnea, highlighting the role of laryngospasm as a key mechanism of airway obstruction during seizures (44, 53).

Seizure activity has been shown to induce high-frequency convulsive activity of the vocal folds, which can occasionally lead to complete airway occlusion. This laryngospasm, when severe, can fully obstruct airflow, precipitating acute hypoxia, ischemic cardiac arrhythmias, respiratory arrest, cardiac arrest, and ultimately death (44, 53). Importantly, laryngospasms have also been observed in human epilepsy, further supporting their clinical relevance (54-57). Moreover, pulmonary edema, a frequent finding in SUDEP, has been proposed as indirect evidence of laryngospasm-related respiratory distress (58-60). The inspiratory effort against a closed airway during obstructive apnea increases pulmonary capillary pressure, which may contribute to the formation of pulmonary edema (61, 62).

The underlying neural mechanisms involve the spread of seizure activity along the pathway from the subiculum to the paraventricular nucleus (PVN) of the hypothalamus (60) and from the PVN to medullary regions (63), where it impacts medullary autonomic nuclei, respiratory centers, and laryngeal motor neurons (53). This seizure-driven autonomic dysregulation exacerbates respiratory dysfunction, further compromising cardiopulmonary stability. Notably, while laryngospasm alone may be sufficient to induce sudden death in some instances, it is not always a necessary condition for fatal seizure-induced obstructive apnea (53). Instead, the critical factor is the strong autonomic co-activation, superimposed on an already heightened sympathetic tone, leading to cardiopulmonary collapse (44, 53).

1.3.1.2. Central apnea

Ictal central apnea (ICA) remains likely underdiagnosed in this population, occurring exclusively during focal seizures, particularly in temporal lobe epilepsy (TLE) (48, 64, 65). ICA is observed in up to 80% of temporal lobe seizures, as recorded on scalp EEG, with similar frequencies found in both

mesial and neocortical TLE (64). Notably, ICA can precede electrographic seizure onset in 33% of cases, and it is the first clinical manifestation in nearly 49% of seizures, underscoring its potential as a biomarker for seizure detection (64, 65). Typically, ICA episodes are transient, ranging from 10 to 185 seconds (66).

Although ICAs are generally benign in the context of focal seizures, prolonged episodes, particularly when associated with marked and sustained hypoxemia, may present clinical risks in a subset of patients. In contrast to obstructive apnea, which typically arises from laryngospasm and mechanical airway occlusion, ICA is characterized by a cessation of respiratory effort despite maintaining an open glottis, implicating brainstem-mediated suppression of respiratory rhythmogenesis. Experimental models have demonstrated that ICA is accompanied by minimal autonomic dysregulation, including only modest activation of the laryngeal nerve and minimal alterations in cardiac function. Collectively, these findings support the hypothesis that ICA, when occurring independently, is unlikely to be intrinsically life-threatening, as it fails to elicit a substantial autonomic response in the absence of active respiratory effort.

Recent evidence from stereo-EEG studies has advanced understanding of the cortical network underlying ICA (67, 68). Electrical stimulation of mesial temporal and paralimbic structures, specifically the amygdala, hippocampus (head and body), anterior parahippocampal gyrus, and antero-mesial fusiform gyrus, reliably induced transient central apnea in 13 out of 19 patients undergoing SEEG monitoring. In contrast, stimulation of the insula, cingulate cortex, subcallosal area, orbitofrontal cortex, and lateral or basal temporal cortices failed to elicit apnea. The duration of apnea correlated with both stimulation intensity and duration, implicating these mesial structures as key nodes in a limbic-paralimbic respiratory control network (67, 68).

1.3.2. Cardiac changes

A large number of studies have investigated the complex inter-relationship between the brain and the heart in patients with epilepsy. Ictal cardiac disturbances are increasingly recognized in both focal and generalized seizures, especially those originating from the temporal lobe, which show strong autonomic involvement. These disturbances include a range of dysregulations such as ictal tachycardia, bradycardia, increases or decreases in BP (69, 70), and, more rarely, cardiac asystole (34, 71). While these changes are often transient and clinically insignificant, there are rare cases where seizure-induced cardiac dysfunction can lead to severe arrhythmic events, which pose a potential risk of life-threatening outcomes.

The following sections will provide a detailed analysis of cardiac alterations.

1.3.2.1. Ictal tachycardia

Ictal tachycardia, or ictal tachyarrhythmia, is classically defined as an excessive elevation in HR during seizures, typically surpassing 100 beats per minute (bpm) (72-76). However, its definition varies considerably across studies, with some using a threshold of more than 10 bpm above baseline (77, 78). In contrast, others adopt higher cutoffs, such as 120 bpm or more (79-81), highlighting the heterogeneity in reported criteria (82). Nevertheless, despite these methodological differences, ictal tachycardia emerges as the most frequently observed cardiac alteration during epileptic seizures, occurring in approximately 82% of patients, with intra-individual variability, as not all seizures in a given patient exhibit this symptom (82, 83). The prevalence of ictal tachycardia is comparable between focal and generalized tonic-clonic seizures, affecting 64–71% of cases. However, its magnitude tends to be greater in focal seizures that progress to bilateral tonic-clonic seizures compared to focal seizures that do not generalize (83). Notably, this phenomenon is more frequently observed in mesial temporal lobe seizures than in extratemporal or non-lesional epilepsy (34, 82-88). Garcia et al. reported that 78% of temporal lobe onset seizures were associated with changes in HR (84), while Weil et al. found that 62% of such seizures showed similar alterations (85), compared to only 22% and 11% for extratemporal seizures, respectively (84, 85).

Ictal tachycardia is characterized by a rapid HR acceleration, typically reaching its peak within the first 60 seconds of seizure onset. The magnitude of this increase varies considerably, ranging from 34% to 60% above baseline and occasionally exceeding 140 bpm. Postictally, HR generally returns to baseline within minutes, although the duration of recovery is modulated by both seizure severity and duration (82, 83). Several studies have shown that HR alterations can precede electroencephalographic (EEG) seizure onset, although findings vary depending on methodology and seizure type (34, 77, 82, 87, 89, 90). Schernthaner et al. (1999) reported preictal HR increases in 76% of seizures recorded non-invasively and in 45.7% of seizures monitored with intracranial depth electrodes (82). Leutmezer et al. (2003), using scalp EEG, observed that 75.9% of seizures were associated with HR increases preceding EEG onset, by an average of 14 seconds in temporal lobe seizures and 8 seconds in extratemporal seizures (87). These data illustrate the variability across studies, likely reflecting differences in seizure localization, seizure classification, and criteria for defining ictal onset.

Caution is warranted when interpreting the temporal relationship between autonomic changes and seizure onset, particularly when using scalp EEG. Early ictal discharges, especially in focal aware or subclinical seizures, may escape detection due to the limited sensitivity of scalp recordings. This limitation was underscored by Casale et al. (2023), who compared simultaneous scalp EEG and stereo-EEG (SEEG) in patients undergoing pre-surgical evaluation. Of the 172 seizures included in this study, 100 (58%) were observed both on scalp EEG and SEEG, whereas 72 (42%) seizures were detected on SEEG only. Notably, 67% of focal aware and subclinical seizures were not detected on scalp EEG. While seizures originated from a wide range of brain regions (including mesial temporal, frontal, insula/lateral temporal, lateral temporal, and occipital), no statistically significant differences in detection rates were found across regions. However, a majority of seizures (65%) originated from the mesial temporal region, which may reflect a sampling bias given the limited number of seizures analyzed in the study, thus representing a key limitation of these findings (91).

Ictal tachycardia results from seizure-induced autonomic dysregulation involving multiple hierarchical structures of the central nervous system. At the cortical level, regions such as the medial prefrontal cortex exert top-down modulation of autonomic output. In contrast, the temporal lobe, including the amygdala, anterior hippocampus, and insular cortex, plays a crucial integrative role in regulating sympathetic activity. Intracranial EEG investigations have demonstrated a strong correlation between ictal tachycardia and localized high-frequency epileptic discharges in the anterior hippocampus and amygdala, reinforcing their central involvement in seizure-related cardiovascular changes (82). At the brainstem level, the NTS processes afferent cardiopulmonary and baroreceptor inputs, contributing to the generation of autonomic output. Seizure activity across any of these regions may disrupt the balance between sympathetic and parasympathetic tone, often favoring sympathetic activation and producing a rapid increase in heart rate (82, 83, 92).

Heart rate variability (HRV) analyses further support this autonomic shift. Power spectral analysis in a small cohort revealed reciprocal high-frequency power peaks between 10 seconds before and 24 seconds after seizure onset, with values exceeding baseline for up to 30 seconds pre-ictally, suggesting a reduced parasympathetic influence (93, 94).

1.3.2.2. Ictal bradycardia

Ictal bradycardia, or ictal bradyarrhythmia, is defined as a transient reduction in HR below 60 bpm (90). Although significantly less prevalent than ictal tachycardia, occurring in fewer than 5% of seizures (74, 95, 96), it is

particularly associated with focal epilepsy, especially TLE. Consistently, a systematic review by Tinuper et al. examining 60 cases of ictal bradycardia found that 76% of patients with well-localized ictal discharges exhibited seizure foci in the temporal or frontotemporal lobes (95).

The degree of bradycardia is variable, with reported cases reaching as low as 44 bpm (90). In the most severe cases, the HR may drop below 40 bpm, as observed in 0.24% of seizures in a cohort of 3,377 cases (97).

The mechanisms underlying ictal bradycardia remain incompletely understood but are hypothesized to involve excessive parasympathetic activation and/or sympathetic inhibition (34, 98). These autonomic alterations likely result from seizure activity originating in or propagating to key structures within the CAN, including the insular cortex and limbic regions, which significantly influence cardiovascular control.

1.3.2.3. Ictal asystole

Ictal asystole is defined as a complete cessation of sinus node activity lasting at least three seconds, typically resolving spontaneously within 60 seconds (97). A progressive ictal bradyarrhythmia generally precedes it and has been reported almost exclusively in focal epilepsy, particularly in drug-resistant TLE, with approximately 90% of cases associated with impaired consciousness and no consistent lateralization (82, 97).

The pathophysiology of ictal asystole is thought to involve aberrant activation of central autonomic circuits, particularly excessive vagal output. Two principal mechanisms have been proposed: seizure-induced enhancement of vagal tone via propagation to medullary autonomic centers, and direct effects of epileptic discharges on postganglionic cardiac parasympathetic fibers (71). Schuele et al. (2008) described ictal asystole observed in 10 patients with focal epilepsy, 8 with TLE, and 2 with extratemporal epilepsy. In most cases, the asystole pattern, along with EEG slowing consistent with cerebral hypoperfusion, closely resembled that seen in vasovagal syncope, supporting a vagally mediated mechanism via brainstem reflex pathways (71, 99). However, in the XTLE cases, asystole may have resulted from secondary hypoxia due to prolonged tonic contraction and ictal apnea, rather than direct involvement of autonomic reflex centers (71, 99).

While ictal asystole is often self-limiting and not typically considered intrinsically life-threatening (100), it may paradoxically abort seizures by

inducing a sharp drop in systemic blood pressure and cerebral perfusion, thereby disrupting ongoing epileptic activity (44).

1.3.2.4. Blood pressure

While seizure-induced HR alterations have been extensively characterized (34, 82, 101), peri-ictal fluctuations in arterial BP remain less comprehensively investigated, primarily due to methodological constraints in continuous, non-invasive BP monitoring. Arterial BP, defined as the force per unit area exerted by circulating blood on arterial walls (102), is dynamically regulated by an intricate interplay between cardiac output and total peripheral resistance (TPR) (103). Seizure activity typically induces a transient elevation in BP; however, paradoxical BP reductions have also been reported, reflecting the heterogeneous effects of epileptic discharges on central autonomic circuits (98, 104).

A recent study employing continuous non-invasive BP monitoring in 37 patients with focal epilepsy undergoing video-EEG recordings demonstrated that mean arterial pressure, systolic arterial pressure, and diastolic arterial pressure increased by 20–30% on average during focal seizures, with values returning to baseline within 10 minutes following seizure cessation (98). This hypertensive response was further corroborated by Jayachandran et al., who reported ictal hypertension in 26.3% of patients (105). These peri-ictal BP elevations followed a time course similar to the ictal HR increase and occurred independently of any changes in oxygen saturation (106). Interestingly, focal seizures with impaired awareness elicited a more pronounced hypertensive response compared to those without impairment (98). Although less frequently observed, ictal hypotension was also reported, occurring in 8.7% of cases (105). Moreover, intra-individual reproducibility of peri-ictal BP changes was observed in patients experiencing multiple seizures of the same semiology, suggesting a seizure-specific autonomic signature (104, 106). The predominant autonomic pattern observed was a concurrent increase in BP and HR, likely reflecting a generalized activation of the sympathetic nervous system induced by seizures. However, in a subset of patients, a paradoxical dissociation was noted, characterized by ictal decreases in BP despite elevations in HR. This latter pattern likely represents a compensatory baroreceptor reflex, where the drop in BP triggers an increase in HR to help restore blood pressure, highlighting the complex interplay of autonomic regulation during seizures (98, 104).

In the context of generalized convulsive seizures, data on peri-ictal BP dynamics remain limited due to the confounding effects of seizure-related motor activity

on measurement accuracy. Nevertheless, evidence suggests two distinct ictal BP response patterns (69, 104, 107). Pattern 1, observed in two generalized convulsive seizure episodes across two patients, was characterized by a concomitant increase in BP and HR, likely mediated by seizure-induced activation of the sympathetic nervous system and catecholaminergic release (108). Conversely, Pattern 2, documented in two other generalized convulsive seizure episodes, exhibited an initial hypertensive response followed by a rapid and pronounced hypotensive phase. This latter pattern is hypothesized to result from ictal propagation to autonomic control centers within the central nervous system rather than a Valsalva-mediated reflex, which temporarily affects BP due to straining or holding breath. (104, 109).

Postictally, BP typically normalizes within minutes, either declining from ictal hypertension or recovering from ictal hypotension (69, 98). Importantly, baroreflex sensitivity, a fundamental mechanism for short-term BP regulation, is preserved following focal seizures but markedly impaired in the early postictal phase of generalized convulsive seizures (110, 111). This dysfunction is thought to result from a combination of metabolic-driven skeletal muscle hyperemia, excessive catecholamine release, and transient brainstem impairment (104, 107). The baroreflex, which ensures BP homeostasis by modulating HR, stroke volume (SV), and TPR, operates via afferent signaling to the NTS. An increase in BP enhances baroreceptor afferent firing, leading to inhibition of cardio-acceleratory neurons within the VLM and activation of cardio-inhibitory neurons in the nucleus ambiguus (NA) and dorsal vagal nucleus (DVN), thereby reducing HR, SV, and TPR. Conversely, a BP reduction results in disinhibition of cardio-acceleratory pathways, enhancing sympathetic outflow to restore BP to baseline levels (104, 112).

1.3.3. Cardiovascular and respiratory mechanisms underlying SUDEP

SUDEP is defined as the sudden, unexpected, witnessed or unwitnessed, non-traumatic, and non-drowning death in individuals with epilepsy, with or without evidence of a preceding seizure, in the absence of documented status epilepticus (SE) and where post-mortem examination does not reveal a structural or toxicological cause of death (113). Cases where autopsy confirms this classification are termed "definite SUDEP," whereas cases without autopsy confirmation are considered "probable SUDEP." This broad definition encompasses heterogeneous cases, and differentiating between seizure-related and seizure-independent SUDEP may be relevant for mechanistic studies, as their pathophysiology is likely distinct (113).

The risk of sudden death in epilepsy patients is more than 20 times higher than in the general population (113). In patients with chronic refractory epilepsy attending specialized epilepsy centers, SUDEP is the leading cause of premature death, accounting for 10–50% of all deaths (113). Population-based studies estimate the incidence at approximately 0.35 cases per 1,000 person-years, rising to 1–2 cases per 1,000 person-years in patients with chronic epilepsy, and reaching 3–9 cases per 1,000 person-years in those with severe, refractory seizures (114).

Most SUDEP cases follow a seizure, with generalized tonic-clonic seizures being the most frequently implicated (34). Moreover, A significant proportion of SUDEP cases occur at night, often while patients are in bed, suggesting an association with nocturnal seizures (115). Nocturnal seizures have been identified as a risk factor for SUDEP, particularly in individuals with nocturnal frontal lobe epilepsy, where seizures predominantly occur during sleep (115).

Although seizures induce substantial cardiovascular changes, including tachycardia and BP fluctuations, cardiac arrhythmias are not the primary cause of SUDEP (34). Instead, respiratory failure is increasingly recognized as the central pathophysiological mechanism. Studies in video-EEG monitoring units have shown that life-threatening seizure events and SUDEP most often result from pulmonary dysfunction, including ictal and postictal apnea and neurogenic pulmonary edema (34). Pulmonary edema arises from increased pulmonary vascular pressure resulting from heightened sympathetic activity, which leads to pulmonary vasoconstriction and elevated left atrial pressure (34). Further evidence suggested that pulmonary edema might also be an indirect evidence of laryngospasm-related respiratory distress (44, 54, 61).

Stewart et al. (2018,2020) described a cascade of events that culminates in SUDEP (44, 54).

1) Seizure-induced activation of autonomic and respiratory brainstem centers leads to first-level autonomic activation, which is characterized by irregular ventilation and laryngospasms, causing partial airway obstruction, leading to moderate hypoxemia.
2) Obstructive apnea, resulting in rapid oxygen desaturation and compensatory autonomic responses to maintain core blood flow.
3) Respiratory arrest, where inspiratory effort ceases due to severe hypoxia, coinciding with the "terminal apnea" described in the MORTEMUS study (116).

4) Progression to respiratory failure, where spontaneous breathing is no longer possible. If airway obstruction persists beyond RA, hypoxic cardiac failure ensues, ultimately leading to cardiac arrest and death.

Laryngospasms are critical in SUDEP, as they induce airway obstruction and obstructive apnea, leading to severe respiratory compromise and severe hypoxemia (44). This sustained oxygen deprivation is a key determinant in seizure-induced mortality, as demonstrated by extensive animal studies linking ictal hypoxia to fatal outcomes (44, 117-121). Notably, central ictal apneas, which have a markedly smaller effect on oxygen saturation, are typically transient and rarely contribute to SUDEP. This contrast highlights the dominant role of prolonged hypoxemia (44). The MORTEMUS study further substantiated this link, showing that terminal apnea consistently precedes cardiac arrest, thereby reinforcing the hypothesis that respiratory dysfunction, rather than primary cardiac failure, is the principal pathophysiological mechanism underlying SUDEP (54, 116).

Several mechanisms contribute to the increased occurrence of SUDEP at night. Postictal respiratory depression is exacerbated by sleep-related reductions in arousal and brainstem reflexes. Normally, hypoxia or hypercapnia triggers autonomic responses to restore airway patency and increase ventilation; however, postictal depression of these reflexes leads to prolonged apnea and fatal hypoxia (34). Additionally, prone positioning post-seizure can exacerbate airway obstruction, particularly when combined with secretions or bedding occlusion (54).

Refractory epilepsy is the second most significant risk factor for SUDEP (114). Patients with drug-resistant epilepsy, particularly those with TLE, often exhibit chronic autonomic dysfunction, typically characterized by a shift toward sympathetic dominance (34, 122). Recurrent uncontrolled seizures and repeated activation of CAN structures may contribute to this dysregulation, which tends to worsen with disease progression and seizure frequency. Such alterations in cardiovascular autonomic control are considered one of the potential mechanisms underlying SUDEP (123). Beyond seizure-related changes, interictal alterations in autonomic function have also been reported, suggesting more persistent dysfunction. For instance, reduced heart rate variability, impaired parasympathetic reactivity, and blunted baroreflex sensitivity have been observed in patients with drug-resistant TLE, indicating chronic parasympathetic impairment (123). Such findings support the hypothesis that ongoing interictal dysfunction may lower the threshold for more severe autonomic disturbances during seizures and increase

vulnerability to SUDEP. Additionally, frequent seizures may contribute to progressive structural and functional alterations not only in brainstem regions but also in other central autonomic networks, which are critical for maintaining respiratory and cardiovascular control (124). Evidence from neuroimaging studies suggests that epilepsy is associated with brainstem atrophy, particularly in areas such as the periaqueductal gray and medulla oblongata, which are key hubs for autonomic regulation (124). A recent morphometric analysis demonstrated that volume loss in these regions correlates with reduced heart rate variability, indicating impaired autonomic control (125). Furthermore, in patients who later died of SUDEP, the extent of brainstem volume loss was inversely correlated with the time between MRI and death, suggesting that more severe atrophy may accelerate SUDEP risk (125). These findings imply that both structural degeneration and autonomic dysfunction may co-evolve in drug-resistant epilepsy, compromising the brain's ability to maintain homeostasis during and between seizures and increasing susceptibility to a fatal autonomic collapse (124, 125).

2. Animal model of epilepsy

Animal models are crucial for understanding the pathophysiological mechanisms of epilepsy and for developing novel therapeutic strategies. While early studies utilized large mammals such as cats and dogs, rodents have become the predominant models due to their well-characterized neuroanatomy, ease of genetic manipulation, and cost-effectiveness (126-128). More recently, zebrafish have gained interest as a high-throughput model for genetic and pharmacological screenings (126, 129). The choice of a model depends on the specific research question, as different paradigms capture distinct aspects of epileptogenesis, seizure propagation, and associated cellular and network dysfunctions.

In the following sections, we will first focus on focal epilepsy models, with particular emphasis on temporal lobe epilepsy (TLE). Given its central role in this thesis, the kainic acid (KA) model, one of the most widely used and well-characterized models of TLE, will be described in detail, including its pathophysiological mechanisms, routes of administration, and progression toward chronic epilepsy. The pilocarpine model, another established paradigm for inducing TLE, will also be briefly discussed. Subsequently, we will address models of generalized seizures, including acute chemically and electrically induced seizures, as well as genetically predisposed absence epilepsy models. Finally, a comparative summary table will synthesize the key features of all experimental models described, highlighting their relevance, induction methods, administration routes, affected brain regions, and main clinical correlates.

2.1. Focal Temporal Lobe Epilepsy model: Status epilepticus models

SE is a prolonged state of self-sustaining seizure activity associated with excitotoxicity, neuroinflammation, and network reorganization (126). Experimental SE can be induced via prolonged electrical stimulation (e.g., kindling models targeting the hippocampus or amygdala) (130) or chemical convulsants, such as KA and pilocarpine (131, 132).

The KA model, a glutamate receptor agonist, administered by systemic or intracerebral injection, induces limbic seizures leading to chronic epilepsy. This model will be discussed in greater detail in the following subsection.

2.2. The kainic acid of temporal lobe epilepsy

Focal epilepsy is the most prevalent form of epilepsy in both adults and children (133), with TLE accounting for approximately 60% of cases (134). Among

patients with drug-resistant TLE, hippocampal sclerosis (HS) represents the most common histopathological abnormality (135). The CA1 region exhibits the most severe neuronal loss, with up to 80% degeneration, followed by the CA4 region and the dentate gyrus. Structural alterations in the dentate gyrus (DG) often include granule cell dispersion (GCD) and mossy fiber sprouting (MFS). GCD is characterized by an expansion of the granule cell layer beyond 10 layers, leading to a blurred boundary between the granule cell and molecular layers (135, 136). In physiological conditions, the mossy fiber axons of glutamatergic granule cells project to CA4 and CA3 via the mossy fiber pathway. However, in MFS, aberrant recurrent collaterals establish excitatory, asymmetric synapses with the apical dendrites and spines of neighboring granule cells within the molecular layer, potentially forming a pathological recurrent excitatory circuit (137). To better investigate this predominant form of epilepsy, a critical need emerged for an experimental model that accurately replicates the pathophysiological characteristics of TLE, allowing for the investigation of unresolved scientific questions and the development of targeted therapeutic approaches.

2.2.1. Mechanisms of action

The KA model was first established by Ben-Ari and colleagues (138, 139), who demonstrated that intra-amygdaloid injections of KA rapidly induce recurrent secondarily generalized convulsive seizures, ultimately leading to fatal SE unless an antiepileptic agent is administered. Beyond the initial damage within the amygdaloid complex, a secondary and progressive neuronal loss was observed in the CA3 region of the dorsal hippocampus, which mirrors the histopathological alterations seen in patients with TLE (138-140).

KA, or kainate, was isolated and extracted from a red alga (Digenea simplex found in tropical and sub-tropical waters (141). Chemically, KA is a heterocyclic analogue of glutamic acid (L-glutamate), exhibiting neurotoxicity that is 30 times greater than that of glutamate, and acting as an agonist of ionotropic kainate receptors (KARs) (142). KA exerts both presynaptic modulatory and direct postsynaptic excitatory effects primarily by binding to KARs. This activation leads to the excessive stimulation of KARs as well as indirect overactivation of other glutamate receptors, including NMDA receptors and AMPA receptors (143). This cascade results in membrane depolarization and increased neuronal firing, which can cause an osmotic imbalance and eventual rupture of the postsynaptic membrane. Simultaneously, the excessive activation of these glutamate receptors induces a substantial intracellular influx of calcium ions (Ca^{2+}), critically impacting mitochondria and the endoplasmic

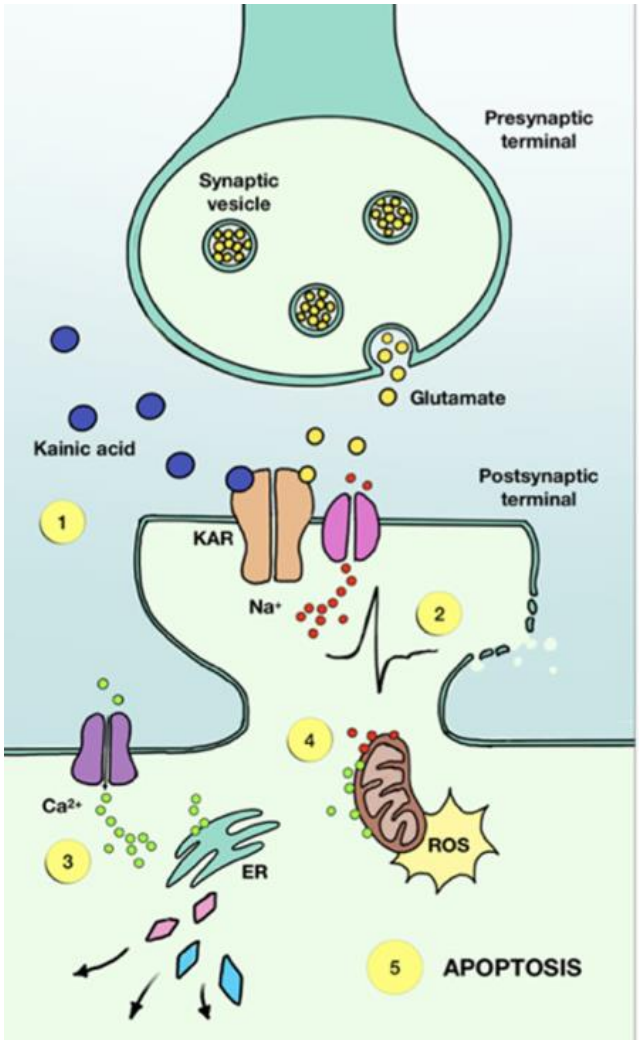

Figure 3 illustrates the complex mechanisms of KA-induced neuronal damage. KA binds to KARs, causing membrane depolarization and neuronal firing (1). Excessive firing leads to osmotic imbalance and rupture of the postsynaptic membrane (2). Calcium influx activates enzymes, such as phospholipases, endonucleases, and proteases, which can damage cellular structures (3). Elevated Ca^{2+} also disrupts mitochondrial function and increases ROS production (4). These events collectively promote apoptosis (5). ER: endoplasmic reticulum, KAR: kainic acid receptor, ROS: reactive oxygen species. Red circles represent Na^{+} ions, green circles represent Ca^{2+} ions, yellow circles represent glutamate molecules, and flower symbols represent KA. Figure extracted from: Rusina, E., et al. (2021). "The Kainic Acid Models of Temporal Lobe Epilepsy (144).

reticulum. The elevated intracellular Ca^{2+} triggers the activation of various intracellular enzymes, such as phospholipases, endonucleases, and proteases, all of which contribute to the degradation of cellular structures. Moreover, the rise in intracellular Ca^{2+} disrupts mitochondrial function, leading to impaired energy production and further cellular damage. In parallel, sodium (Na^{+}) and chloride (Cl^{-}) ions contribute to the neurodegenerative process, and extracellular potassium (K^{+}) dynamics are also implicated in KA-induced excitotoxicity. Additionally, KA administration promotes the excessive generation of reactive oxygen species (ROS) and reactive nitrogen species, amplifying the neurotoxic cascade. These free radicals play a critical role in exacerbating neuronal damage, contributing to the progression of cell injury and culminating in apoptosis. Collectively, these mechanisms act synergistically, potentiating one another and driving the neurodegenerative effects observed following KA exposure (142, 144) (*Figure 3).* KARs are expressed at varying levels in the amygdala, entorhinal cortex, basal ganglia, and cerebellum (140). They are also highly expressed in the hippocampus, with KA1 subunits (also known as GluK4) being highly expressed in CA3 pyramidal cells, and KA2 (GluK5) subunits being highly expressed in both CA1 and CA3 pyramidal cells. Therefore, the high affinity of KA1 and KA2 receptors to KA, combined with their high rates of expression in the CA3 region of the hippocampus, renders this region highly susceptible to excitotoxic damage induced by KA and often makes the hippocampus the seizure onset zone in this model (140).

2.2.2. Administration routes: advantages and limitations

KA can be administered via two routes: intracerebral and systemic (140, 144). Intracerebral injections typically target the hippocampus or amygdala and generate a more localized model of TLE, with more controlled and predictable histopathological alterations. In rats, intracerebral injection of KA doses ranging from 0.4–2.0 μg results in SE within 5–30 minutes (144-146), with low lethality (typically <10%) (144, 147). This method induces focal hippocampal lesions, predominantly in the ipsilateral CA3 subfield, with some involvement of CA1 and CA4, regardless of the injection site (144, 146, 148-150). Additionally, MFS (146, 151-153) and GCD in the DG are observed (144, 147). Thus, intracerebral administration confers several advantages, including high reproducibility, controlled and localized neuronal damage, and a low mortality rate. However, it also presents notable limitations, primarily its invasive nature, as it requires surgical intervention for the implantation of a cannula prior to KA administration. In some studies, mild anesthesia during injection to facilitate SE

induction, which may influence the epileptogenesis process due to antiepileptogenic effects of anesthesia (147, 154).

In contrast, systemic KA administration is more commonly used in broader studies due to its less invasive nature; however, it may require higher or repeated doses (5mg/kg i.p. according to the Hellier protocol)(155) to achieve similar effects due to variability in brain bioavailability (140, 144). SE develops within two hours after systemic administration, lasting approximately 5–9 hours if untreated with an additional drug injection (144, 156-159), with mortality rates around 22%, which can be reduced to 5–6% with repeated low-dosage (2.5mg/kg) injections (160). Following systemic administration, the first signs of neuronal damage appear within 48 hours, predominantly affecting the CA1, CA3, and CA4 hippocampal subregions (140, 144, 157, 161, 162). The typical pattern of damage includes necrosis of pyramidal cells, gliosis, and MFS (163), along with involvement of extrahippocampal regions such as the amygdala (164), subiculum, entorhinal cortex, thalamus, caudoputamen (157), substantia nigra, and hypothalamus (165). Systemic administration leads to more extensive lesions, affecting both temporal and extratemporal brain regions, resulting in higher mortality rates compared to intracerebral injections (140, 144).

2.2.3. Epileptogenesis: From induction to chronic state

Following seizure induction and histopathological damage, a latency period precedes the onset of spontaneous seizures, marking the initiation of epileptogenesis. During this phase, seizure frequency gradually increases, reflecting a progressive reorganization of brain networks. The transition from acute inflammation to a chronic epileptic state is driven by complex molecular and cellular mechanisms, including alterations in synaptic transmission, neuronal excitability, and network plasticity (166-168). These processes progressively enhance neuronal synchrony, ultimately establishing a stable epileptic condition characterized by spontaneous recurrent seizures independent of external triggers.

The dynamics of epileptogenesis in the KA model have been explored in a few studies, across different administration routes (146, 147, 155, 156, 168). Given its relevance to this thesis, we focus on the systemic KA model. Williams et al. (2009) investigated epileptogenesis in Sprague-Dawley rats subjected to repeated systemic KA injections (5 mg/kg) until self-sustained SE was elicited, defined by ≥10 convulsive seizures per hour for at least three hours (stages III-V) (156). Seizure evolution was assessed through nearly continuous EEG monitoring over 100 days in KA-treated rats (n=7) and saline-injected controls

(n=6). No seizures, convulsive or nonconvulsive, were detected in controls, confirming the specificity of KA-induced epileptic activity (156).

Using radiotelemetry-based surface cortical and bilateral hippocampal EEG recordings combined with semiautomated seizure detection, Williams et al. quantified electrographic seizure frequency over 100 days post-SE. Their findings demonstrated a progressive, sigmoid-like increase in seizure frequency. A key observation was the emergence of seizure clustering. Interseizure interval analysis showed that seizures were not randomly distributed but occurred in clusters, with intra-cluster intervals <4 hours and inter-cluster intervals spanning 1–4 days. This pattern suggests that clustering is an intrinsic feature of epileptogenesis, potentially amplifying overall seizure burden (156).

Building on these findings, Van Nieuwenhuyse et al. (2015) conducted a long-term study using continuous depth EEG monitoring in six rats over 30 weeks, starting before KA administration (168). Their results confirmed a mean latency of 7 ± 1 days to the first spontaneous seizure (range: 4–10 days) (168). By fitting seizure rate progression to a Boltzmann sigmoid function, they identified four distinct phases in epileptogenesis: (1) Latent period – characterized by the absence of detectable seizures. (2) Slow growth phase – a gradual increase in seizure frequency, reaching >5 seizures/day at 67.5 ± 6.3 days post-SE. (3) Exponential growth phase – rapid seizure escalation culminating in a plateau, with a mean transition time of 122.3 ± 79.0 days. (4) Plateau phase – stabilization of seizure frequency at persistently high levels, though with significant inter-individual variability (14.5–48.6 seizures/day) (168).

These findings reinforce the concept of epileptogenesis as a progressive and nonlinear process. However, substantial inter-individual variability was observed in seizure dynamics, highlighting the complexity of the underlying mechanisms (156, 168).

2.3. The pilocarpine model of temporal lobe epilepsy

Similar to KA, the pilocarpine model is widely used to induce chronic TLE. Pilocarpine acts as an M1 muscarinic acetylcholine receptor agonist, promoting continuous excitatory neuronal activity that leads to brain tissue damage (169). Turski et al. (1983) initially described the pilocarpine model, which demonstrated that systemic intraperitoneal administration of pilocarpine in rodents induced a sequence of automatisms and motor limbic seizures progressing to status epilepticus. Subsequent analysis revealed extensive

neuronal injury in the olfactory cortex, amygdala, thalamus, neocortex, hippocampus, and substantia nigra (Turski et al., 1989) (170-174). Compared to the KA model, which produces more selective and delayed damage, particularly in the CA3 region of the hippocampus, the pilocarpine model induces broader and earlier excitotoxic injury, especially in the dentate gyrus, where granule cells are otherwise relatively resistant. Silver staining studies confirm more widespread and intense neuronal damage with pilocarpine than KA, particularly in cortical, limbic, and hypothalamic structures (165, 175).

The pilocarpine model offers a robust and reproducible method to induce SE and the transition to chronic epilepsy, enabling investigation into seizure dynamics, neurodegeneration, synaptic plasticity, and epileptogenesis. It also promotes marked neurogenesis and mossy fiber sprouting (165, 175). However, the model's high mortality rate and extensive irreversible damage limit its utility in some experimental contexts, particularly when modeling subtle epileptogenic mechanisms or testing neuroprotective agents.

2.4. Generalized seizure models

Generalized seizure models are designed to investigate seizure initiation and propagation across widespread neuronal networks. Among acute models, the maximal electroshock (MES) seizures induce generalized tonic-clonic seizures via high-intensity electrical stimulation through corneal or auricular electrodes (126, 176, 177). Unlike KA-induced seizures, which originate focally and evolve into chronic epilepsy, MES-induced seizures are acute, making this model particularly suitable for preclinical screening of anticonvulsant compounds (126). Similarly, pentylenetetrazol (PTZ), a non-competitive GABA_A receptor antagonist, triggers generalized seizures when administered systemically, leading to a sequence of behavioral manifestations ranging from myoclonic jerks to tonic-clonic convulsions (126, 178, 179). Like KA, PTZ disrupts the balance between excitation and inhibition, albeit through distinct pharmacological mechanisms. While MES and PTZ models are highly reproducible and widely used for screening AMS compounds, they primarily reflect acute seizure activity rather than chronic epilepsy.

Audiogenic seizure models represent another generalized approach, which are triggered by high-intensity acoustic stimuli in genetically susceptible strains, such as Krushinsky-Molodkina rats, DBA/2 mice, and Wistar audiogenic rats (126, 180-183). Seminal neuroethological, electrophysiological, cellular, and molecular studies have established the Wistar Audiogenic Rat (WAR) strain as a robust and reliable model for investigating the complexity and emergent properties of epileptogenic networks (184). However, since seizures in this

model are triggered by external stimuli rather than occurring spontaneously, its relevance to spontaneous epileptic conditions remains limited (126).

In addition to these well-known and characterized models, others include closed head injury models for post-traumatic epilepsy, systemic NMDA administration to induce seizures via glutamatergic excitation, and flurothyl inhalation for controlled generalized seizures through GABA_A receptor antagonism. Each model has distinct advantages and limitations (126).

2.5. Absence seizures models

Absence seizures, characterized by brief episodes of behavioral arrest and spike-and-wave discharges (SWDs) in the 2.5–4 Hz range in humans, are commonly modeled using genetic absence epilepsy rats from Strasbourg (GAERS) (185-187) and WAG/Rij rats (188). However, in these animal models, the frequency of SWDs is notably higher, typically with a higher frequency (9–11 Hz) during the first 1–2 seconds of the seizure, followed by a decrease to 7–8 Hz (185, 189). These models exhibit spontaneous non-convulsive seizures with well-defined electrophysiological signatures, making them highly relevant for investigating potential mechanisms and selection of AEDs (190). The minimal motor activity during absence seizures is advantageous for electrophysiological recording with minimal movement contamination; however, they display minimal autonomic alterations in comparison with other epilepsy type, such as TLE, which may limit their utility in studying systemic effects of epilepsy (191).

Model	Seizure Type	Induction Method	Chronicity	Administration Route
KA	Focal (TLE)	Chemical (KA, glutamate analog, KAR agonist)	Acute (SE) or Chronic (SRS)	Intracerebral (hippocampus, amygdala) or systemic (i.p.)
Pilocarpine	Focal (TLE)	Chemical (M1 muscarinic agonist)	Acute (SE) or Chronic (SRS)	Intracerebral (hippocampus) or systemic (i.p.)
Kindling	Focal (TLE)	Electrical (repeated subthreshold stim.)	Chronic	Intracerebral electrode (hippocampus, amygdala)
MES	Generalized (tonic-clonic)	Electrical (high-intensity)	Acute	Corneal/auricular electrodes
PTZ	Generalized	Chemical (GABA_A antagonist)	Acute or Chronic	Systemic (i.p., s.c.)
Audiogenic (e.g., WAR, DBA/2 mice)	Generalized	Acoustic stimulation (genetically susceptible strains)	Acute or Chronic (repeated exposure)	Auditory stimulus
GAERS /WAG Rij rats	Generalized (absence)	Genetic	Chronic	Spontaneous (no external induction)

Table 1: Summary table of experimental epilepsy models. Models are categorized based on seizure type (focal vs. generalized), induction method (chemical, electrical, genetic), chronicity (acute seizures, status epilepticus [SE] induction, or spontaneous recurrent seizures [SRS]), and route of administration.

3. The vagus verve

3.1. Anatomy and fiber types

The vagus nerve (cranial nerve X) is the longest cranial nerve, playing a critical role in both autonomic and somatic functions by linking the viscera to the brain. It comprises afferent (sensory) and efferent (motor) fibers in an approximate ratio of 80% and 20% efferent fibers. Its primary function is sensory, relaying peripheral information to the central nervous system. The vagus nerve originates from four distinct nuclei in the medulla oblongata and, after exiting the skull via the jugular foramen, traverses the superior and inferior ganglia, which house sensory neuron cell bodies as illustrated in *Figure 4*.

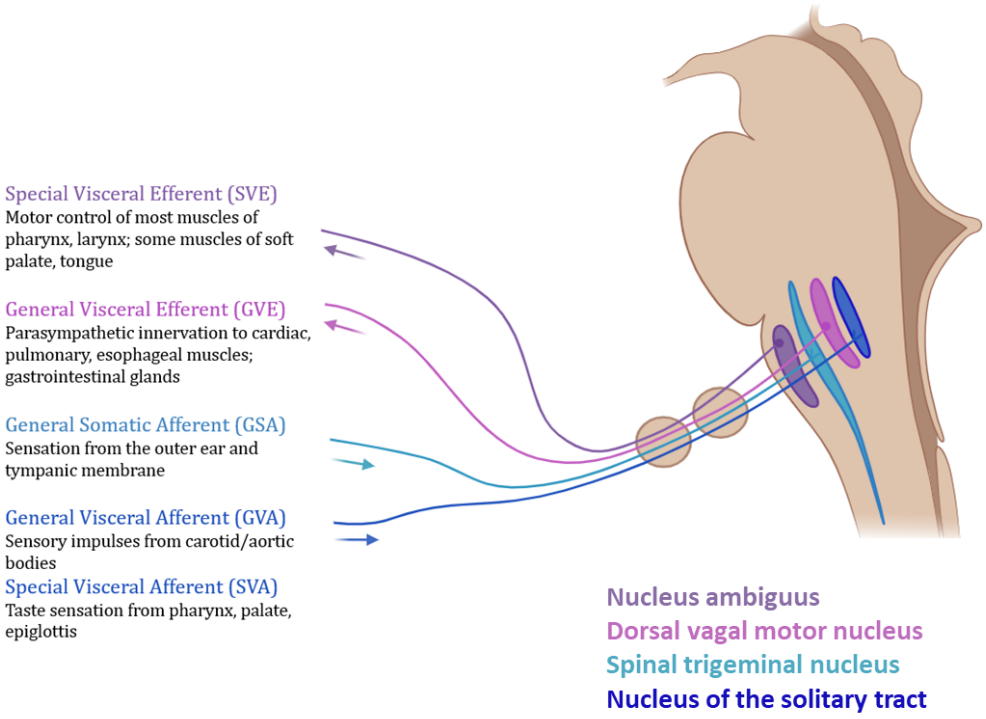

Figure 4 illustrates the afferent and efferent components of the vagus nerve, along with their central and peripheral projections.

The efferent (motor) component of the vagus nerve consists of:

- Special visceral efferent (SVE) fibers, originating from the NA, which innervate most muscles of the pharynx, larynx, soft palate, and the

palatoglossus muscle of the tongue. These fibers are essential for swallowing and phonation.
- General visceral efferent (GVE) fibers, arising from the dorsal motor nucleus of the vagus, which provide parasympathetic innervation to the cardiac, pulmonary, and gastrointestinal (GI) systems, modulating visceral functions such as HR, respiratory activity, and digestive processes.

The afferent (sensory) component, which constitutes the majority of vagal fibers, includes:

- General somatic afferent (GSA) fibers, with cell bodies in the jugular (superior) ganglion, convey sensory input from the external ear and tympanic membrane to the spinal trigeminal nucleus.
- General visceral afferent (GVA) fibers, with cell bodies in the nodose (inferior) ganglion, transmit interoceptive signals from the carotid and aortic bodies to the solitary nucleus.
- Special visceral afferent (SVA) fibers, with cell bodies in the nodose (inferior) ganglion, carry gustatory information from the pharynx, soft palate, and epiglottis to the solitary nucleus.

3.1.1. Distribution and central connections of the vagus nerve:

As the vagus nerve descends within the carotid sheath alongside the carotid arteries and the internal jugular vein, it gives rise to multiple branches:

- The pharyngeal branch, containing both motor and sensory fibers, which innervates most pharyngeal and palatal muscles while also conveying chemoreceptive information from the carotid body.
- The superior laryngeal nerve, which bifurcates into:
    - An internal branch, responsible for sensory innervation of the mucosa from the epiglottis to the supraglottic larynx.
    - An external branch, which controls the cricothyroid muscle and modulates pitch regulation.
- Superior cardiac branches, which integrate into the cardiac plexus to regulate autonomic cardiac function.

In the thoracic region, the vagus nerve follows distinct anatomical pathways on the right and left sides:

- On the right, it passes anteriorly to the subclavian artery before giving rise to the right recurrent laryngeal nerve, which loops around the subclavian artery and ascends to the larynx.

- On the left, the left recurrent laryngeal nerve emerges at the level of the aortic arch, looping beneath it before ascending toward the larynx.

These recurrent laryngeal nerves provide motor innervation to all intrinsic laryngeal muscles except the cricothyroid and relay sensory input from the infraglottic larynx.

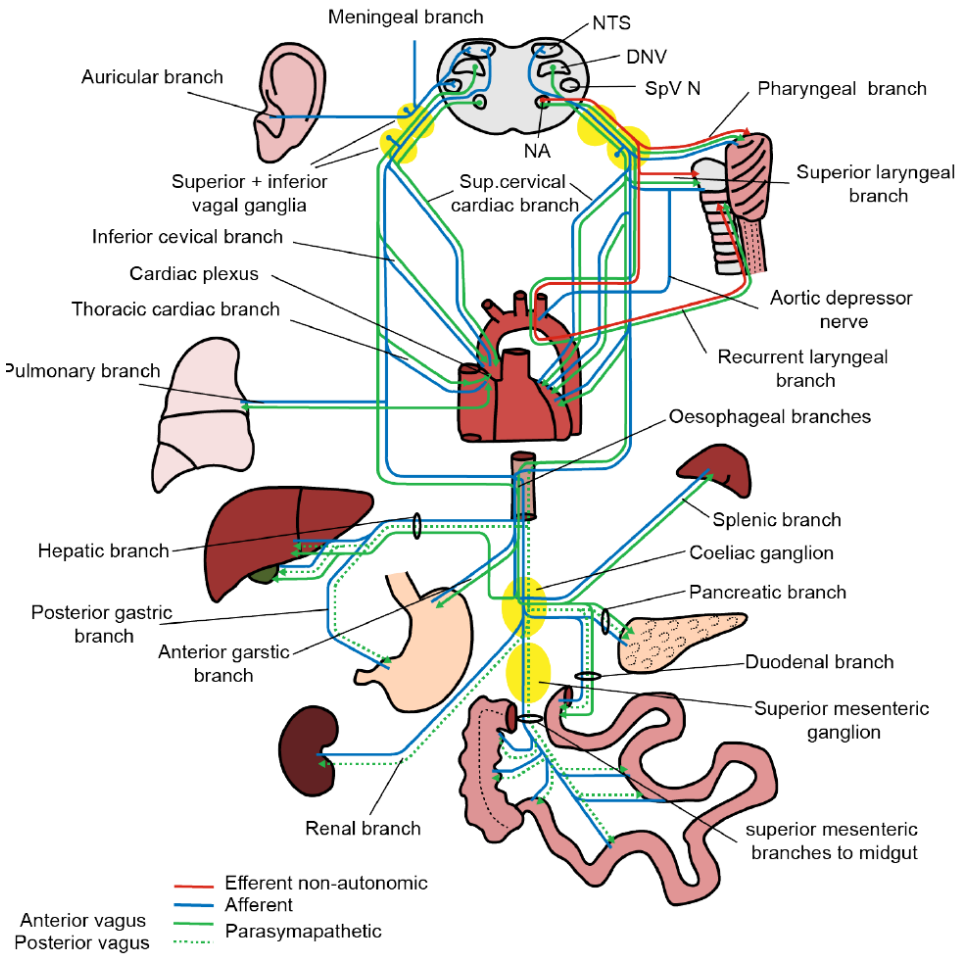

Figure 5 shows the representation the distribution and central connections of the vagus nerve. All cervical and thoracic branches are bilateral but have been omitted for clarity. The green solid line represents the anterior vagal trunk, and the green dotted line indicates the posterior vagal trunk. The vagus nerve divides into these two trunks: the anterior trunk, primarily derived from the left vagus nerve, gives rise to hepatic, celiac, and anterior gastric branches, including the nerves of Latarjet, which innervate the pylorus and proximal duodenum. NA: nucleus ambiguus; NTS: nucleus tractus solitarii; Sp V N: spinal trigeminal nucleus. Figure extracted from: Clancy JA, Deuchars SA, Deuchars J. The wonders of the Wanderer. Exp Physiol. 2013 *(192).*

As it extends into the thorax and abdomen, the vagus nerve gives rise to additional branches that contribute to the cardiac, pulmonary, esophageal, gastric, and celiac plexuses, thereby orchestrating the autonomic control of visceral organs (193, 194). *Figure 5* illustrates the extensive distribution and innervation of the vagus nerve.

3.2. Functional vagal afferents in key visceral organs

3.2.1. Cardiac innervation

The vagus nerve plays a key role in cardiovascular homeostasis by conveying sensory information from the heart to the central nervous system. Approximately 5–6% of all nodose ganglion sensory neurons are dedicated to cardiac afferents (195, 196). These afferents, derived exclusively from the nodose ganglion, innervate both atria and ventricles, where they monitor pressure, stretch, and chemical signals essential for modulating autonomic responses (196-198). Vagal afferents are conventionally classified as mechanoreceptors (1) and chemoreceptors (2).

(1) Mechanosensitive cardiac vagal afferents are primarily myelinated Aδ fibers. These fibers terminate in the epicardium and endocardium and respond to mechanical deformation of the myocardium during different phases of the cardiac cycle (196, 197, 199, 200). Depending on their subtype, they encode either ventricular filling (preload) or systolic pressure changes (afterload), and are activated by physiological and experimental changes in cardiac load, such as aortic occlusion or volume expansion (201, 202).

(2) Chemosensitive afferents, by contrast, are predominantly unmyelinated C fibers and outnumber mechanosensitive afferents significantly (196, 197). These fibers exhibit low basal activity and slow activation kinetics. They respond to chemical mediators such as bradykinin, prostaglandins, and reactive oxygen species, contributing to cardiac nociception and inflammation signaling (196, 200).

Centrally, both fiber types project to the NTS, particularly its dorsomedial subregion, which is critically involved in cardiovascular reflex control (203). Second-order neurons in the NTS relay information to the NA and dorsal motor nucleus of the vagus, forming the basis for parasympathetic efferent output (204). Additionally, ascending projections from the NTS extend to higher-order centers involved in autonomic integration (196, 205).

3.2.2. Respiratory innervation

The respiratory tract receives dense vagal sensory innervation, with nearly 20% of all vagal afferents terminating in the lungs and airways (206). These afferents arise from two distinct embryological lineages: nodose ganglion neurons, which exhibit a visceral phenotype, and jugular ganglion neurons, which share features with somatosensory neurons. Sensory terminals are broadly distributed along the airway epithelium and associated structures, including neuroepithelial bodies, smooth muscle, vasculature, and submucosal glands (206).

Mechanosensitive pulmonary afferents are primarily composed of myelinated Aβ and Aδ fibers, which are derived from nodose neurons. They are categorized functionally as slowly adapting receptors (SARs) and rapidly adapting receptors (RARs) (206). SARs are highly sensitive to lung inflation and maintain tonic activity during sustained stretch, reflecting their close association with airway smooth muscle. Their persistent discharge encodes static lung volume, thereby contributing to the fine-tuning of inspiratory timing and the termination of inspiration through negative feedback mechanisms (206, 207). In contrast, RARs respond preferentially to dynamic mechanical stimuli such as bronchospasm or mucus-induced obstruction. Characterized by rapid adaptation, typically within 1–2 seconds, to sustained inflation, RARs terminate predominantly within or beneath the airway epithelium. They are especially responsive to changes in dynamic lung compliance and airway irritants (206). These afferents are critically involved in reflexive responses such as coughing, sighing, and bronchoconstriction.

Although primarily responsive to mechanical forces, both SARs and RARs can be secondarily activated or modulated by a variety of endogenous and exogenous substances, including acetylcholine, histamine, bradykinin, capsaicin, and substance P, which may amplify their sensitivity or trigger reflex inhibition of airway smooth muscle (206, 208). As a result, these afferents play an essential integrative role, encoding lung inflation, mechanical distortion, and obstruction.

In contrast, chemosensitive afferents consist of unmyelinated C fibers and lightly myelinated Aδ fibers, originating from both nodose and jugular ganglia (209, 210). These fibers are activated by noxious chemical stimuli, including capsaicin, acid, and inflammatory mediators, and express a variety of ligand-gated and G protein-coupled receptors (206, 208). Pulmonary C fibers contribute to neurogenic inflammation, bronchoconstriction, and modulation of respiratory drive.

Central projections are highly organized: SARs terminate in the medial and ventrolateral NTS, engaging inhibitory pump cells and inspiratory neurons, while RARs project to the caudal and medial NTS, providing glutamatergic excitation to respiratory networks (206, 211). Nodose-derived C and Aδ fibers primarily target the commissural and dorsolateral NTS, whereas jugular afferents preferentially project to the paratrigeminal nucleus, suggesting distinct roles in somatic-visceral integration (206).

3.2.3. Gastrointestinal innervation

The vagus nerve provides dense afferent innervation to the GI tract, mediating sensorimotor integration critical for digestion and visceral homeostasis. Vagal afferents target both muscular and mucosal layers, forming specialized terminals that enable bidirectional communication with the enteric nervous system and epithelial cells (212).

Mechanoreceptors in the GI tract include intraganglionic laminar endings (IGLEs) and intramuscular arrays (IMAs). Both originate from myelinated A-type fibers and are distributed along the smooth muscle layers of the esophagus, stomach, and intestines. IGLEs, located at myenteric ganglia, act as tension receptors, while IMAs, arranged along smooth muscle, detect stretch, especially in sphincteric regions (213-215).

Chemosensitive afferents within the gut are predominantly unmyelinated C fibers. These fibers terminate in the mucosa, where they detect luminal stimuli including nutrients, acids, and microbial metabolites. Some of these afferents form glutamatergic synapses with enteroendocrine cells, facilitating rapid detection of gut content changes (216).

Central projections of GI vagal afferents primarily terminate in the medial and commissural NTS, where they relay mechanical and chemical information from the gut wall (217). Muscle-derived mechanoreceptors project to NTS regions involved in motor reflex circuits, while mucosal chemosensors activate distinct populations of second-order neurons influencing satiety, nausea, and gut motility (218). Neurotransmission is predominantly glutamatergic, with additional contributions from serotonin and ATP in the mucosal pathways.

3.3. The role of vagal anatomy in guiding therapeutic neuromodulation

Several aspects of vagus nerve anatomy have been previously investigated and described. However, a detailed understanding of the transverse (horizontal) and longitudinal (vertical) fascicular organization of the vagal trunk,

particularly in relation to the target organs innervated and the functions mediated, remains limited (219). Previous studies have commonly estimated fiber counts by analyzing spatially confined segments of the nerve and extrapolating these findings to the entire vagus nerve. This approach relies on the assumption of a uniform fiber distribution both within and across fascicles, as well as a linear and continuous organization of fibers along the nerve's longitudinal axis. However, it remains unclear whether such uniformity exists, or if certain fiber types show preferential localization within specific fascicles or even sub-fascicular sectors (219).

This anatomical uncertainty is not purely of academic interest: it carries significant implications for the development of bioelectronic medicine targeting the vagus nerve. In particular, the design of selective neuromodulation strategies, aiming to activate specific functional pathways while avoiding off-target effects, relies on precise knowledge of fascicular organization. As VNS is increasingly employed in clinical contexts, ranging from epilepsy and depression to stroke and obesity (220-230), the need for anatomical specificity becomes critical. While current clinical VNS devices typically employ a non-selective bipolar cuff electrode delivering cyclic stimulation to the cervical vagus nerve, this approach may inadvertently engage non-target fibers, contributing to variable efficacy and undesirable side effects (20, 231, 232). Indeed, although VNS leads to a seizure reduction exceeding 50% in approximately 45–60% of patients after six months of therapy (20), it is also frequently associated with adverse effects such as voice alteration, coughing, dyspnea, and headaches, likely due to incidental activation of motor or autonomic fibers (231, 232). While not typically limiting, these effects have prompted interest in whether more selective stimulation could enhance therapeutic specificity by targeting relevant fiber populations.

The potential for selective stimulation depends on two key anatomical principles: fiber-size selectivity and spatial selectivity. Then, designing stimulation strategies that exploit these principles requires a thorough understanding of how fascicles and fibers are organized along both the vertical (rostro-caudal) and horizontal axes of the nerve (219, 233).

Recent studies have begun to address this gap by generating high-resolution anatomical maps of the vagus nerve and its projections. Jayaprakash et al. (2023) investigated the spatial organization of fascicles within the swine vagus nerve using high-resolution micro-computed tomography and quantitative histology (219). Their findings revealed two complementary patterns of fascicular organization along the longitudinal axis of the nerve. First, from a

functional perspective, sensory and motor fascicles are spatially segregated in the upper cervical portion of the vagus nerve, near the nodose ganglion. As the nerve descends caudally toward the thoracic region, these functionally distinct fascicles increasingly converge, resulting in a more intermixed configuration (219). Conversely, from a target-specific perspective, fascicles projecting to peripheral organs such as the larynx, heart, and lungs exhibit a greater degree of separation in the lower cervical and upper thoracic segments. These organ-specific fascicles progressively merge as they ascend rostrally toward the nodose ganglion, leading to a gradual loss of spatial specificity at more proximal levels (219). In parallel, immunohistochemical analysis at the single-fiber level revealed that different morphological fiber types are distributed non-uniformly across fascicles: myelinated afferents and efferents tend to occupy separate fascicles. In contrast, small unmyelinated afferents are more broadly distributed (219).

Building on these anatomical insights, the authors investigated whether spatially selective stimulation could differentially recruit functionally distinct fiber populations. To this end, they developed a multi-contact cuff electrode capable of stimulating discrete sites along the nerve's circumference (219). In acute experiments on anesthetized swine, stimulation through different contacts evoked distinct physiological responses associated with specific organ systems: changes in HR (cardiac vagal fibers), respiratory rate (pulmonary innervation), and laryngeal muscle contraction (somatic motor fibers) (219). These effects were accompanied by evoked compound action potentials (eCAPs) recorded at a second site, confirming the activation of specific fiber types with differing conduction velocities (Aα/β versus Aδ/B fibers), depending on the stimulation site (219).

In addition to spatial selectivity, the longitudinal (rostro-caudal) organization of fascicles adds another layer of complexity. Previous studies have shown that fascicles undergo extensive branching and merging along the length of the vagus nerve (219, 233-235). Thus, conceptualizing fascicular anatomy as a linear map may be misleading; a curvilinear model more accurately reflects the true anatomical structure, especially in humans (233). This is particularly relevant for designing stimulation strategies that aim to target fibers based on their spatial localization along the nerve.

Many of these insights have emerged from studies in large animal models, particularly swine, whose vagus nerve closely mirrors the anatomical and fascicular complexity of the human vagus nerve (236-238). In contrast, rodent models possess predominantly mono- or bifascicular vagus nerves. This

anatomical simplicity significantly limits their translational relevance, especially in the context of spatially selective stimulation strategies or the development of advanced bioelectronic interfaces. Although selective VNS has been demonstrated in rodents (239) and sheep (240), with studies showing targeted stimulation of baroreceptive fibers to reduce blood pressure without bradycardia (239) and function-specific modulation of heart or respiratory rate (240), the limited fascicular organization in these species constrains the extrapolation of such results to the more complex human vagus nerve.

Taken together, these anatomical studies underscore the crucial importance of understanding both the structural organization and functional dynamics of the vagus nerve in advancing selective neuromodulation therapies. While the anatomical mapping of the vagus nerve provides the foundational knowledge necessary for developing precise and targeted stimulation devices, it is equally important to understand how the nerve functions in terms of signal transmission. This includes how different fascicles and fiber types process and relay specific information from peripheral organs.

4. Vagus nerve activity recording

Over the past two decades, numerous studies have explored vagus nerve recordings in animal models and, more recently, in humans, for various research objectives. Several types of electrodes can be used to record neural activity: intraneural electrodes, which allow for close proximity to nerve fibers, enabling the recording of Single Unit Activity (SUA) (241-250), and extraneural electrodes, such as cuff (239, 251-267) or hook electrodes (255, 266, 268-274), which record the summation of action potentials, referred to as Compound Action Potentials (CAP). These various studies, along with the type of electrode used and their objectives, are summarized in the tables presented in Appendix 2 from pages 158 to 169.

4.1. Electrodes

Two main categories of electrodes are distinguished: intraneural and extraneural. The choice of electrode type plays a crucial role in signal acquisition, as it determines the nature of the neural activity recorded. Generally, recording selectivity increases with the level of invasiveness of the electrode.

4.1.1. Extraneural electrodes

The principal types of extraneural electrodes include hook electrodes and cuff electrodes. Variants of these configurations, cuff-like electrodes, have also been described in the literature. For instance, Falcone et al. (2020) employed de-insulated microwires wrapped around the nerve, effectively mimicking a cuff configuration (260).

The primary advantage of extraneural electrodes lies in their minimal invasiveness, which allows neural signal acquisition without penetrating the nerve or causing long-term damage (275). However, due to the spatial separation between the recording contacts and the nerve fibers, the recorded signal reflects the summed activity of multiple fibers across the entire nerve cross-section. Consequently, both the sensitivity and spatial specificity of extraneural recordings are generally limited. This signal, representing the summed electrical response of multiple nerve fibers, is referred to as a CAP.

Hook electrodes represent the most basic form of extraneural interfaces. They are composed of metal wires shaped into hooks, allowing the nerve to be positioned within the curvature of the electrode, as illustrated in *Figures* 6.A-6.B from the Silverman et al. (2018) study (266). Due to the absence of any fixation mechanism securing the electrode to the nerve, this configuration is suitable only for acute experimental settings, where stability over extended periods is not required.

Cuff electrodes, or cuff-like electrodes, address the issue of nerve fixation, thereby enabling their use in chronic experimental setups. Moreover, Cuff electrodes significantly reduce background noise and increase the signal-to-noise (SNR) ratio as compared to hook electrodes (*Figure 6*) (255, 266). A typical cuff electrode consists of a silicone cuff incorporating two or three platinum contacts, which are embedded within the inner surface of the cuff. Once positioned around the nerve, the electrode ensures stable contact with the epineurial surface, providing a direct interface for both electrical stimulation and signal recording. Additionally, the electrically insulating properties of the

surrounding material enhance sensitivity and improve the SNR by minimizing interference from surrounding tissues.

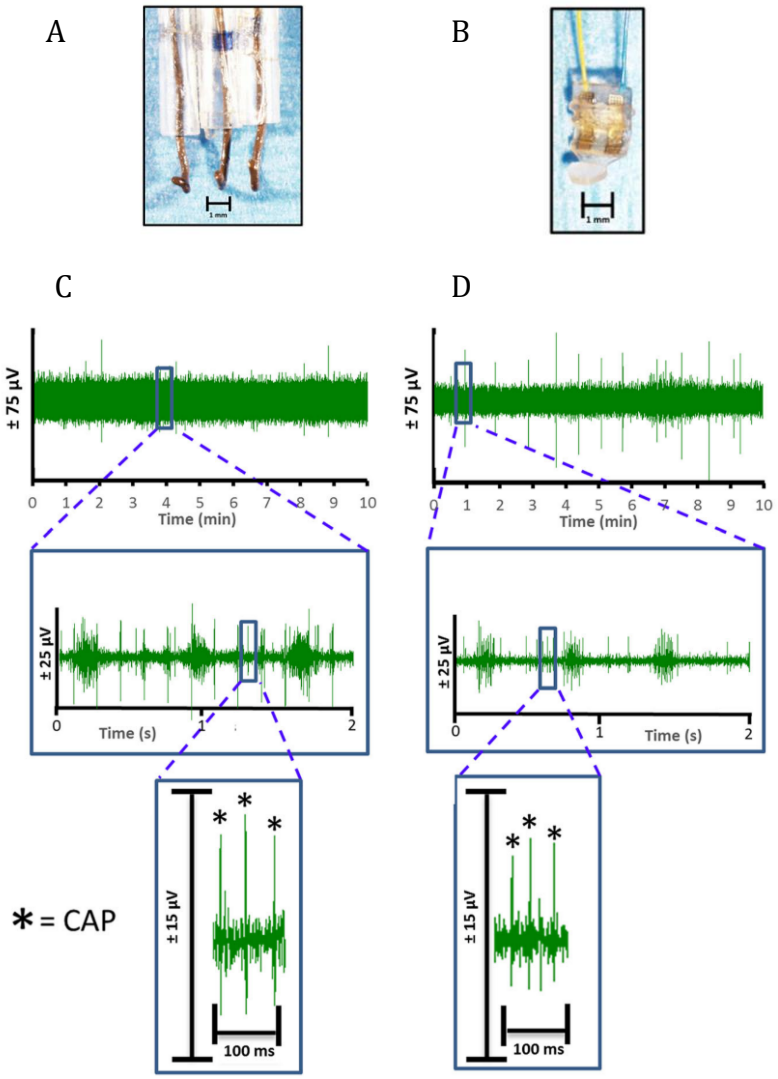

Figure 6. Electrophysiological recording setup and comparison of vagus nerve signals, adapted from Silverman et al. (2018). (A) Lab-made hook electrode with three leads used to record cervical vagus nerve activity. (B) Commercial cuff electrode (Cortec) used for similar recordings. (C) Representative neurograms recorded using the hook electrode over a 10-minute baseline period in Balb/c mice (n = 72), shown at full scale and magnified in 2-second and 100 ms windows. (D) Representative neurograms recorded using the cuff electrode under the same conditions (n = 25), shown at the same magnifications for comparison (266). Figure extracted from: Silverman, H. A., et al. (2018). "Standardization of methods to record Vagus nerve activity in mice".

Cuff electrodes have demonstrated long-term biocompatibility and have been used safely for extended periods, typically for stimulation purposes (276). Notably, they are widely employed in clinical applications, such as VNS, where they provide a stable and well-tolerated platform for therapeutic neuromodulation.

4.1.2. Intraneural electrodes

Intraneural electrodes penetrate the nerve tissue, allowing the recording contacts to be positioned near individual nerve fibers. Depending on the configuration of the electrode and the precision of its implantation, this approach enables the recording of SUA, corresponding to the action potentials of individual neurons. Recent studies have demonstrated the feasibility of such recordings from the human vagus nerve using intraneural microelectrodes. Multiple types of these electrodes have been developed for such applications. Tungsten or stainless-steel microelectrodes, for example, are commonly used in acute experimental paradigms due to their ease of insertion and high spatial resolution. These electrodes can be inserted percutaneously and guided to the nerve using imaging modalities such as ultrasonography, as demonstrated by Ottaviani et al. (2020) (249) and Patros et al. (2024) (250). When optimally positioned and oriented, these electrodes may permit the recording of SUA. This was illustrated in Ottoviani's (2020) study, where a dorsolateral approach allowed for the manual advancement of a microelectrode to the human cervical vagus nerve while avoiding vascular structures. Depending on the electrode's position within the nerve, multiple axonal firing patterns were recorded. Some of these displayed rhythmic modulations tightly coupled to physiological signals such as cardiac intervals and blood pressure fluctuations, while others showed no clear correlation with systemic activity. In the recording illustrated in *Figure 7*, the recording showed a tonically firing axon whose discharge covaried with the cardiac interval and blood pressure fluctuations. The presence of consistent spike morphology and clear superposition of action potentials confirmed single-unit resolution (*Figure 7*). However, their mechanical rigidity and invasiveness limit their suitability for chronic implantation.

Recently, a novel class of intraneural electrodes based on carbon nanotube (CNT) yarns has shown promise for chronic SUA recordings (244). First introduced by McCallum et al. (2017), CNT electrodes exhibit excellent flexibility, mechanical compliance, and axon-like dimensions, making them well suited for implantation within nerve fascicles (244).

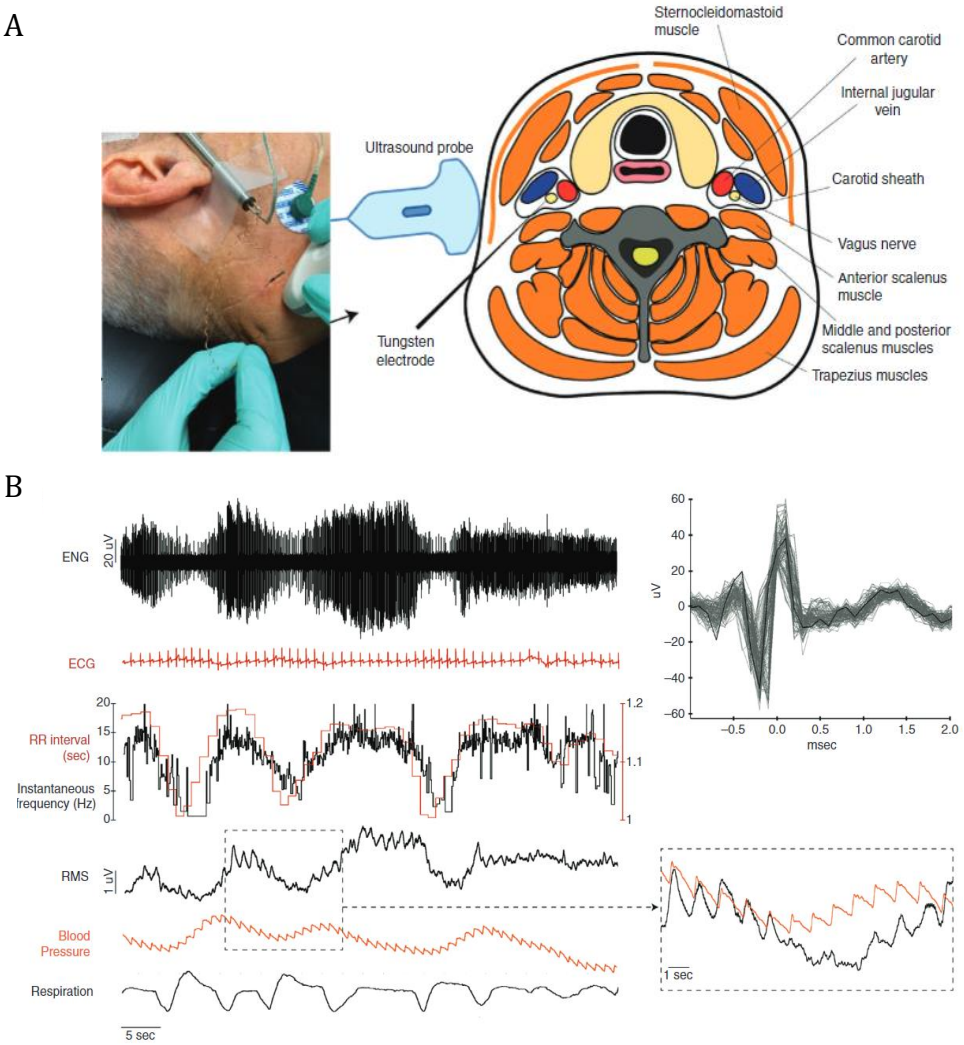

Figure 7 illustrates the experimental approach used to penetrate the human cervical vagus nerve, along with representative microelectrode recordings obtained from one participant. (A) Schematic representation of cervical anatomy and the dorsolateral trajectory of the manually advanced microelectrode toward the right vagus nerve, carefully avoiding the carotid artery and jugular vein. (B) A tonically firing axon displayed covariation with the cardiac interval. The RMS of the neurogram showed modulation corresponding to blood pressure fluctuations. Variations in spike amplitude were attributed to minor microelectrode displacements caused by neck movement. Superimposed spikes in the right panel confirm that this was a single-unit recording. Figure extracted from: Ottaviani, M. M., et al. (2020). "In vivo recordings from the human vagus nerve using ultrasound-guided microneurography (249).

In this study, CNT electrodes were chronically implanted in two autonomic nerves in rats (*Figure 8*), the glossopharyngeal and vagus nerves, with recordings obtained under anesthesia for up to 16 weeks (244). The electrodes maintained low impedance and high signal-to-noise ratios (SNR > 10 dB) throughout the experimental period, confirming the long-term stability of the interface. Furthermore, distinct unit activities were successfully isolated from the recordings and classified into functionally distinct groups using offline clustering and classification algorithms (*Figure 8*) (244). CNT yarn electrodes have since been employed in several studies to investigate physiological modulations of vagus nerve activity (VNA), including components related to respiration, BP regulation, as well as responses to hypoxia and feeding behavior, further confirming the reliability of this method (244-247, 277). Notably, this type of electrode has also been tested in freely moving rats, demonstrating promising recording capabilities while maintaining a low SNR (247). This advancement facilitates longitudinal investigations of vagal nerve activity, enabling the detection and decoding of spontaneous neuronal spiking patterns in relation to diet changes, therapeutic interventions, and behavioral changes, research avenues that have previously been inaccessible.

4.2. Signals

4.2.1. The Vagus Nerve Electroneurogram (VENG) signal

Several studies have characterized the VENG in various animal models using different electrode types and configurations, thereby further confirming the authenticity and reliability of the recorded neural activity. Some of these studies are listed in *Table 8*: Methodological aspects. Silverman et al. (2018) were among the first to compare hook and cuff electrodes in mice (266). Hook electrodes were custom-made tripolar silver wires, while the cuff electrode was a commercially available bipolar sling electrode from CorTec. Signal characterization focused on spike components and firing rates. Recordings with hook electrodes showed an average spike rate of 4.2 ± 0.4 spikes/s, compared to 5.3 ± 0.8 spikes/s with cuff electrodes over 10-minute periods (266).

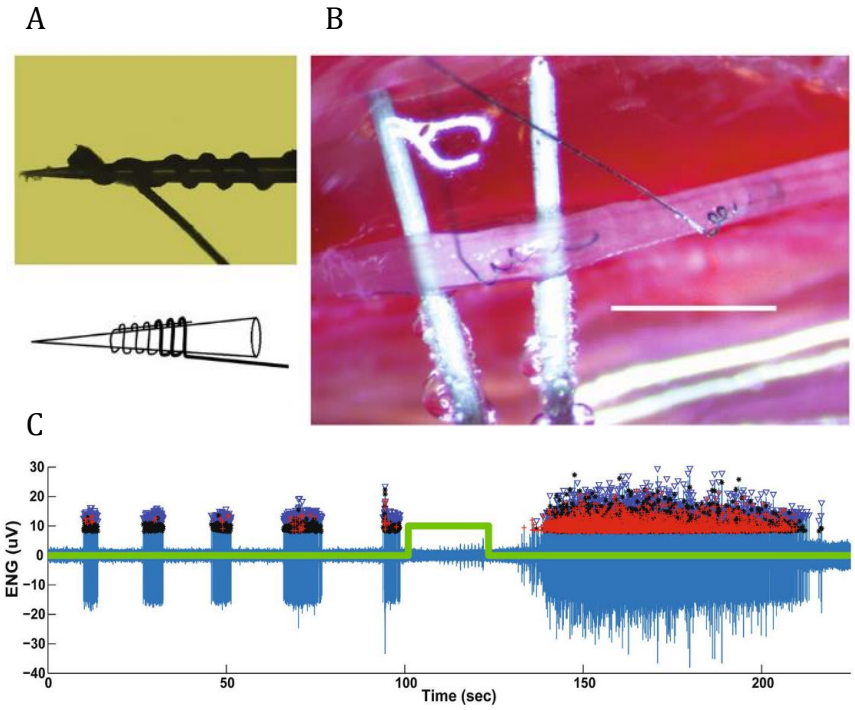

Figure 8 illustrates (A) CNT yarns wrapped around the tip of a tungsten microneedle used for implantation into the nerve. (B) Two CNT yarns were implanted in the rat vagus nerve, spaced approximately 2 mm apart, enabling differential recording of neural activity (scale bar = 2 mm). (C) Processed spontaneous neural activity recorded from the vagus nerve 16 weeks post-implantation (blue trace). The green trace shows the trigger signal marking a hypoxia event administered to the anesthetized rat. Markers indicate identified neural spikes and cluster groupings used for activity classification. Figure extracted from: McCallum GA, Sui X, Qiu C, Marmerstein J, Zheng Y, Eggers TE, et al. Chronic interfacing with the autonomic nervous system using carbon nanotube (CNT) yarn electrodes (244).

To assess the physiological modulation of VNA, the effect of food intake was examined. Mice that had been fed exhibited a notably higher spike rate compared to fasted mice, with a marked increase in the total number of spikes observed in the fed group (266). This significant difference highlights the sensitivity of VNA to changes in physiological states, further supporting the interpretation that the VENG reflects genuine neural activity associated with autonomic processes.

Stumpp et al. (2020) extended this approach, using a true tripolar configuration for both hook and micro-cuff electrodes to enhance VENG signal quality (255). Importantly, they identified two distinct burst types in the VENG: (1) high-amplitude bursts synchronized with the negative peaks of the respiratory

signal, and (2) lower-amplitude bursts at frequencies corresponding to the HR. While respiration-related bursts were observed with both electrode types, heart-rate-related bursts were only detected using cuff electrodes, suggesting these electrodes provide clearer and more reliable detection of cardiac signals (255). These temporally structured patterns indicate that the VENG captures physiologically relevant rhythmic activity linked to cardiorespiratory dynamics. These findings align with the earlier work of Harreby et al. (2011), who performed a power spectral density analysis of VENG recorded with bipolar stainless-steel hook electrodes (269, 278). Their analysis revealed that energy levels in the VENG peak between 1 and 5 Hz, and that VENG activity fluctuates in phase with both the cardiac and respiratory cycles, with respiratory-related fluctuations being the most prominent.

Additionally, topical application of lidocaine to the nerve abolished all recorded spiking activity within 30 seconds, providing further evidence for the neural origin of the signal (*Figure 9*) (255). Cuff electrodes yielded more stable signals with higher root mean square (RMS) amplitudes and significantly fewer artifacts (0.12 ± 0.15%) than hook electrodes (30.06 ± 13.98%), confirming their suitability for reliable and repeatable recordings (255).

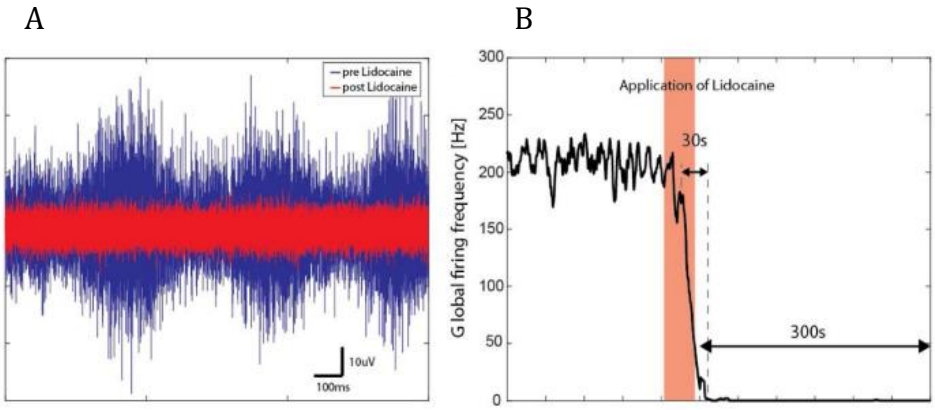

Figure 9 illustrates an experiment from the study by Lars Stumpp (2020), demonstrating the silencing effect of lidocaine on vagus nerve activity. (A) Segment of a 2.5-second recording of vagus electroneurogram (VENG) activity under baseline conditions (blue trace) compared to after topical application of lidocaine to the nerve (red trace). Burst activity associated with respiration and heartbeat is completely abolished following lidocaine administration. (B) Timeline of global vagus nerve firing frequency, derived from the timestamps of all detected spikes. The red box marks the period during which lidocaine was applied to the nerve, indicating a marked suppression of neural activity. Figure extracted from Stumpp, L., et al. (2020). Recording of spontaneous vagus nerve activity during Pentylenetetrazol-induced seizures in rats (255).

To further validate the physiological relevance of the method, seizures were pharmacologically induced under anesthesia using PTZ, while VENG, ECG, and video recordings were simultaneously acquired. The VENG signal exhibited abrupt changes in firing frequency that coincided with alterations in respiratory and cardiac rhythms, as well as with behavioral events captured on video (255). These results highlight the ability of the VENG to dynamically track autonomic and functional state changes in vivo, reinforcing its value as a reliable tool for peripheral neural monitoring.

From this global VENG signal, distinct components such as the cardiac-related VENG (crVENG) (251-253, 269) or respiratory-related activity (254, 258) can potentially be extracted. It is essential to distinguish between the firing rate and the study of spike profiles when considering CAPs and SUA, as the recording method and experimental setup determine whether CAPs or SUA are recorded, each with its unique characteristic waveform and features.

4.2.2. crVENG

The coherent averaging/crVENG profile has been used as a metric for seizure detection in papers by Harreby, Nielsen, or Sevcencu (251, 253, 269). To create a CrVENG, the VENG signals were recorded in relation to the R-peak of the heartbeat. This was done by extracting segments of the VENG signal, or "sweeps," triggered by the R-peak. Each sweep of the VENG signal lasted from 70ms before the R-peak to 150 ms after the R-peak, totaling 220 ms (269). The strength of the VENG signal (its energy or power) was calculated in small time intervals, each lasting 10 ms (there were 22 intervals in each sweep). All the VENG sweeps recorded within a 20-second period were averaged together to produce the CrVENG profile (269).

In the study by Harreby et al. (2011), the authors found that the VENG profile derived from the left vagus nerve typically displayed a prominent peak around the R-peak of the ECG, followed by a smaller peak approximately 50 ms later. A sharp drop was observed between these peaks, with a low and steady plateau around 100 ms after the R-peak (269). In contrast, the VENG profile from the right vagus nerve also showed a peak around the R-peak. However, the pattern was less distinct and more variable across animals, indicating greater inconsistency in its morphology (269). These results suggest that the crVENG profile is more consistent and pronounced in the left vagus nerve compared to the right. This observation aligns with the findings of Einthoven et al., who noted that the left vagus nerve in dogs exhibited more prominent oscillations tied to the cardiac cycle than the right vagus nerve.

4.2.3. Respiratory-related profile

The respiratory component of the VENG signal, as previously discussed, is clearly evident and prominent under anesthesia. Sevcencu et al. (2018) extracted a respiratory-related profile from the VENG recorded in pigs using a tripolar cuff electrode (254). To isolate this component, the recorded data were first filtered to retain frequencies between 800 Hz and 10 kHz. The signals were then squared to calculate the power of the VENG activity and further subjected to low-pass filtering (below 2 Hz) to isolate frequencies associated with respiration. Additionally, the respiratory cycle signal itself was filtered to remove high-frequency noise (below 35 Hz) (254). An automatic peak detection algorithm was used to identify inspiration peaks in the respiratory cycle, which were then visually confirmed. Segments of the signal surrounding each inspiration peak were extracted and averaged to generate stable respiratory profiles (254). This approach enabled the characterization of respiratory-related fluctuations within the broader VENG signal, capturing variations linked explicitly to the respiratory cycle. Notably, the relationship between the amplitude of the respiratory-related profile and lung inflation was quantified, revealing a strong linear correlation in all nine pigs. As lung inflation increased, the amplitude of the respiratory-related profile also increased predictably, with R^2 values ranging from 0.85 to 0.99, demonstrating the method's sensitivity to changes in respiratory volume (254).

4.2.4. CAP

Extraneural electrodes, due to their broader surface contact with the nerve and relative distance from individual axons, primarily record the summed electrical activity of multiple nerve fibers. These fibers can be either afferent or efferent, and may be myelinated or unmyelinated, contributing variably to the overall signal. As a result, the recorded signal represents a composite of this heterogeneous activity. When action potentials from different fibers are not synchronized or propagate in opposing directions, the resulting CAPs may appear attenuated or less distinct. Additionally, the configuration and spatial orientation of the electrode in relation to the nerve critically influence the morphology and detectability of these recorded waveforms.

The impact of electrode contact spacing on VENG signal quality was systematically investigated by Stumpp et al. (2020) (255). Using hook electrodes with 1 mm or 2 mm inter-contact spacing, and cuff electrodes with 2 mm or 4 mm spacing, they demonstrated that increasing the anode-cathode (AC) distance improved signal detectability. Specifically, a 1 mm AC distance in hook electrodes often resulted in VENG signals where burst modulations were

obscured by background noise and barely discernible (255). In contrast, increasing the AC distance to 2 mm or greater significantly enhanced burst visibility within the signal. Quantitative analysis showed that the RMS amplitude of the signal increased proportionally with contact spacing, with each doubling of the AC distance resulting in an approximate fourfold increase in RMS amplitude (255). This finding highlights the significance of electrode design parameters in achieving optimal signal quality for reliable neural recordings.

The inter-contact distance also plays a critical role in shaping the morphology of the recorded signal. CAPs can exhibit either biphasic or triphasic waveforms, with their temporal width being influenced by the spacing between recording contacts. In the study by Stumpp et al. (2021), the majority of CAPs displayed a triphasic morphology, with most having a duration of less than 1.5 milliseconds (257).

4.2.5. SUA

Intraneural electrodes with small contact areas inserted directly into the nerve can enable the recording of SUA, attributed to the firing of individual nerve fibers. Compared to extraneural electrodes, fewer fibers contribute to the recorded signal, resulting in minimal overlap and improved resolution of discrete neural events. Jiman et al. (2020) described a monopolar recording configuration in which a single electrode was in contact with the vagus nerve, while a ground wire was implanted subcutaneously in the cervical region and a reference electrode was placed in the surrounding tissue or fluid (277). In this setup, the spike shape is less influenced by electrode geometry, unlike in CAP recordings. As a result, SUA waveforms typically appeared biphasic with durations of approximately 1.5 ms. The signal amplitude varied considerably depending on the relative position of the electrode to the active axon, with reported peak-to-peak amplitudes ranging from 23 to 92 μV in the rat vagus nerve, using carbon fiber microneedle arrays (277).

In contrast, McCallum et al. utilized a bipolar configuration with two CNT yarn electrodes inserted into the nerve with an inter-electrode spacing of 2 mm for differential acquisition. In this configuration, the spike waveforms exhibited a triphasic shape, with a duration of approximately 2 ms and amplitudes ranging from 30 to 60 μV peak-to-peak, as estimated from published recordings (244).

A similar bipolar configuration was employed by Marmerstein et al. (2021), who recorded VNA in both anesthetized and awake animals for up to 11 weeks (245). They observed robust neural activity in both states, with an increased

incidence of large action potentials during wakefulness. The recordings included individual spikes and short bursts, often exceeding 100 μV in peak-to-peak amplitude (245).

4.3. Modulation of VNA during epileptic seizures

Several studies have examined how acute, chemically induced seizures modulate VNA, as reflected in VENG recordings. Harreby et al. (2011) were the first to specifically investigate alterations in the crVENG during seizures, using a bipolar hook electrode configuration in a rat model (269).

To quantify such changes, the authors introduced a metric based on energy variations within the crVENG waveform (269). Specifically, two intra-profile time windows (I1 and I2) were defined within each crVENG cycle. These intervals could be positioned anywhere within the temporal bounds of the crVENG waveform and varied in duration (in 10-ms steps). The Intrabeat Energy Difference (IBED) was then calculated as the difference in average signal energy between these two intervals:

IBED = crVENG(I2) – crVENG(I1).

To enable cross-subject comparisons, the IBED was standardized for each animal by subtracting the individual baseline mean (IBED_baseline) and dividing by the corresponding standard deviation (SD), yielding a standardized IBED (sIBED) (269). Using this approach, and based on optimization analyses of the left VENG signal, early seizure detection was consistently achieved in all PTZ-treated rats (269). Importantly, alterations in the crVENG signal were accompanied by bradycardia and respiratory disturbances, indicative of seizure-related autonomic dysregulation (269). This method effectively captured subtle pre-ictal changes in vagal nerve activity, underscoring the potential of crVENG as a physiological biomarker for seizure prediction.

These findings were further supported in a subsequent study by Nielsen et al. (2013), which applied the same methodology to a porcine model (251). In all three pigs tested, early seizure prediction was successfully achieved prior to the onset of tonic-clonic manifestations. Subsequently, the crVENG was also found to be associated with fluctuations in BP, suggesting that this metric may reflect not only direct cardiac modulation but also indirect neural effects (251). In a study by Sevcencu et al. (2016), bilateral cervical VNA was recorded in anesthetized pigs using cuff electrodes while seizures were chemically induced with PTZ (253). A significant pre-ictal increase in vagal activity was observed, followed by suppression during the tonic-clonic phase and a marked rebound

postictally (253). These changes were accompanied by preserved afferent input and suppressed efferent output, suggesting a disruption of baroreflex function during seizures and potential involvement in postictal cardiac depression (253).

All of these studies were conducted using the PTZ model of epilepsy. However, alternative models exist that more closely replicate the focal onset and regional specificity of human epileptic seizures.

Sakamoto et al. (2008) were the first to systematically investigate the autonomic effects of seizures by administering high doses of kainic acid (10–12 mg/kg, intra-arterially) in urethane-anesthetized rats, with simultaneous recordings from the vagus nerve, cervical sympathetic ganglion, and renal nerve (120). In 44 animals, KA-induced seizures presented as an initial phase of high-frequency EEG activity that evolved into slower, high-amplitude discharges, followed by low-voltage EEG, cycling continuously, and culminating in a convulsion-free status epilepticus. A pronounced increase in VNA was observed during seizures. To evaluate baroreflex integrity, phenylephrine (PE; vasoconstrictor) and nitroprusside (NP; vasodilator) were administered prior to seizure induction to characterize baseline autonomic responses. Under baseline conditions, PE increased mean arterial pressure (MAP) and significantly elevated VNA. However, during seizures, PE induced only minimal additional changes in VNA, suggesting vagal output was already saturated. Similarly, NP caused a modest, non-significant reduction in VNA during seizures (120). These findings suggest that seizure-induced vagal activation approaches a physiological ceiling, rendering baroreflex-mediated modulation largely ineffective during ictal periods.

Another particularly valuable contribution in this regard is the study by Naggar et al. (2022), which investigated seizure dynamics in a KA-induced epilepsy model under urethane anesthesia (241). The authors simultaneously recorded VNA, cervical sympathetic nerve or ganglionic activity, EEG, ECG, and arterial BP in 16 rats. Seizures were induced by systemic administration of KA. Neural activity was captured using invasive linear array electrodes, consisting of four platinum/iridium wires embedded in a small epoxy trough, enabling simultaneous assessment of both branches of the ANS. This configuration allowed for a detailed evaluation of sympathetic–parasympathetic balance, a critical factor in the context of SUDEP (241).

Seizures were categorized into four types based on associated HR dynamics and EEG characteristics: (1) bradycardia-associated seizures, (2) tachycardia-

associated seizures, (3) self-terminating seizures, which ceased due to cerebral hypoperfusion (evidenced by prolonged bradyarrhythmia and EEG suppression), and (4) seizures that progressed to death (241). Interestingly, in the most severe outcomes, self-terminating seizures and seizure-related death, autonomic activity increased during the ictal period until a critical threshold was reached, resulting in abrupt HR reduction (>50%). This was followed by a sharp decline in both seizure and autonomic activity (241).

The findings revealed that persistent parasympathetic activation during seizures was associated with fatal outcomes, while sustained sympathetic tone during the postictal period appeared to be protective, particularly in self-terminating seizures, highlighting the complex interplay between sympathetic and parasympathetic systems in determining seizure outcomes and reinforce the relevance of autonomic monitoring in SUDEP research (241).

CHAPTER 2 : Fundamental hypothesis and objectives

The primary objective of this thesis is to investigate the dynamics of VNA during epileptic seizures, with the aim of identifying physiologically relevant biomarkers to support the development of closed-loop VNS systems. As outlined above, epileptic seizures are frequently accompanied by autonomic manifestations, involving both sympathetic and parasympathetic components (34). The vagus nerve, as a major pathway mediating bidirectional communication between the brain and peripheral organs, plays a central role in autonomic regulation. Characterizing how VNA is modulated across different seizure states may offer novel insights into seizure-related autonomic dysfunction and improve physiological seizure detection strategies.

This thesis is organized into two complementary parts: the first focuses on acute experiments performed under anesthesia using an induced seizure model, while the second addresses the translation of these findings to chronic recordings in awake, freely moving rats exhibiting spontaneous epileptic seizures.

Question 1: Is VNA modulated during KA-induced seizures under anesthesia, and can specific signal features be extracted to enable reliable seizure detection?

Several studies have demonstrated that PTZ-induced seizures under anesthesia are associated with modulation of VNA, from which relevant features for seizure detection can be extracted (251, 257, 269). However, these findings are based exclusively on the PTZ model, which involves systemic administration of PTZ via the lateral tail vein, widespread, non-specific neuronal hyperexcitability throughout the brain. Mechanistically, PTZ acts as a non-competitive GABA_A receptor antagonist, reducing GABAergic inhibition and promoting generalized neural excitation (279). Because of its systemic action and limited spatial specificity, the PTZ model provides little control over the initial site of seizure onset, making it challenging to attribute VNA changes to specific brain regions.

Experimental evidence suggests that PTZ-induced hyperexcitability often originates within the brainstem's reticular formation before propagating to cortical areas via the anterior thalamic nuclei (280-283). Given the brainstem's integral role in autonomic regulation, such activation may directly influence

vagal output via brainstem nuclei. While helpful in studying generalized seizure mechanisms and autonomic involvement, the PTZ model is less representative of focal epilepsy, where seizures originate in discrete brain regions and may or may not secondarily generalize.

To address this limitation, we aimed to evaluate VNA modulation in a more spatially controlled model of focal epilepsy using direct intra-hippocampal injection of KA, a clinically relevant seizure focus in human TLE. Under anesthesia, KA-induced seizures typically present as non-convulsive events with minimal or absent motor manifestations, thereby reducing the risk of motion-related artifacts in the recorded signal.

Hypothesis 1: Focal hippocampal KA injection under anesthesia induces non-convulsive seizure activity, which may propagate to CAN structures, resulting in measurable modulation of VNA.

The hippocampus, while traditionally linked to cognitive functions, has established anatomical connections to components of the CAN, including the hypothalamus and amygdala. Through these connections, seizure activity arising in the hippocampus has the potential to influence downstream brainstem autonomic centers that regulate vagal output, either through direct engagement of parasympathetic efferents or via afferent relay of broader autonomic (including sympathetic) changes (92).

Previous work has shown that systemic KA administration under anesthesia can reliably induce seizures (120, 284, 285). While systemic administration remains common, focal intracerebral delivery provides enhanced experimental control, allowing for precise localization of seizure initiation.

We hypothesize that hippocampal seizures induced by focal KA injection may lead to detectable changes in VNA, reflecting possible recruitment of central autonomic pathways.

Hypothesis 2: Distinct VNA signal features can be extracted during KA-induced seizures to enable specific seizure detection.

While several VNA-derived features (crVENG, spike detection) have demonstrated excellent performance in detecting PTZ-induced seizures, with some reports showing 100% specificity and sensitivity (257, 269), these findings stem from a generalized seizure model in which early brainstem activation may drive strong and consistent autonomic responses. Such dynamics inherently favor VNA-based detection, including early detection, as

the brainstem harbors key vagal regulatory nuclei and may modulate vagal output before cortical seizure manifestations become evident.

By using the focal KA model of hippocampal seizures, this study aims to determine whether VNA contains reliable signal features that can discriminate ictal from non-ictal states under more spatially constrained and clinically relevant conditions. We hypothesize that seizure-related changes in VNA can be reliably identified and used to detect seizure activity.

Question 2: Is it feasible to chronically record VNA in awake, freely moving rats, and how is VNA modulated during spontaneous recurrent seizures in a chronic epilepsy model?

Previous studies have established the feasibility of chronic VNA recordings in awake, non-epileptic rodents. For instance, Falcone et al. (2020) demonstrated stable longitudinal recordings of spontaneous compound action potentials in the mouse vagus nerve using a flexible cuff electrode, with consistent signal-to-noise ratios and electrode impedance over several weeks. Additionally, Miki et al. (2025) achieved simultaneous recordings of cervical VNA and renal sympathetic nerve activity (RSNA) in conscious rats, employing pharmacological blockade to dissect afferent and efferent vagal components, thereby elucidating vagal-sympathetic interactions critical to autonomic homeostasis.

To date, however, chronic VNA recordings in awake epileptic rodents during spontaneous recurrent seizures have not been reported. This gap limits our understanding of the dynamic autonomic changes accompanying focal epilepsy under physiological conditions. Addressing this, the present study aims to evaluate the technical feasibility of chronic cervical VNA recordings in freely moving epileptic rats and to characterize the modulation of vagal activity associated with spontaneous seizures in a clinically relevant chronic epilepsy model.

Hypothesis 3: VNA exhibits state-dependent modulation, with greater activity observed during sleep compared to wakefulness.

Autonomic tone is known to vary across behavioral states, with sleep, particularly NREM stages, being associated with a shift toward parasympathetic dominance. HRV studies consistently show increased vagal drive and respiratory regularity during sleep, in contrast to the more dynamic and reactive autonomic state observed during wakefulness (286, 287).

Given the vagus nerve's role as a primary parasympathetic pathway, we hypothesize that direct neural recordings will reflect this state-dependent modulation, with greater and more sustained VNA observed during sleep relative to wakefulness.

Hypothesis 4: VNA undergoes dynamic modulation during spontaneous focal seizures in the KA model of TLE, reflecting seizure-related autonomic disturbances.

TLE is frequently associated with autonomic dysregulation during both interictal and ictal periods, characterized by reduced heart rate variability, a shift toward sympathetic dominance, and decreased vagal tone. These alterations reflect functional disturbances within the CAN, which includes seizure-relevant regions such as the hippocampus, amygdala, insula, and brainstem nuclei.

While sympathetic activation predominates during seizures, physiological changes like increased heart and respiratory rates are conveyed centrally via vagal afferents, potentially triggering compensatory parasympathetic responses to restore autonomic balance. Acute studies in anesthetized rats have demonstrated that KA-induced seizures, particularly severe or fatal ones, can produce sustained vagal activation during ictal phases.

Based on this, we hypothesize that a subset of focal hippocampal seizures in the KA model secondarily generalize and induce measurable autonomic disturbances, as reflected by modulation of VNA.

CHAPTER 3 : Modulation of VNA in acute KA-induced seizures

1. Preface

The following section is based on the manuscript published in Frontiers of Neurosciences under the title: "Vagus Nerve Electroneurogram (VENG)-Based Detection of Acute Kainic Acid Induced Seizures".

2. Vagus Nerve Electroneurogram (VENG)-Based detection of acute kainic acid-induced seizures

2.1. Abstract

Seizures produce autonomic symptoms, mainly sympathetic but also parasympathetic in origin. Within this context, the vagus nerve is a key player as it carries information from the different organs to the brain and vice versa. Hence, exploiting vagal neural traffic for seizure detection might be a promising tool to improve the efficacy of closed-loop VNS. This study developed a VENG detection algorithm that effectively detects seizures by emphasizing the loss of spontaneous rhythmicity associated with respiration in acute intrahippocampal KA rat model. Among 20 induced seizures in six anesthetized rats, 13 were detected (sensitivity: 65%, accuracy: 92.86%), with a mean VENG-detection delay of 25.3 ± 13.5 seconds after EEG-based seizure onset. Despite variations in detection parameters, 7 out of 20 seizures exhibited no ictal VENG modifications and remained undetected. Statistical analysis highlighted a significant difference in Delta, Theta, and Beta band evolution between detected and undetected seizures, in addition to variations in the magnitude of HR changes. Binomial logistic regression analysis confirmed that an increase in delta and theta band activity was associated with a decreased likelihood of seizure detection. These results suggest the possibility of distinct seizure spreading patterns between the two groups, which may result in differential activation of the autonomic central network. Despite notable progress, limitations, particularly the absence of respiration recording, underscore areas for future exploration and refinement in closed-loop stimulation strategies for epilepsy management. This study constitutes the initial phase of a longitudinal investigation, which will subsequently involve reproducing these experiments in awake conditions with spontaneous recurrent seizures.

2.2. Introduction

Since its recognition as a viable therapy in 1988, VNS has been employed to treat drug-resistant epilepsy, with over 125,000 patients implanted worldwide (19). Distinguished by its minimal invasiveness, VNS has demonstrated significant efficiency, with 45-60% of patients experiencing over 50% reduction in seizure frequency after a minimum treatment duration of six months (20).

Initially, VNS utilized an open-loop system delivering electrical pulses based on a predetermined ON-OFF cycle. Featured in the device, magnets enable patients or caregivers to administer supplementary therapy manually. When magnet-activated stimulation was concurrently applied with VNS therapy, it demonstrated further clinical advantages, such as decreased seizure severity and an ability to terminate seizures (288, 289), highlighting the therapeutic value of stimulating the vagus nerve proximal to seizure onset.

The introduction of the AspireSR VNS device in 2014 marked a significant advancement by employing a closed-loop system that delivers stimulation in response to ictal tachycardia, as 82% of seizures are characterized by HR increases during the pre-ictal or ictal phases according to literature (34, 82). Challenges persist, despite the proven clinical benefits of a closed-loop system compared to traditional open-loop stimulation (21, 290, 291). Multicentric clinical studies referred to in the literature as “E-36” (29) and “E-37” (30) highlighted a specificity concern, with only about 50% of seizures showing a significant ictal tachycardia (>20% HR increase), indicating significant variability in ictal HR changes among patients. Also, there is a concern about nonseizure-related detections ranging from 0.4 to 1.6 detections per hour at the maximum threshold of 70% and up to 6.6 and 6.9 for the minimum threshold of 20% (29) and 30% (30), indicating a moderate specificity (31). Hence, there is a need to increase the specificity of seizure detection strategies.

EEG remains the gold standard for seizure detection in a clinical setting. It is utilized in RNS therapy, which boasts a remarkable efficacy with a 75% median reduction in seizure frequency at nine years (18). However, the high invasiveness of this therapy and its limited approval worldwide underscore the necessity for alternative, less invasive detection methods. Given the extensive autonomic dysfunctions induced by seizures, including changes in cardiac and respiratory patterns (34, 86, 292), exploring biomarkers that integrate multi-organ information represents a promising innovative approach to seizure detection.

As the vagus nerve is accessed during electrode implantation for VNS and is the primary parasympathetic relay of the nervous system, recording the nerve using the same implanted electrode could contribute to the development of a novel method for seizure detection. In a study of systemic KA injection in urethane anesthetized rats, the vagus nerve and the cervical sympathetic ganglion were recorded with invasive linear array electrodes to determine seizure-related modifications in the ANS (241). They found that in the severe outcomes (self-terminating seizures with severe bradyarrhythmia and seizure-related death), ANS activity increased during seizures until it caused a drastic HR reduction (>50%), in which case seizure and ANS activity decreased dramatically (241). Specifically, parasympathetic nerve activity was maintained during seizures, resulting in death, and the persistence of sympathetic tone was important for survival during the late vulnerable period in self-terminating seizures (241, 293). Hence, patterns of VNA could give indications of seizure characteristics and therefore be proposed as a biomarker for seizure detection. Indeed, prior studies have successfully extracted a cardiac-related profile from the VENG as a biomarker to detect PTZ-induced seizures in rats (269). However, none of these studies recorded the vagus nerve with non-invasive electrodes, with the final goal of extracting an ictal VENG pattern for seizure detection. Also, in addition to HR changes, seizures are also characterized by respiratory dysrhythmias and, in severe cases, hypopneas and apneas (44, 66, 118, 294-296). In a study investigating VNS as a potential treatment for refractory hypertension, respiratory components were successfully extracted from the VENG, as a potential biomarker to differentiate between exercise-induced increase in BP and pathological hypertension (254). Therefore, respiratory-based VENG activity is measurable and can be proposed as a novel way of detecting seizures.

Our previous work introduced non-invasive monitoring of the vagus nerve to detect systemic PTZ-induced generalized seizures in rats, using a microcuff electrode around the left cervical portion of the vagus nerve. This VENG-based detection showed independence from movement artifacts and outperformed heart-rate-based seizure detection algorithms (255, 257). Nonetheless, PTZ's limitations, including its tendency to induce hyperexcitability and interictal spikes shortly after administration, prompted our focus on acute intrahippocampal KA-induced seizures. This model mimics human TLE characteristics, including associated autonomic dysfunctions like respiratory abnormalities, apnea, and BP and HR changes, thus reinforcing the relevance of this model for advancing seizure detection research (140, 292).

This investigation aims to refine our seizure detection algorithm by exploring respiratory-derived ictal VENG modifications in an anesthetized acute intrahippocampal KA model using implantable cuff electrodes. This study will be extended to awake conditions to confirm the detection feasibility for potential future closed-loop stimulation strategies.

2.3. Methods

2.3.1. Animals

Six male Wistar rats (Local breeding facility, UCLouvain, Belgium), with an average weight of 296,8 ± 50,2g, were housed in a 12h day/night cycle in a temperature- and humidity-controlled environment with 'ad libitum' access to food and water. The protocol has been approved by the Animal Experimental Ethical Committee of UCLouvain University and the Brussels environment committee under the reference 2022/UCL/MD/066.

2.3.2. Surgical procedure

Initially, all animals were anesthetized using a combination of ketamine (100 mg/kg) and xylazine (7 mg/kg) administered intraperitoneally. To maintain anesthesia, half the initial dose was administered as soon as a withdrawal reflex was observed. On average, each animal received two maintenance injections, totaling 200 mg/kg of ketamine and 14 mg/kg of xylazine.

A rectal probe was inserted to monitor and control body temperature, and a heating pad was used to maintain a constant temperature of 37.5°C. The animals were then securely positioned in a stereotaxic frame (David Kopf Instruments, Tujunga, USA) for the implantation procedure. Custom-made epidural electrodes, consisting of a 4.8 mm stainless-steel screw (Bilaney, Germany), were implanted at specific coordinates relative to the Bregma: for the frontal electrode (+) [anteroposterior (AP) +2mm, mesolateral (ML) ±3mm], reference electrode (Ref) [AP +6mm, ML ±0mm], and ground electrode (GND) [AP −5mm, ML +3mm] in the parietal region (297). The differential EEG recording was obtained between the frontal (+) and parietal (Ref) electrodes.

An additional procedure involved drilling a hole into the skull above the right hippocampus for KA injection with the coordinates [Right Hippocampus (RH) AP −5.6mm, ML −4.5mm]. Following this, the left vagus nerve was exposed at its cervical portion, and a tripolar micro-cuff electrode (Microprobes, Gaithersburg, USA) was carefully implanted around the nerve for vagus nerve recording. To ensure the electrode remained in place, the sternomastoid and sternohyoid muscles were sutured over it. The implanted cuff electrodes have specific dimensions: 300 μm inner diameter, 100 μm contact width, and 4mm

contact spacing. The recording setup was designed to reject common noise, with signal amplitudes from two channels being differentially analyzed. In cases of signal amplitude disparity between the two channels, the channel with the amplitude closest to the mean was retained. Electrode impedance was measured before the surgery, with acceptable levels defined as lower than 30 KOhms (kΩ). Several experiments were previously performed to confirm the genuine origin of the VENG recorded signals with tripolar microcuff electrodes (255, 298).

Finally, following Eindhoven's lead II reference, three lab-made tungsten electrocardiogram (ECG) electrodes were implanted subcutaneously to monitor cardiac activity.

2.3.3. Experimental procedure

Post-surgery, each animal was carefully placed within a Faraday cage, with their head fixed in the stereotaxic frame to ensure minimal movement and interference during the recording phase. For the administration of KA, a 25G Hamilton microliter syringe, preloaded with a KA solution (0.4 µg/0.2 µl; Hello Bio, Princeton, USA) as per Bragin et al. (145) was mounted to the stereotaxic frame. This setup allowed for precise delivery of KA into the right hippocampus, targeting the coordinates previously established during the surgical procedure.

The electrophysiological data collection encompassed EEG, ECG, and VENG recordings, providing a comprehensive overview of the induced seizure activity and its effects. Initially, a 20-minute baseline recording was captured to establish the background activity levels for each animal. Following this, the KA solution was injected into the hippocampus at a controlled rate of 0.1µl/min (DV: 4.5mm deep), aiming to induce acute seizure episodes. This injection phase was immediately succeeded by a 20-minute ictal recording session to capture the seizure manifestations. After the ictal recording, the epileptic activity was stopped by a mixture of Diazepam (20mg/kg) and Ketamine (50mg/kg), administered intraperitoneally, as recommended by Martin and Kapur (299) and Vermoesen et al. (300). This led to a final 20-minute post-ictal recording period. The experimental sequence concluded with the euthanasia of the animals through CO2 asphyxiation, ensuring a painless and ethical end to their participation in the study.

2.3.4. Data acquisition and filtering

For data acquisition in this study, a suite of custom-made amplifiers was employed, including two amplifiers for the EEG, one for the ECG, and two for the VENG. Each type of signal was subjected to specific band-pass filtering

(hardware and software) to ensure the integrity and quality of the recorded signals. ECG signals were filtered between 1-70 Hz, EEG signals between 0.5-70 Hz to cover key EEG bands, while VENG filtering was between 300 Hz and 3 kHz is based on nerve fiber conduction velocities to capture relevant physiological signals accurately (264, 301, 302). This filtering process was crucial for isolating the relevant frequency bands and minimizing noise in the recorded data.

Signal digitization was conducted at different sampling frequencies tailored to each signal type to capture the necessary temporal resolution and detail: EEG signals at 250 Hz, ECG at 40 kHz, and VENG at 80 kHz. This approach allowed for comprehensive data analysis, effectively capturing the intricacies of each signal type.

Data acquisition was facilitated by a USB-6212 multifunction I/O device (National Instruments, Austin, USA). The recorded data were then processed and stored using a custom-developed application in Matlab R2022a (MathWorks, Natick, USA). This setup ensured that the data were not only captured with high fidelity but also organized and accessible for subsequent analysis, laying the groundwork for the detailed investigation of the induced seizures and their physiological manifestations. The acute monitoring system and its physiological amplifiers were previously validated (255, 298).

2.3.5. Data analysis

This section details the methodologies for analyzing the various physiological signals recorded during the experiment. The analysis includes determining seizure onset and duration from EEG, EEG band power evolution, ECG-derived HR and respiration activity, and VENG-based seizure detection derived from respiratory pattern changes. Each sub-section provides a step-by-step description of the signal processing and analysis techniques used.

2.3.5.1. EEG seizure onset and duration

Seizure events were identified by periods of low-voltage, high-frequency (>5Hz) rhythmic spiking activity, evolving into high-voltage low-frequency SWDs lasting at least 10 seconds. The end of the seizure was defined as the last spike observed on the EEG (168). The onset and offset of these seizure events determined the total seizure duration.

2.3.5.2. Individual ictal EEG band power evolution calculation

Spectral power was computed through Fourier transform over an 8-second sliding window with 50% overlap. A pre-ictal window, mirroring the ictal

duration, was selected for normalization against the mean spectral power. This normalized spectral power, smoothed with a 5-sample moving average window, was expressed as a percentage change relative to the pre-ictal state.

2.3.5.3. ECG-derived ictal HR changes

Instantaneous HR was determined by measuring the interval between successive R peaks in the QRS complex. This approach allowed for calculating the mean instantaneous HR over 10-second intervals. We compared the HR at seizure onset against the maximum and minimum HR recorded during the seizure to ascertain the extent of HR variation (peak increase/decrease). Additionally, we evaluated the mean HR increase or decrease during the seizure by comparing the average instantaneous HR within the seizure window to the baseline pre-ictal period, which was matched in duration to the ictal window (average HR increase/decrease). This comparative analysis facilitated a detailed understanding of the cardiac responses associated with seizure activity.

2.3.5.4. ECG-derived respiration calculation

Respiration frequency was estimated through the amplitude modulation of R peaks within the ECG's QRS complex, reflecting the mechanical and electrophysiological effects of inspiration and expiration. This method provides an indirect measure of respiratory activity during the experimental protocol [38].

2.3.5.5. VENG-based seizure detection

We aimed to detect acute seizure-related changes by focusing on alterations in respiration-related VENG bursts. The integrity of the VENG signal was assessed by evaluating the synchronization of these bursts with the frequency and phase of ECG-derived respiration (*Figure 10.2-10.3*), as previously implemented by Charlton et al. (303), Patros et al. (304), and Sevcencu et al. (254). First, upper and lower-bound envelopes were computed to determine the peak-to-peak values, thereby measuring the distance between these envelopes. This peak-to-peak amplitude signal was subsequently smoothed with a 100 ms averaging window to minimize noise and stabilize the signal for analysis.

Following smoothing, a Fast Fourier Transform (FFT) was applied to isolate the primary low-frequency components that match the overall main respiratory frequency (Rf) within the VENG envelope signal. Centered on this identified respiratory frequency a narrow band-pass filter as shown in equation 1, was employed to track the amplitude of respiratory components within the surroundings of Rf over time. As respiratory frequency deviates from the

narrow band range, the amplitude of the narrowed bandpass filtered signal decreases.

$$Low\ cutoff\ frequency = \frac{R_f}{2}\ \ and\ High\ cutoff\ frequency = 3R_f \quad (1)$$

Our seizure detection algorithm calculates a ratio using two distinct moving averaging windows: a smaller foreground (Fg) window and a larger background (Bg) window. By methodically sliding these windows across the signal and comparing the ratio to a given threshold equation 2, abrupt respiratory changes can be identified.

$$\frac{F_g}{B_g} < th \quad (2)$$

Normally, the Fg/Bg ratio is expected to hover around 1, indicating stable respiratory amplitude under non-seizure conditions. However, seizures prompt abrupt changes in respiratory frequency, leading to a notable decrease in this ratio. To optimize detection sensitivity, we experimented with various sizes for the Fg (3, 5, and 10 seconds) and Bg (30, 60, and 90 seconds) windows, and the thresholds for this ratio were methodically adjusted between 0.4 to 0.7, in increments of 0.05. This process allowed us to detect abrupt deviations in respiratory frequency, indicative of seizure activity, thus highlighting the intricate relationship between respiratory dynamics and seizure occurrences.

2.3.6. Statistical analysis

The statistical framework of our study was designed to evaluate the efficacy of our seizure detection algorithm. The sensitivity of seizure detection was determined by calculating the ratio of true positive detections to the total number of seizures observed. Additionally, the positive predictive value (PPV), which provides insight into the accuracy of the seizure detections, was derived by dividing the number of true positive detections by the sum of true positive and false positive detections.

To further refine our understanding of the algorithm's performance, Receiver Operating Characteristic (ROC) curves were constructed. These curves plot the sensitivity of the seizure detection against the PPV for various combinations of foreground/background (Fg/Bg) window lengths and detection thresholds. Sensitivity represents the proportion of true positives correctly identified by the algorithm, while PPV indicates the proportion of detected events that are

true positives. The ROC curves are a critical tool for assessing which combination of these parameters yields the most effective detection strategy.

All statistical analyses were performed using GraphPad Prism version 10.1.2 (GraphPad Software, Boston, Massachusetts USA) and JASP 0.18.3.0. Seizures were categorized into two groups: detected seizures (d) and undetected seizures (ud). Normality of data was assessed using the Shapiro-Wilk Test. Parametric and non-parametric unpaired t-tests and Mann-Whitney U tests (MWU) were conducted to compare mean band power evolution between groups, with significance determined at $p < 0.05$. Data were expressed as mean±SD. Logistic regression analyses were performed only for physiological parameters that showed a significant difference in parametric and non-parametric t-tests. Binomial logistic regressions were employed to ascertain whether the likelihood of seizure detection significantly correlates with various predictive variables, including the evolution of individual Delta, Theta and Beta bands, and Maximum HR changes (305). Logistic regression outcomes were reported in terms of log odds ratios (OR), 95% confidence intervals (CI), and p-values, with a p-value of less than 0.05 denoting a statistically significant correlation between the detection outcomes and the predictive variables under investigation. Additionally, regression coefficient, standard error, R2 de McFadden and area under the curve (AUC) were added in the table. Our study implemented uniform subject cohorts, standardized anesthesia protocols, and controlled environmental conditions to mitigate potential confounders in logistic regression analyses.

2.4. Results

2.4.1. Characterization of the induced seizures

In our study, we observed a range of two to five KA-induced seizures per animal (n=6), with a total of 20 recorded seizures (*Table 2*). The average duration of these seizures was 53.1 ± 19.1 seconds. Remarkably, during the entirety of the ictal recordings, no motor manifestations were detected, attributed to the constant state of anesthesia under which the seizures were induced. Notably, two seizures were triggered immediately following the injection of KA. In contrast, the remaining 18 seizures manifested after a mean delay of 8.8 ± 4 minutes post-injection, with seizures occurring at an average interval of 4.8 ± 3.2 minutes.

When examining the EEG band activity for all seizures collectively, we noted a modest elevation in the delta and theta frequency ranges, with delta activity increasing by 43.6 ± 107.5% and theta by 18 ± 103%. However, the most

pronounced changes were observed in the faster EEG frequency bands: alpha band activity surged by 91.7 ± 93.1%, beta by 240.4 ± 235.93%, and gamma by 286.3 ± 318.3%. This differential increase in EEG band activity underscores the varied neurophysiological impact of KA-induced seizures, highlighting significant alterations in brain activity, particularly within the higher frequency bands.

	No. sz (EEG)	Avg. duration (s)	Mean HR changes (%)	Max HR changes (%)	No. detected sz	Mean delay (s)	Sensitivity (%)	PPV (%)
RAT 1	5	52.9 ± 19.3	3.0 ± 1.6	6.8 ± 2.8	5	14.6 ± 4.6	100	100
RAT 2	3	57.13 ± 32.1	−0.7 ± 0.8	−3.1 ± 0.8	3	16.2 ± 2.7	100	100
RAT 3	3	31.2 ± 0.9	−3.5 ± 0.6	−13.6 ± 2.7	3	18.4 ± 3.4	100	100
RAT 4	4	70.7 ± 8.8	−4.5 ± 4.0	−12.0 ± 5.6	2	48.4 ± 18.2	50	100
RAT 5	3	43.4 ± 10.3	−0.2 ± 0.2	−0.6 ± 0.1	0	–	0	0
RAT 6	2	60.9 ± 2.3	−0.9 ± 1.1	−4.9 ± 5.9	0	–	0	0

Table 2: Summarizes seizure characteristics per animal, including the count of seizures (No sz), average duration, mean HR changes throughout the seizure, maximum HR changes during the seizure, the number of seizures detected by the algorithm (using Fg5/Bg90, Threshold: 0.5), the mean delay between EEG seizure onset and VENG seizure detection onset, and specificity/positive predictive value.

2.4.2. HR during acute KA-induced seizures

The primary HR change outcome was ictal bradycardia in five out of six rats (RAT2-6). During the ictal phase, the mean average HR across all seizures in all rats decreased by 2.1 ± 2.3%, and the mean peak had a more pronounced decrease of 7.6 ± 6% compared to pre-ictal phase. These findings are detailed individually for each rat in *Table 2*.

The remaining rat (1/6) demonstrated ictal tachycardia, characterized by a mean average HR increase of 3 ± 1.6% and a mean peak increase of 6.8 ± 2.8% relative to the pre-ictal HR stage.

2.4.3. VENG during acute KA-induced seizures

Characterization of ictal modification of VENG signal revealed that seizures could be categorically divided into two distinct groups. The first group of 13 seizures, with a depicted representation in *Fig. 10.A*, was characterized by a noticeable disruption in the rhythmicity of respiration-related VENG bursts during seizures. The majority of this group (10 out of 13 seizures) exhibited a reduction in the mean amplitude during seizures, averaging 5.04 ± 3.44 μV. Specifically, a subset of these seizures (3 out of 13) was marked by an increase in the mean VENG signal amplitude, averaging 56.23 ± 41.17 μV. The second group, as illustrated in *Figure 10.B*, was distinguished by an absence of

discernible changes in VENG activity in response to the seizures, both in terms of amplitude and rhythmicity related to respiration in the signal.

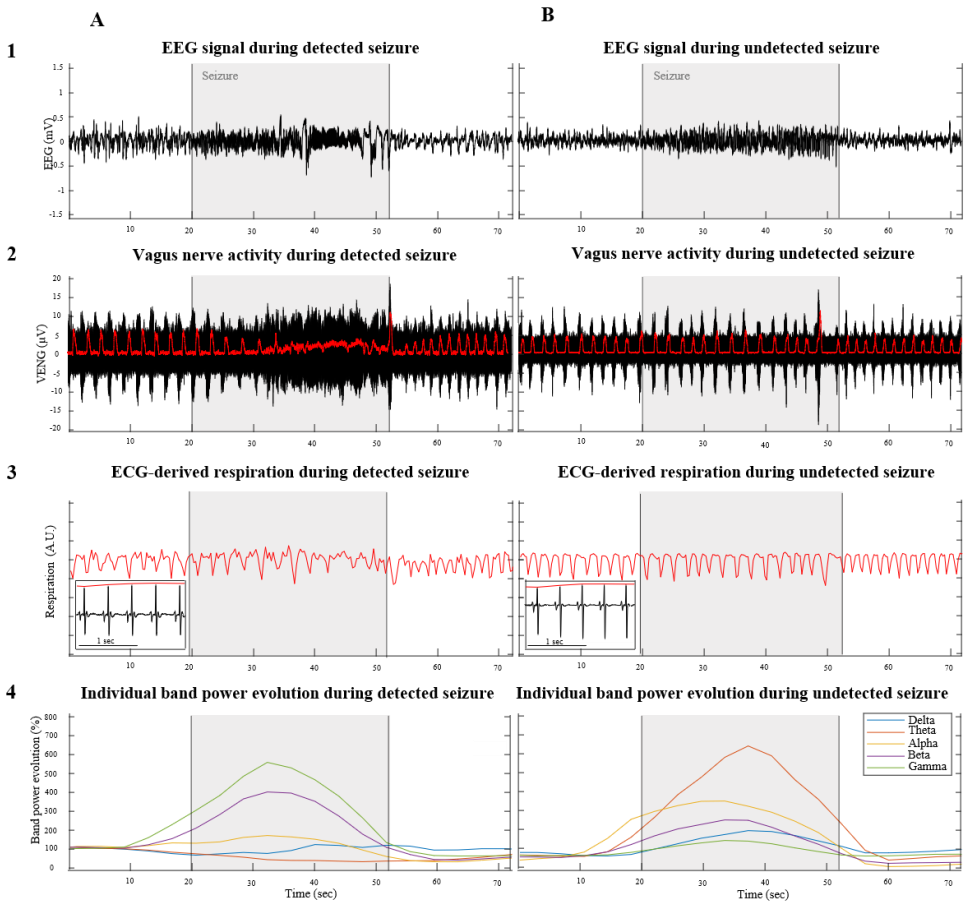

Figure 10: Illustrates a comparative analysis of physiological parameters between VENG-detected (A) and undetected (B) seizures induced by KA injection into the right hippocampus of two different rats (RAT3 and 5), weighing 215 g and 306 g, respectively. The top row displays the EEG signal across three phases: pre-ictal, ictal, and post-ictal. The second row depicts vagus nerve activity during the same periods, with respiration-related VENG bursts (indicated by the red line in row 2) synchronizing with respiration derived from modulation QRS complexes of the ECG during in/expiration (red line in row 3). The bottom row represents the individual EEG band spectrum evolution during the recorded seizures, normalized by the pre-ictal period, emphasizing the heightened activity in each band during the ictal period.

This differential response in VENG signal amplitude and rhythmicity to KA-induced seizures provides valuable insights into the variability of ANS reactions among individual subjects, potentially contributing to a more nuanced understanding of seizure dynamics and their impact on VNA. Furthermore,

these changes in amplitude and rhythmicity within the VENG signal were leveraged by the detection algorithm, confirming that 13 out of 20 seizures exhibit alterations, while the remaining 7 do not.

2.4.4. VENG-based seizure detection

In our study, a comprehensive approach was adopted to refine the parameters for optimal VENG-based seizure detection across the six rats (RAT1-6) involved in ictal recordings. We explored nine distinct combinations of foreground/background (Fg/Bg) window lengths, alongside seven detection thresholds ranging from 0.4 to 0.7, incremented by 0.05. This comprehensive analysis aids in identifying the most effective parameters for optimizing the algorithm's performance in seizure detection.

For each Fg/Bg window combination, a ROC curve was generated by evaluating the sensitivity and PPV at each threshold level (illustrated in *Figure 11*). Each curve symbolizes a specific Fg/Bg pairing, with individual points along the curve representing different detection thresholds. It was observed that higher thresholds led to less restrictive detection criteria, compromising accuracy. The thresholds were arranged such that they increased from right to left along the curve.

A notable observation from the black curve (*Figure 11*, Fg5/Bg90) reveals that the first point on the left (threshold: 0.7) achieved the highest sensitivity (65%) but the lowest accuracy (38.9%), indicating an overly permissive threshold. Conversely, the second highlighted point (threshold: 0.5) was identified as the optimal balance between sensitivity and accuracy, successfully detecting 13 out of 20 seizures (sensitivity: 65%) with only one false detection (PPV: 92.8%). The lowest tested threshold (0.4) resulted in the detection of 8 out of 20 seizures (sensitivity: 34.8%), accompanied by one false detection (PPV: 88.9%). Following the ROC curve analysis, the optimal parameters were set at Fg5/Bg90 and the detection threshold to 0.5. With these parameters, the VENG algorithm managed to detect 13 out of 20 seizures, recording a mean delay of 25.3 ± 13.5 seconds between the EEG onset and VENG detection onset (*Table 2*).

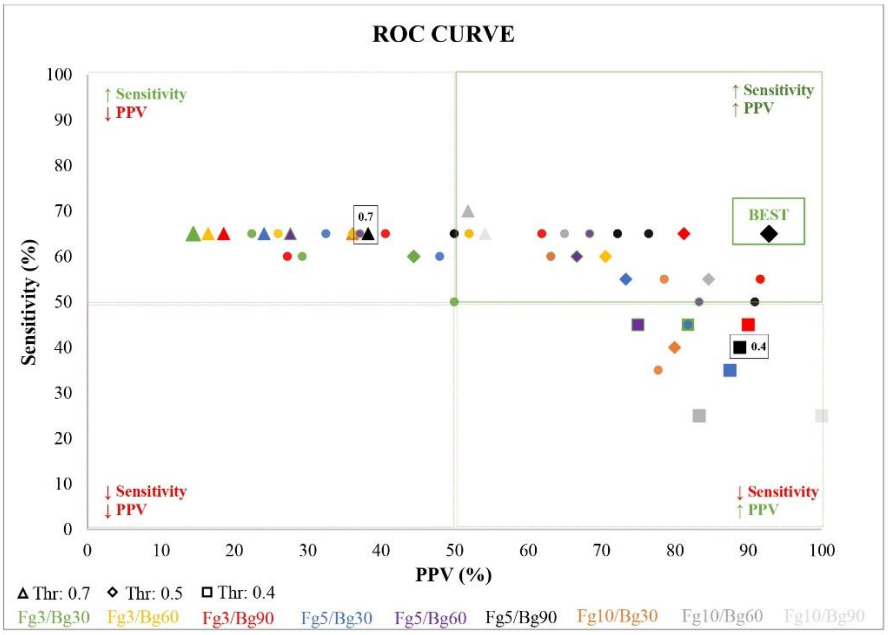

Figure 11: Illustrates Receiver Operating Characteristic (ROC) curves, depicting the predictive performance of various detection parameters, including the detection threshold and Foreground/Background (Fg/Bg) window length. The x-axis represents the accuracy or positive predictive value (PPV), while the y-axis represents the true positive rate (TPR), also known as sensitivity. Each curve corresponds to a unique combination of Fg/Bg window sizes, with points along the curves indicating different detection thresholds, ranging from 0.70 (on the left) to 0.40 (on the right), with a step decrement of 0.05. Optimal detection parameters, determined by maximal sensitivity and positive predictive value, are highlighted at a detection threshold of 0.5 and an Fg/Bg length of 5/90 s.

2.4.5. Comparative analysis of seizure spread through ictal band power evolution and HR changes between undetected and detected seizures.

We compare the mean ictal band power evolution for each individual band to investigate potential differences in seizure spread between the two groups. The statistical analysis revealed a significant difference in the evolution of the Delta band (p-value: 0.0136), with undetected seizures exhibiting a mean increase of 117.6 ± 116% compared to the detected group with a mean change of 0 ± 79.6% (*Figure 12*). Similarly, significant differences were found in the Theta band (p-value: 0.0236), where the undetected group displayed a mean increase of 83.6 ± 145.6%, contrasting with the detected group with a mean decrease of -28.4 ± 38.2% (*Fig. 12*). Additionally, in the faster Beta band, a significant difference in band power evolution was observed (p-value: 0.0297), indicating faster activity

in the detected group (334.9 ± 263.4%) compared to the undetected group (122.4 ± 56.7%) (*Figure 12*). Furthermore, unpaired t-tests revealed a significant difference in the ictal HR changes between the two groups, with the detected group showing an absolute mean change of 9.03 ± 5.5% contrasted with the undetected group, which showed an absolute HR change of 4.42 ± 3.7% (*Figure 12*).

The observed variations in individual EEG band power evolution between detected and undetected seizures suggest the possibility of distinct seizure spreading patterns between the two groups. This may result in differential activation of the autonomic central network. This observation is further supported by the differential HR changes observed between the two groups, indicating potential differences in the underlying mechanisms of seizure propagation.

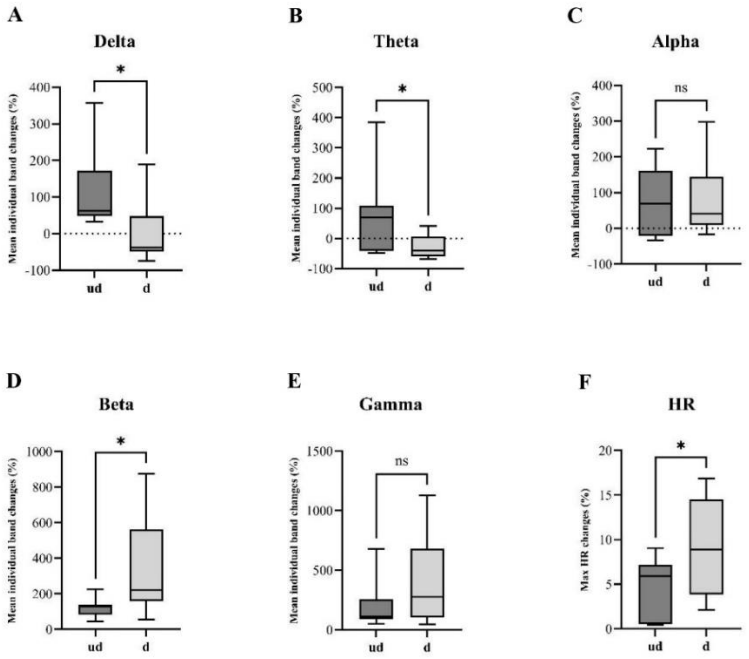

Figure 12: Illustrates a comparative analysis of seizure spread and HR changes between undetected seizures (ud, n = 7) and detected seizures (d, n = 13). Boxplots resulting from the Mann–Whitney U-test reveal a significant increase in panel (A) delta (p-value: 0.0136) and (B) theta (p-value: 0.0236) band power in undetected seizures. Conversely, detected seizures exhibit a significantly higher increase in faster (D) beta band (p-value: 0.0297) power. Additionally, unpaired t-tests reveal a significantly steeper HR changes (F) in detected seizures compared to undetected seizures. While no significant differences were observed in panel (C) Alpha and (E) Gamma bands. *p<0.05.

2.4.6. Correlation between physiological parameters and VENG-based seizure detection efficacy

We conducted binomial logistic regression analyses to explore which physiological parameters affect VENG signal-based seizure detection. These focused on examining the associations between detection outcomes and several predictive variables, such as the evolution of individual EEG band power and average HR changes (ictal versus pre-ictal periods).

The binomial logistic regression revealed a nuanced interplay between VENG-based seizure detection and EEG band power evolution. Notably, an increase in theta band activity was associated with a decreased likelihood of seizure detection ([OR]: 0.976, 95% [CI]: [-0.047;-0.001], p-value: 0.038*), suggesting an impact of theta band fluctuations on the efficacy of seizure detection (*Table 3*). A similar trend was observed with delta band activity, although the correlation approached the statistical significance threshold (OR: 0.986, CI: [-0.029;0], p-value: 0.051)(*Table 3*). Conversely, an increase in beta band activity showed a tentative correlation with enhanced seizure detection (OR: 1.013, CI: [-0.003;0.029], p-value: 0.099), albeit not reaching statistical significance (*Table 3*).

Furthermore, the logistic regression analysis highlighted a correlation between HR changes and seizure detection, indicating that a more pronounced HR change is associated with a higher likelihood of detecting a seizure (OR: 1.248, CI: [-0.032;0.475], p-value: 0.086) (*Table 3*).

	Coefficient	Error	OR	*p*-value	95% CI		McFadden R^2	AUC
					Lower bound	Upper bound		
Delta	−0.015	0.007	0.986	0.051	−0.029	0	0.246	0.835
Theta	−0.024	0.012	0.976	0.038*	−0.047	−0.001	0.303	0.813
Beta	0.013	0.008	1.013	0.099	−0.003	0.029	0.261	0.802
HR	0.222	0.129	1.248	0.086	−0.032	0.475	0.158	0.736

*$p<0.05$.

Table 3: Presents the outcomes of logistic regression analyses, displaying the regression coefficients along with their corresponding error terms, the odds ratios with their 95% confidence intervals, Wald statistic-derived p-values, McFadden's R2, and the area under the Receiver Operating Characteristic (ROC) curve.

2.5. Discussion

This study demonstrates the feasibility of seizure detection based on respiratory-derived ictal VENG modifications using an implantable cuff electrode in an acute intrahippocampal KA model. Our algorithm successfully identified 13 out of 20 seizures with an accuracy of 92.9% and an average delay

of 25.3 ± 13.5 seconds. However, 7 out of 20 seizures remained undetected, exhibiting distinct EEG characteristics and autonomic symptoms, suggesting potential differences in seizure spread and involvement of the autonomic central network.

Respiratory modulation of the VNA is well established in the literature in both animal models and human studies. Previous research using a porcine model has shown that vagal recordings with cuff electrodes exhibit morphological similarities within the neural activity profile with respect to actual respiratory patterns, in both duration and frequency (254). Further, studies involving awake human subjects have utilized intraneural recordings from the left vagus nerve, revealing modulations attributed to both cardiac and respiratory functions (304). Notably, respiratory modulation was observed to be more substantial (45%) compared to cardiac modulation (23%), suggesting a stronger respiratory influence on VNA (304). In the current study, the baseline recordings showed that ECG-derived respiratory activity aligned well with the respiratory-related vagus nerve bursts, supporting previous findings and validating our setup (303).

Our results suggest an ictal disappearance of spontaneous vagus nerve bursts related to respiration. This is potentially explained by well-recognized respiratory arrhythmia observed during seizures. In humans, seizures can be characterized by hypopneas (117) and, in severe cases, obstructive apnea and respiratory arrest, leading to sudden death (44, 66, 118, 294-296). Similarly, animal studies on KA rats have shown seizure-induced suppression of phrenic nerve activity (306), which is the only motor nerve innervating the diaphragm, hence a potential explanation for reduced respiratory frequency. In another study using an acute KA rat model, respiratory efforts were observed during bradycardic seizures (241). These respiratory efforts, characterized by gasps, were later explained by airway obstruction. This aligns with the emerging consensus that seizures can lead to obstructive apnea (307-309), which could, in severe cases, be followed by bradycardia, terminal apnea, and eventually death (307-309). These autonomic alterations result in an increased flow of information through the vagus nerve, wherein bidirectional transmission can either increase or decrease signal amplitude. The modulation of rhythmicity may stem from respiratory irregularities disrupting respiration-related bursts or heightened information transit, masking these bursts. While our experimental setup did not directly measure apneas, the disturbances observed in respiratory-derived VENG signals during seizures could serve as potential biomarkers for seizure detection.

A previous investigation has explored a seizure detection algorithm based on VENG activity in the PTZ model, focusing on cardiac-related changes (269). Their method involved identifying variations in the extracted CrVENG, obtained through R-peak triggered averaging of VENG energy. Notably, all seizures were detected with a mean delay of 103 ± 51 seconds before the onset of the tonic-clonic phase (269). However, this study used hook electrodes, which are unsuitable for human application. Additionally, this algorithm exclusively relied on cardiac-related changes without exploiting all the potential of VENG detection associated with other non-cardiac physiological changes.

A more recent algorithm adopted a spike detection approach, quantifying VENG activity by analyzing extra-neural spikes or CAPs (257). This method involves computing a detection metric by averaging spike frequency and amplitude and determining the ratio between two sliding Foreground (Fg) and Background (Bg) windows. All seizures were detected with 100% sensitivity and specificity, with 3 out of 6 seizures identified during the early stage, exhibiting a mean delay of 426 ± 126 seconds (7.10 ± 2.1 minutes) before the tonic-clonic stage. The remaining 3 out of 6 seizures were detected with a mean delay of 9.6 ± 5.4 seconds after the onset of the tonic-clonic stage. Analysis of spiking activity in the vagus nerve has become the focus of a growing number of studies with diverse objectives. Most studies have explored vagus nerve spiking activity in non-epileptic related diseases such as inflammatory response (273), intestinal/gastric extension, or hypoxia (244). This study provides a novel application of spiking analysis in the context of epilepsy.

By optimizing our new detection algorithm's parameters, including varying Fg/Bg window lengths and setting detection thresholds (0.4 to 0.7 with increments of 0.05), we identified an optimal setup with an Fg/Bg window length of 5/90 seconds, coupled with a threshold of 0.5. This configuration allowed for detecting 13 out of 20 seizures, with a mean delay post-ictal onset of 25.3 ± 13.5 seconds, verified against concurrent scalp EEG recordings. However, it is noteworthy that RAT4 exhibited an extended detection time latency, with 2 out of 4 seizures detected at a mean delay of 48.36 ± 18.17 seconds. In contrast, the 11 seizures detected in the first three rats (RAT1-3) demonstrated a detection delay of 16.09 ± 2.67 seconds. Moreover, despite variations in algorithm parameters, 7 out of 20 seizures exhibited no ictal VENG modifications and remained undetected.

Our investigation explored the hypothesis that detected seizures might exhibit higher severity than undetected seizures, potentially explaining the absence of autonomic changes in the latter group. Since the conventional Racine scale is

inadequate for assessing seizure severity due to the absence of clinical manifestations under anesthesia (178, 310), we chose to explore individual band power evolution to identify potential differences in EEG characteristics that could indicate different seizure spread patterns or severity. Grouping all seizures together revealed a notable increase in gamma and beta bands during seizures, with detected seizures showing faster EEG activity. Binomial logistic regression further confirmed that the detection appeared to be correlated with a steeper increase in beta (OR: 1.013, CI: [-0.003;0.029], p-value: 0.099), and a smaller increase in theta ([OR]: 0.976, 95% [CI]: [-0.047;-0.001], p-value: 0.038*) and delta (OR: 0.986, CI: [-0.029;0], p-value: 0.051) band power. Moreover, we hypothesized that detected seizures may propagate differently and engage the autonomic central network to a greater extent than undetected seizures, which might involve distinct subcortical pathways. In addition, undetected seizures exhibit a significantly higher increase in delta (p-value: 0.0136) and theta band (p-value: 0.0236), which has already been described in the literature - reflecting a potential mechanism underlying temporal lobe seizures, which were characterized by impaired consciousness without motor activity (311). These seizures were associated with large amplitude slow EEG activity, and neuroimaging signals decreased in the frontal and parietal cortices, contrary to the fast poly-spike activity and high blood flow in limbic structures and subcortical regions. Thus, they proposed the "network inhibition hypothesis," in which seizure activity propagates to subcortical regions necessary for cortical activation, such as the lateral septum, allowing the cortex to descend into an inhibited state of unconsciousness without motor manifestation during focal secondary generalized seizures (311).

Correlation between VENG alterations and ictal HR changes showed that seizures were characterized by bradycardia in most rats. Among the rats studied, 1 out of 6 displayed ictal tachycardia, characterized by a mean average increase of 3 ± 1.6% and an average peak increase of 6.8 ± 2.8% relative to pre-ictal HR values. In 5 out of 6 rats, we observed a mean average HR decrease of 2.1 ± 2.3% and an average peak decrease of 7.6 ± 6% relative to pre-ictal HR values. Binomial logistic regression analysis revealed a correlation between detection and higher HR changes, with the VENG-detected seizure group exhibiting more pronounced alterations. This underscores the meaningful association between ictal VENG changes and cardiac variations, aligning with findings from other studies (241, 269).

This study encountered several limitations that warrant acknowledgment. First, the size of the experimental group was insufficient to allow for separation

into two distinct groups: a training group for refining detection parameters and a test group for validation. Moreover, the small sample size limits the strength of the conclusions drawn from the logistic regression analyses. Future studies should increase the number of rats to test the algorithm's performance and obtain a more robust representation of seizure characteristics, thereby reinforcing the results presented in the logistic regression analyses. Alternatively, evaluating algorithm performance in spontaneous recurrent seizures induced by KA could further strengthen the results, highlighting the longitudinal aspect of the KA model. Second, KA injection provokes multiple seizures characterized by a high-frequency onset evolving into spike-wave discharges. Usually, we are able to induce two to five seizures in our animals. However, defining the offset became more and more challenging for later seizures, primarily due to increasing interictal activity. While this does not represent a significant limitation, it may result in a slight variation in seizure duration. This consistency in identifying seizure onset allowed us to accurately determine the delay between EEG seizure onset and VENG seizure onset, ensuring the reliability of our findings, which is a major challenge in the context of seizure detection. Additionally, anesthesia might influence the autonomic modifications during seizures, as it is known in the literature that ketamine decreases parasympathetic tone, homeostatic reflex and vagal activity (312, 313). However, the anesthesia protocol was uniformly applied across all animals in our cohort. Deep anesthesia maintenance was confirmed by the predominant presence of delta waves during the baseline period, constituting the largest proportion of observed waves (54.8 ± 2.6%), followed by theta waves (22.5 ± 6.4%). Finally, a major limitation is the lack of respiration recording, which hinders the direct correlation between ictal VENG modulation and respiratory dysregulation, such as apneas or tachypnea during seizures. While direct respiratory recording was not feasible in our experimental protocol, literature supports indirect estimation of respiratory rate from ECG-derived R peak amplitude modulation (303, 314), a method successfully applied previously in our group (255, 257). Stump et al. demonstrated synchrony between ECG-derived respiration and VENG signal bursts, indicating potential for correlating these measures to understand respiratory dynamics during seizures (255, 257).

Although RNS remains the most reliable detection method and demonstrates high efficacy, due to its highly invasive nature and restriction to focal epilepsy, other closed-loop stimulation strategies should be considered. VNS is applicable to both pediatric and adult populations and is effective for epilepsy of both lesional and non-lesional origin, whether focal or generalized (20).

Additionally, VNS improves not only seizure frequency but also comorbidity factors, such as depression (315). However, there is a critical need to enhance seizure detection for closed-loop VNS. Within this context, our research aims to explore alternative methods for seizure detection. This study underscores the potential of VENG recording as a promising alternative for HR-based seizure detection. This investigation primarily adopts a descriptive approach. Future investigations are needed to confirm the applicability of ictal VENG alterations for spontaneous seizure detection in chronic epilepsy models, and determine sensitivity and specificity in these models, as well as the comparison between only open-loop and combined open and VENG-based closed-loop stimulation. After refining our detection algorithm, expanding the animal cohort will be necessary to gain a more precise understanding of its sensitivity and accuracy. Managing motion constitutes a critical challenge requiring the use of thresholds to reject motion artifacts. Machine learning could assist us in identifying specific patterns in each patient and setting appropriate detection thresholds. This will be addressed in the future, following our investigations in the chronic model. Furthermore, broadening our research to multiple types of seizures is crucial, with the ultimate goal of enhancing the sensitivity of closed-loop VNS devices across all seizure types.

2.6. Contribution

Acedo Reina E, Germany Morrison E, Dereli AS, Collard E, Raffoul R, Nonclercq A, El Tahry R. Vagus nerve electroneurogram-based detection of acute kainic acid induced seizures.

3. Amendment: ROC curve

Although this figure is based on previously published work (*Figure 11*), modifications were made to the ROC representation to improve interpretability and align with conventional standards.

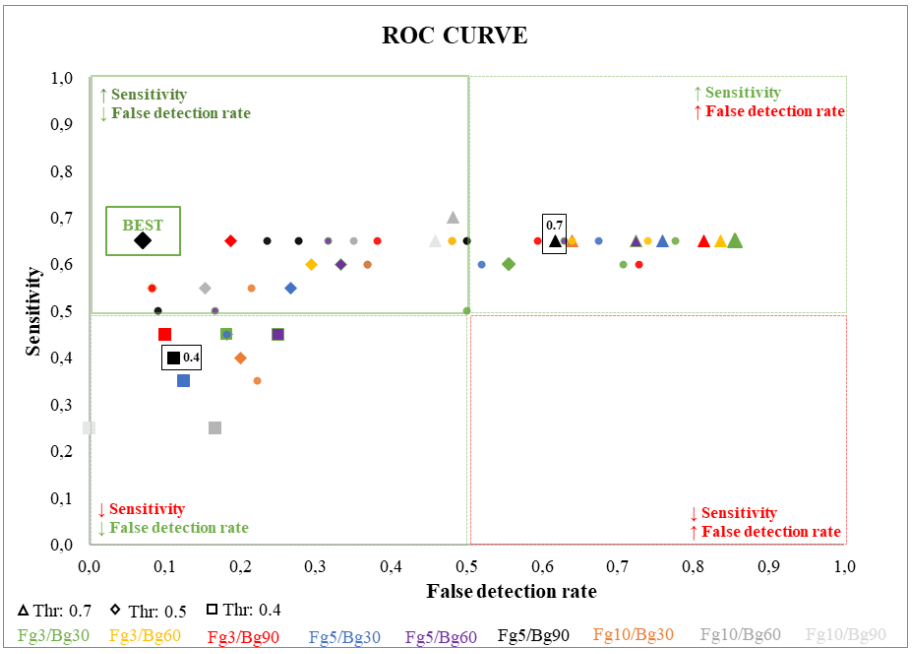

First, the x- and y-axis values were divided by 100 to express all metrics on a normalized scale ranging from 0 to 1. Additionally, the figure was reformatted such that the most optimal detection point appears in the top-left quadrant, consistent with standard ROC visualization practices. To achieve this, the Positive Predictive Value (PPV) originally plotted on the x-axis was replaced by the False Discovery Rate (FDR), computed as (1 – PPV), thereby allowing for a more intuitive interpretation of classifier performance.

To further improve figure readability, given the superposition of nine distinct parameter combinations, data points were not connected by lines. Instead, each color represents a unique Fg/Bg window combination, and each point on a curve corresponds to a detection threshold ranging from 0.40 to 0.70 in 0.05 increments. This range was deliberately restricted to 0.40–0.70 (as opposed to the full 0–1 scale) to avoid overcrowding and to focus on the most relevant portion of the operating curve.

For transparency, individual ROC plots were also generated for each Fg/Bg window configuration, displaying the full set of threshold-dependent curves separately. These are presented below.

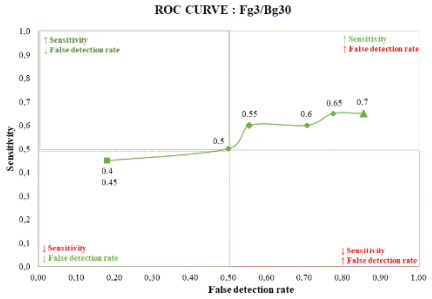
ROC CURVE : Fg3/Bg30
Sensitivity
False detection rate
↑ Sensitivity
↓ False detection rate
↑ Sensitivity
↑ False detection rate
↓ Sensitivity
↓ False detection rate
↓ Sensitivity
↑ False detection rate
0.4
0.45
0.5
0.55
0.6
0.65
0.7

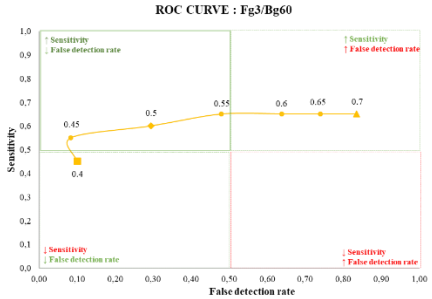
ROC CURVE : Fg3/Bg60
Sensitivity
False detection rate
↑ Sensitivity
↓ False detection rate
↑ Sensitivity
↑ False detection rate
↓ Sensitivity
↓ False detection rate
↓ Sensitivity
↑ False detection rate
0.4
0.45
0.5
0.55
0.6
0.65
0.7

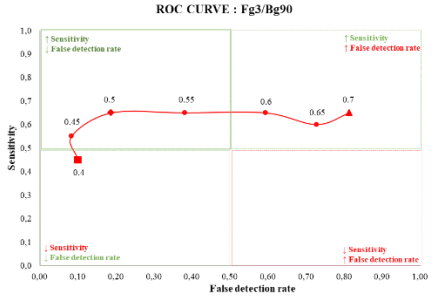
ROC CURVE : Fg3/Bg90
Sensitivity
False detection rate
↑ Sensitivity
↓ False detection rate
↑ Sensitivity
↑ False detection rate
↓ Sensitivity
↓ False detection rate
↓ Sensitivity
↑ False detection rate
0.4
0.45
0.5
0.55
0.6
0.65
0.7

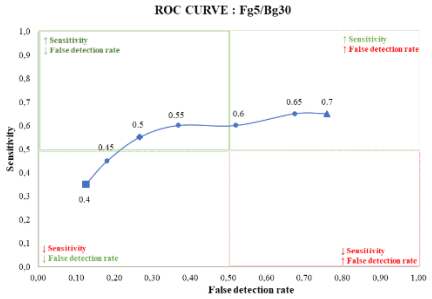
ROC CURVE : Fg5/Bg30
Sensitivity
False detection rate
↑ Sensitivity
↓ False detection rate
↑ Sensitivity
↑ False detection rate
↓ Sensitivity
↓ False detection rate
↓ Sensitivity
↑ False detection rate
0.4
0.45
0.5
0.55
0.6
0.65
0.7

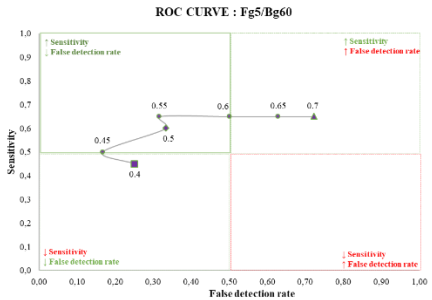
ROC CURVE : Fg5/Bg60
Sensitivity
False detection rate
↑ Sensitivity
↓ False detection rate
↑ Sensitivity
↑ False detection rate
↓ Sensitivity
↓ False detection rate
↓ Sensitivity
↑ False detection rate
0.4
0.45
0.5
0.55
0.6
0.65
0.7

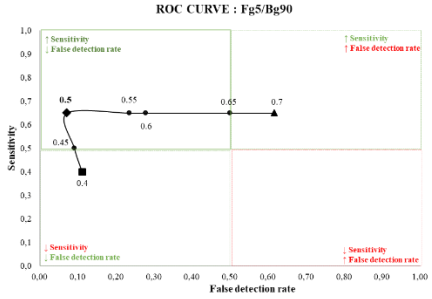
ROC CURVE : Fg5/Bg90
Sensitivity
False detection rate
↑ Sensitivity
↓ False detection rate
↑ Sensitivity
↑ False detection rate
↓ Sensitivity
↓ False detection rate
↓ Sensitivity
↑ False detection rate
0.4
0.45
0.5
0.55
0.6
0.65
0.7

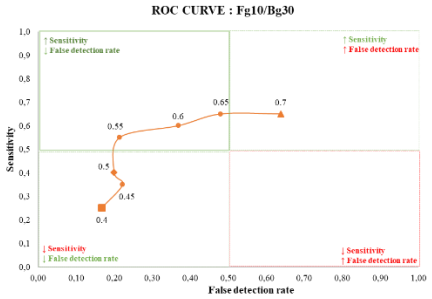
ROC CURVE : Fg10/Bg30
Sensitivity
False detection rate
↑ Sensitivity
↓ False detection rate
↑ Sensitivity
↑ False detection rate
↓ Sensitivity
↓ False detection rate
↓ Sensitivity
↑ False detection rate
0.4
0.45
0.5
0.55
0.6
0.65
0.7

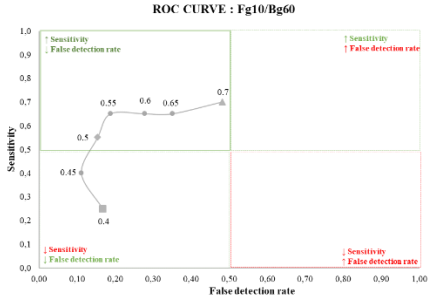
ROC CURVE : Fg10/Bg60
Sensitivity
False detection rate
↑ Sensitivity
↓ False detection rate
↑ Sensitivity
↑ False detection rate
↓ Sensitivity
↓ False detection rate
↓ Sensitivity
↑ False detection rate
0.4
0.45
0.5
0.55
0.6
0.65
0.7

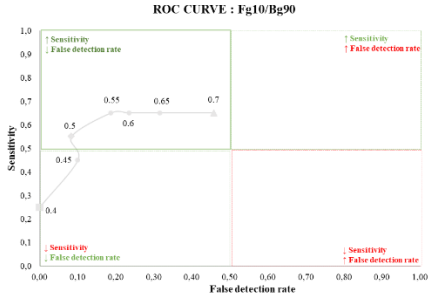
ROC CURVE : Fg10/Bg90
Sensitivity
False detection rate
↑ Sensitivity
↓ False detection rate
↑ Sensitivity
↑ False detection rate
↓ Sensitivity
↓ False detection rate
↓ Sensitivity
↑ False detection rate
0.4
0.45
0.5
0.55
0.6
0.65
0.7

CHAPTER 4 : Modulation of VNA during spontaneous recurrent seizure in the KA model of temporal lobe epilepsy

1. Preface

The following section is based on the manuscript submitted as a Brief Research Report in Frontiers of Neurosciences under the title: "Modulation of Vagus Nerve Activity During Spontaneous Recurrent Seizures in the Kainic Acid Rat Model of TLE".

2. Modulation of vagus nerve activity during spontaneous recurrent seizures in the kainic acid rat model of temporal lobe epilepsy

2.1. Abstract

This preliminary study investigates the modulation of VNA during spontaneous seizures in freely moving rats. VNA was recorded from an intraneural electrode, while an RMS amplitude and CAPs detection were used to quantify VNA. During wakefulness, CAPs frequency was significantly higher than during NREM sleep. However, wakefulness also exhibited a higher proportion of commonly recorded activity between the intraneural and extraneural electrodes, suggesting increased contamination by motion-related artifacts. During seizures, VNA displayed higher activity, supported by a significant increase in RMS amplitude and a trend toward higher CAP frequency. These findings suggest that VNA modulation may reflect seizure dynamics and highlight its potential as a biomarker for seizure detection. Nonetheless, further validation in larger experimental datasets is necessary.

2.2. Introduction

The vagus nerve is the primary parasympathetic relay between the brain and visceral organs (316). It regulates crucial autonomic functions, including breathing, HR, digestion, immune response, and metabolism (213, 277, 317-320). Primarily composed of unmyelinated C-fibers (>80%), it conveys afferent sensory information from visceral organs to the central nervous system (277, 321, 322). Given its integrative role, the VNA represents a key biomarker for monitoring the physiological state of visceral organs, offering significant potential for therapeutic and scientific applications.

Seizures are known to disrupt the autonomic balance. While sympathetic activation is frequently observed across various seizure types, parasympathetic involvement is more complex. It can manifest as either activation or inhibition, leading to bradycardia or respiratory dysrhythmias and, in severe cases, hypopneas and apneas (66, 118, 294-296). These autonomic alterations are correlated with seizure severity and adverse clinical outcomes, with excessive parasympathetic activation identified as a potential risk factor for SUDEP (93).

A recent study in the KA model of TLE in rat indicates that persistent parasympathetic activity during seizures is associated with severe outcomes, while sustained sympathetic tone contributes to survival during the late phase of self-terminating seizures (241). These findings underscore the need for understanding vagal signaling under both physiological and pathological conditions. Investigating VNA as a multi-organ biomarker could provide valuable insights into the mechanisms of autonomic dysfunction in epilepsy. Besides, it would offer a promising approach to refine seizure detection and optimize closed-loop stimulation strategies, such as for VNS therapy.

The feasibility of recording VNA has been demonstrated in both animal models (251-253, 255, 257, 258, 269, 278) and human subjects (250, 304), offering valuable insights into autonomic dynamics during seizures. VNA has been recorded using various electrode types in rodents and larger animal models, demonstrating its feasibility for assessing cardiac-related modulation during PTZ-induced seizures (251, 253, 255, 257, 269, 278) In the KA model, VNA recordings have been used to evaluate seizure detection via respiratory-related components, highlighting their potential for seizure monitoring (258).

However, these studies (251, 253, 255, 257, 258, 269, 278) were all conducted under anesthesia, which may influence autonomic responses during seizures. Anesthetic agents such as ketamine are known to depress parasympathetic tone, homeostatic reflexes, and vagal activity (312, 313), potentially complicating interpretations. Therefore, there is a critical need to develop methods for recording VNA during spontaneous seizures in awake conditions to ensure more physiologically relevant insights.

The KA-induced model is a well-established animal model of chronic epilepsy, mimicking key neuropathological and electroencephalographic features observed in patients with TLE (140). This model is associated with autonomic alterations, including increased susceptibility to homeostatic autonomic cardiorespiratory reflex impairments during recurrent seizures (323, 324), and suppressed phrenic nerve activity, crucial for diaphragmatic function (306).

Given these characteristics, this model provides a good framework for investigating VNA modulation during spontaneous seizures in awake animals.

This study characterizes VNA in awake rats across different physiological states, focusing on spontaneous recurrent seizures in the KA model of TLE, to better understand the autonomic mechanisms underlying seizure dynamics.

2.3. Methods

2.3.1. Animals

The Animal Experimental Ethical Committee of Université Catholique de Louvain (UCLouvain) and the Brussels Environment Committee have approved all experimental protocols under the 2022/UCL/MD/066 reference. Nine male Wistar rats (local breeding facility, UCLouvain, Belgium), with an average age of 62 ± 7.2 days and an average weight of 288.9 ± 22.3g, were housed in a temperature- and humidity-controlled environment with a 12h day/night cycle and ad libitum access to food and water.

2.3.2. Experimental design

Epilepsy was induced in all rats (n=9). Following induction, six rats survived and were housed in the animal facility for five months to allow stabilization of the epileptogenic process (168). After this period, the rats underwent surgical implantation of EEG and vagus nerve electrodes. Of these six rats, four rats survived the surgical procedure. They were immediately transferred to custom-built EEG-video monitoring cages for continuous recording for 2 to 5 days (325) (Timeline is shown in *Figure 14.A*).

2.3.3. SE induction

SE was induced by intraperitoneal injections of KA (5 mg/kg; Hello Bio, Princeton, USA) following the Hellier protocol (155). Clinical seizures were continuously monitored visually and scored according to the Racine scale (178). KA treatment was repeated hourly until the animals displayed stable, self-sustained SE for at least 3 hours. Animals that exhibited excessive motor or lethargic behavior were given reduced dosages (2.5 mg/kg) of KA to avoid exaggerated toxicity and mortality. On average, all rats received 2.3 ± 0.75 injections, corresponding to a mean KA dose of 11.5 ± 3.75 mg/kg. Out of 9 rats, 6 survived the induction of the SE.

2.3.4. Electrode manufacturing

The custom EEG scalp electrodes (including reference and ground electrodes) consist of a 4.8 mm stainless-steel screw (Bilaney, Germany), soldered to a 0.05 mm^2 CSA, 30 AWG silver-plated copper wire, which connects to a 2.54 mm pin.

The custom intraneural/extraneural control electrodes are made of 10 cm, 76.2 µm PFA-coated platinum wire (AM-systems, USA), with insulation removed from both ends and one end soldered to a 2.54 mm pin. Electrodes were quality-checked pre-surgery by measuring absolute impedance to a stainless-steel counter electrode in saline solution at 1 kHz (IMP-2A, Microprobe for life Sciences, USA); acceptable absolute impedance was <1 kΩ for EEG electrodes and <5 kΩ for vagus nerve electrodes.

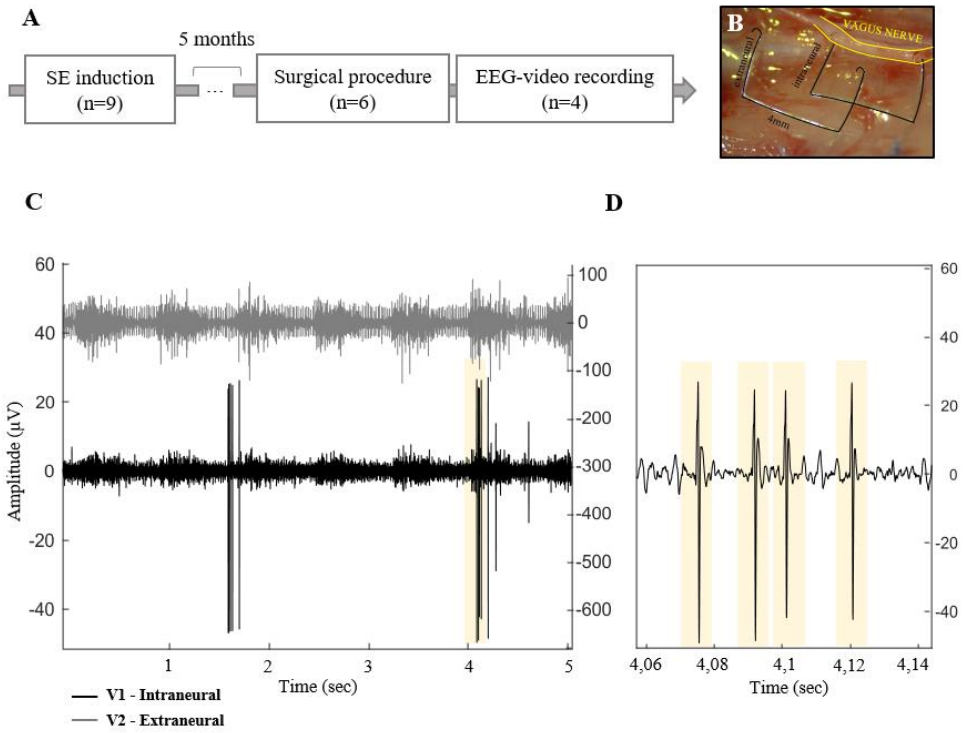

Figure 14. Experimental Design and Illustration of Vagus Nerve Activity (VNA) Signal Acquisition. (A) Experimental Timeline Detailing the Sequential Steps from Epilepsy Induction to Surgical Implantation and EEG-Video Recording. "n" represents the number of animals remaining at each step. (B) Surgical example of intraneural and extraneural electrode implantation in the left cervical vagus nerve. The electrodes are highlighted in black, and the vagus nerve is outlined in yellow. (C) Example of VNA signal recording during NREM Sleep. V1 and V2 signals are displayed in black and gray, with their respective amplitude scales shown on the left and right. (D) Magnified view of the yellow-highlighted section from (C), showing high-amplitude CAPs.

2.3.5. Surgical procedure

Anesthesia was induced with 5% sevoflurane in O2 (Sevotek® 1000 mg/kg) and maintained with 2.5% sevoflurane at 3 l/min (Dräger-Vapor2000, RWD).

Tramadol (5 mg/kg, subcutaneously) and Ketofen (5 mg/kg, subcutaneously) were administered subcutaneously. Body temperature was monitored with a rectal probe and maintained at 37.5°C using a heating pad. The animals were positioned in a stereotaxic frame (David Kopf Instruments) for implantation. Craniotomies were performed with a hand drill (Foredom Instrument), and custom epidural electrodes were implanted at specific coordinates: frontal electrode (+) [anteroposterior (AP) + 2 mm, mediolateral (ML) +3 mm], reference electrode (Ref) [AP + 6 mm, ML + 0 mm], and ground electrode (GND) [AP – 5 mm, ML + 3 mm] in the parietal region (297). The differential EEG recording was obtained between the frontal (+) and parietal (Ref) electrodes.

Following this, the left vagus nerve was exposed at the cervical segment, and two custom intraneural electrodes (4 mm apart) with non-insulated tips were inserted transversely into the nerve. A hook was created to secure the electrodes in position. The external portions were covered with medical-grade silicone. Control extraneural electrodes were placed near the nerve with the same spacing and orientation as the intraneural electrodes (*Figure 14.B*).

Leads from EEG and vagus nerve electrodes were connected to a socket connector and fixed to the skull using UV dental cement (CompoFlow, R&S).

2.3.6. Signal acquisition and filtering

The four surviving rats were housed in a custom chronic monitoring system within a Faraday cage to record spontaneous seizures and VNA (325). This recording system enabled unrestricted movement via a slip ring while allowing real-time acquisition of intraneural VNA, extraneural control signals, EEG, and video. High input-impedance (10 MΩ) amplifiers with 800 V/V gain preserved signal integrity, with low noise (0.5 μV - RMS) ensuring accurate VNA recordings. Signals were bandpass filtered (VNA: 10 Hz–10 kHz; EEG: 0.1 Hz–100 Hz). The system allows recording of two channels for vagus nerve recording (intra/extraneural signal recording) (20 kS/s), one scalp EEG channel (1 kS/s), and video (20 fps, infrared, 5 MP). Post-acquisition, VNA was further filtered (500 Hz–8 kHz) as well as the EEG (0.5 Hz–70 Hz). The system and amplifiers were previously validated (325, 326).

2.3.7. Seizure onset and duration

Seizures were characterized on the EEG by periods of low-voltage, high-frequency (> 5 Hz) rhythmic spiking activity, evolving into high-voltage, low-frequency SWDs that persisted for more than 10 seconds. The end of the seizure was defined as the last spike observed, followed by a depression phase of low voltage (168). Seizures were divided into two categories: non-convulsive

seizures (stages 1–2) and convulsive seizures (stages 3–5), according to the Racine scale (178).

2.3.8. VNA segmentation

To investigate VNA modulation under distinct conditions, two independent segment sets were extracted: one targeting physiological states (NREM/Wakefulness), and another focused on epileptic states (Pre-Ictal/Ictal).

2.3.8.1. Comparison of VNA across physiological states: Segmentation of sleep and wakefulness periods

Each animal's first recording day following surgery was segmented into distinct behavioral states based on concurrent EEG activity and synchronized video recordings. Specifically, we identified 10-second segments of two conditions: (1) NREM sleep, characterized by complete immobility, and (2) active periods (wakefulness), defined by continuous exploration and movement. For each animal (n=4), we extracted 30 segments per condition, pooled for all animals to obtain a total of 120 segments per condition. The first 8 hours post-surgery were excluded to prevent potential confounds from anesthesia and surgical recovery, and the 30 segments per condition (NREM/Wakefulness) were subsequently selected over the next 16 hours, ensuring continuous sampling with an average of two segments per hour. VNA was quantified independently for each segment (detailed in section 2.3.9), and the two conditions (NREM/Wakefulness) were compared using a Wilcoxon signed-rank test.

2.3.8.2. Modulation of VNA during seizures: Segmentation of ictal and pre-ictal periods

Separately, to analyze seizure dynamics, daily EEG recordings from each rat were reviewed to identify spontaneous epileptic seizures. In total, 15 seizures were detected across all animals and all recording days (14 days in total) and extracted as ictal segments, along with their corresponding pre-ictal segments (i.e., the periods immediately preceding seizure onset). Segment durations were defined using three distinct methods:

1) Method 1: Fixed 10-second pre-ictal duration and variable ictal duration: A 10-second pre-ictal segment and an ictal segment covering the entire seizure length.

2) Method 2: Variable ictal and pre-ictal durations (variable length): Ictal and pre-ictal segments of equal duration, both matching the seizure length.

3) Method 3: Fixed 10-second ictal and pre-ictal durations: A 10-second ictal segment (first 10 seconds of the seizure) and a 10-second pre-ictal segment (10 seconds before onset).

For all animals (n=4), we extracted 15 segments per condition (Pre-Ictal/Ictal). VNA was quantified for each segment (detailed in section 2.3.9), and pre-ictal and ictal windows were compared using a Wilcoxon signed-rank test.

2.3.9. VNA analysis

We employed various signal-processing methods to characterize VNA across extracted segments. First, the RMS amplitude was calculated for each segment to provide a measure of the signal's energy. This approach offers a metric for assessing overall VNA fluctuations; however, it does not isolate neural components, as it remains susceptible to contamination from movement artifacts, muscle activity (EMG), and other non-neural sources.

To refine our analysis and capture neural-specific activity, we identified "spiking" events based on local maxima detection, also called "peaks" or "CAPs". This method was applied to both the intraneural electrode (V1) and the extraneural control electrode (V2). Peaks were determined using dynamic thresholding, wherein the 95th percentile of the 10 ms RMS distribution for each recording day was used as a daily threshold. This ensured that only high-amplitude fluctuations, including neural activity and large motion-related artifacts, were considered. A filtering step was added to identify intraneural-specific spiking events considered genuine CAPs, unrelated to any type of common interference, including movement artifacts and surrounding EMG. We assumed that peaks detected in V1 could be due to contamination of V2, if a simultaneous peak was detected in V2. In that regard, a temporal exclusion criterion was applied: a peak detected in V1 within a ±500 µs window of a peak in V2 was rejected. Two metrics were used. CAPs Density was defined as the number of peaks exclusive to V1 normalized by proper segment duration, expressing spiking events considered CAPs. Density of Common Peaks represented the number of temporally coincident peaks in V1 and V2, normalized by proper segment duration, expressing peaks related to surrounding "spiking" activity (e.g., due to movement artifacts and surrounding EMG).

Besides, to evaluate the degree of similarity between V1 and V2 signals, we extracted a spline-interpolated envelope from peaks for each segment and computed the Pearson correlation coefficient. This correlation metric measured shared activity between the two electrodes, allowing us to quantify

the extent of common interference (whatever their shape). A high correlation suggested large contamination (e.g., due to movement, breathing, or cardiac activity), regardless of its shape ("spiky" or not).

Taken together, four metrics were used for the analysis: RMS amplitude, CAPs density, density of common peaks, and envelope Pearson correlation. Among these, three metrics (spike density, RMS amplitude, and envelope Pearson correlation) were used to compare ictal and pre-ictal windows, while two metrics (spike density and RMS amplitude) were used to compute the ictal/pre-ictal ratio to assess VNA modulation between convulsive and non-convulsive seizures.

2.4. Results

2.4.1. VNA modulation between NREM sleep (no motion) and wakefulness (with motion)

The mean VNA amplitude over 24 hours was 6.12 ± 2.3 µVRMS for V1 and 9.73 ± 9.7 µVRMS for V2. *Figure 14.C* shows V1 and V2 signals during NREM sleep, both displaying respiratory modulation. Clear CAPs were observed exclusively in V1, with a peak-to-peak amplitude of ~70 µV and a duration of 2 ms (*Figure 14.D*).

The number of CAPs was significantly larger during wakefulness segments compared to NREM sleep segments (*Figure 15.A*; $p<0.0001$). Additionally, the number of common peaks between V1 and V2 was significantly larger in wakefulness segments than in sleep segments, indicating that wakefulness segments are more affected by motion artifacts and external interference (*Figure 15.B*; $p < 0.0001$). Finally, the proportion of CAPs relative to the total number of detected peaks was significantly higher during sleep segments, confirming that surrounding interferences contaminate sleep less than compared to wakefulness segments (*Figure 15.C*; $p<0.0001$).

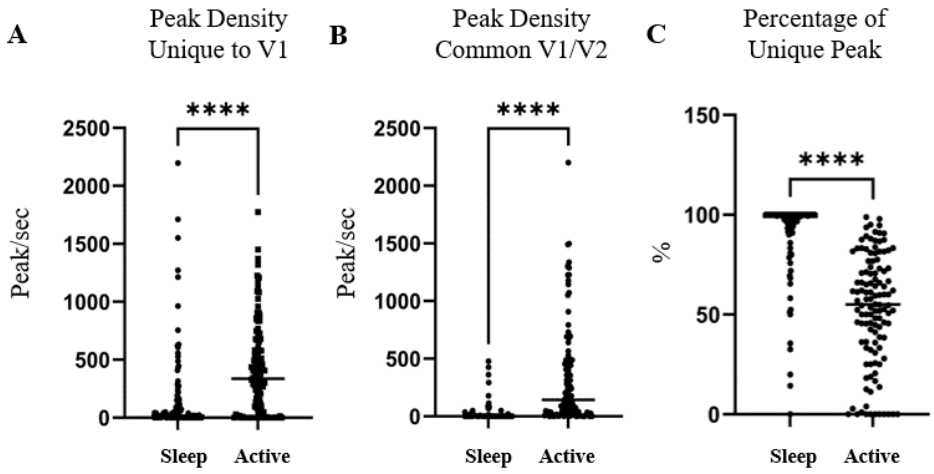

Figure 15. Comparison of VNA activity between NREM sleep segments and Active Wakefulness segments of 10 seconds (n = 120 per condition, sleep/wakefulness). (A) Quantification of neural activity using CAPs Density. (B) Assessment of signal contamination from movement artifacts and external interference using the Common Peaks Density metric. (C) Proportion of CAPs, obtained by dividing the number of peaks unique to V1/CAPs by the total number of peaks detected on V1, providing an estimate of the proportion of neural activity relative to shared artifacts. Statistical comparisons were performed using the Wilcoxon rank-sum test, with significant differences observed in all three metrics (****$p < 0.0001$).

2.4.2. EEG analysis of spontaneous recurrent seizures

A total of 15 seizures were identified. The average seizure duration was 56.4 ± 23.4 seconds. 8 out of 15 seizures were classified as non-convulsive seizures (stage 1-2), while 7 out of 15 were classified as convulsive stage 4 tonic-clonic seizures. Furthermore, in 8 out of 15 seizures, the ictal period was preceded by sleep or a state of very low activity, characterized by an awake but motionless condition. This pre-ictal state was observed in both seizure types: 4 convulsive and 4 non-convulsive seizures.

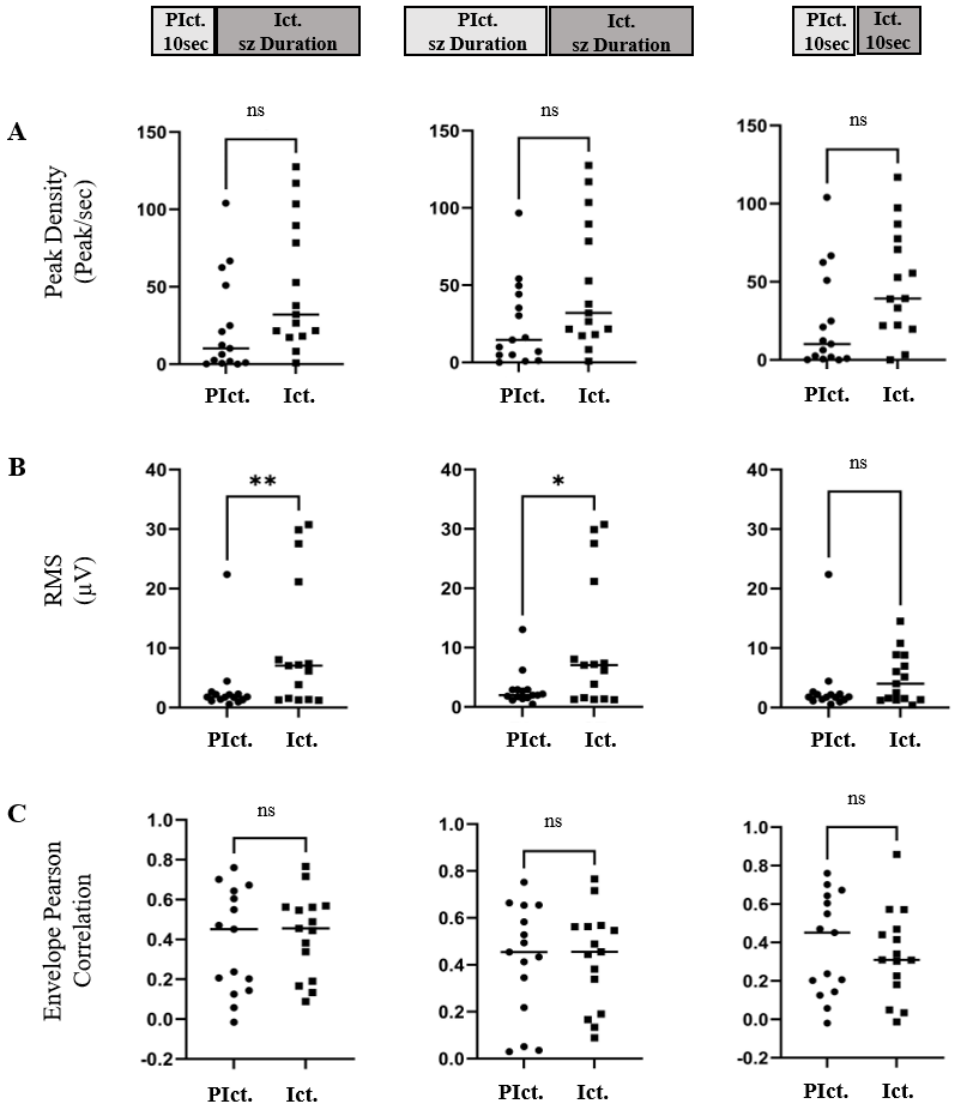

Figure 16. Comparison of Vagus Nerve Activity (VNA) Between Pre-Ictal and Ictal Periods. The columns represent the three distinct signal extraction methods: (A) CAPs Density, (B) RMS, and (C) Envelope Pearson Correlation between V1/V2. The rows depict the three computational metrics employed for comparison. Statistical comparisons between the pre-ictal and ictal groups were performed using the Wilcoxon signed-rank test. Non-significant results are indicated as "ns," while statistically significant differences are denoted as * ($p < 0.05$) and ** ($p < 0.01$).

2.4.3. VNA modulation during seizures

No significant differences in CAPs density were observed between ictal and pre-ictal segments across the three extraction methods (*Figure 16.A*; p = 0.151, 0.208, and 0.153, respectively). Nonetheless, a trend toward elevated VNA during seizures is visible, as indicated by an increased CAPs density in V1 during ictal periods. In method 1, this increase reached a median of 411.3% relative to pre-ictal segments. Consistently, RMS amplitudes were higher in ictal than in pre-ictal segments, with significant differences noted in methods 1 and 2, particularly in method 1 (*Figure 16.B*; p = 0.0034, 0.0103, and 0.120), which exhibited a median amplitude increase of 202.8% in ictal segments. In contrast, Pearson correlation coefficients of the signal envelopes between V1 and V2 did not differ significantly, indicating no measurable change in cross-electrode contamination across seizure states (*Figure 16.C*; p = 0.804, 0.891, and 0.599, respectively).

To further explore VNA modulation across seizure types, ictal/pre-ictal ratios for spike density and RMS amplitude were compared between convulsive (C) and non-convulsive (NC) seizures across the three extraction methods (*Figure 17*). Mann-Whitney tests revealed significantly higher ratios for convulsive seizures in spike density and RMS for the first two extraction methods, and for spike density in the third method, while no significant difference was observed for RMS in the third method.

2.5. Discussion

This preliminary study assessed the feasibility of recording VNA in freely moving epileptic rats and investigated its modulation across different physiological states and during seizures. Our findings demonstrate that chronic VNA recording is achievable and suggest state-dependent variations, with significantly higher VNA CAPs density observed during wakefulness compared to NREM sleep (*Figure 15.A*). No significant differences were found in CAPs density between ictal and pre-ictal periods during seizures (*Figure 16.A*). However, a trend toward increased VNA was noted in ictal segments, with significantly higher RMS values (*Figure 16.B*). Since the Pearson correlation between V1 and V2 showed no significant difference between pre-ictal and ictal windows, suggesting movement artifacts did not drive this RMS difference (*Figure 16.C*), we attributed it to increased VNA. Ictal/pre-ictal ratio analyses further indicated seizure type–dependent effects, with convulsive seizures exhibiting greater increases in spike density across all extraction methods and in RMS for the first two methods (*Figure 17*).

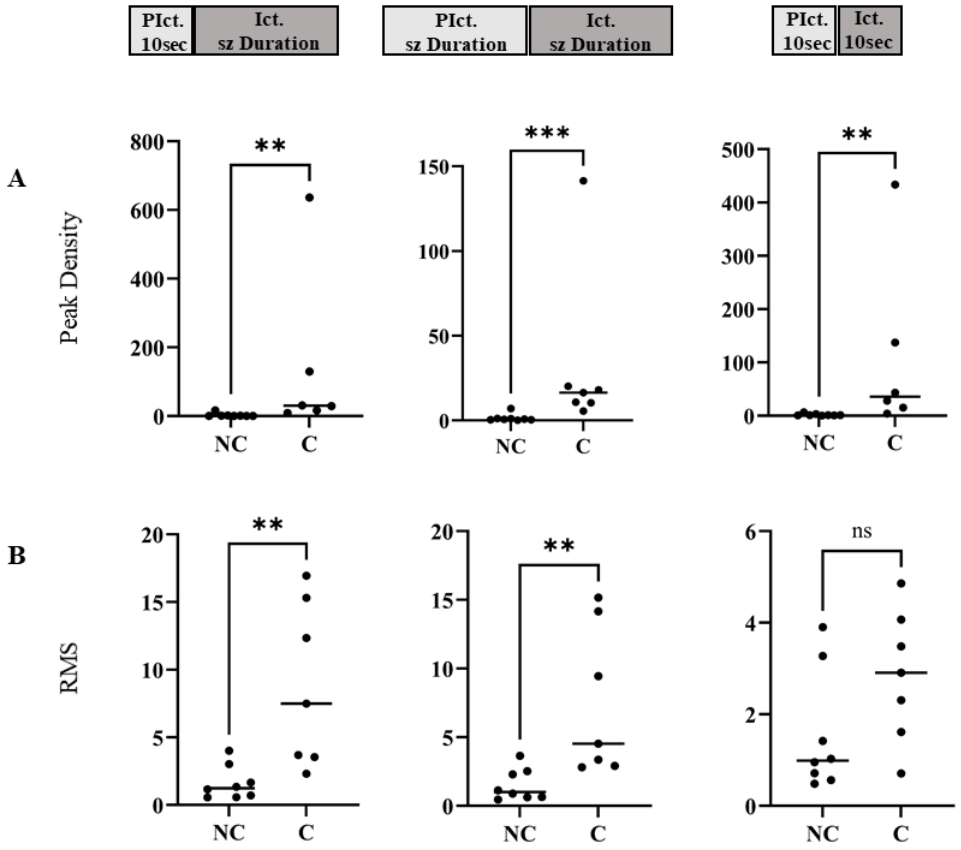

Figure 17. Comparison of Ictal/Pre-Ictal Ratios of Spike Density and RMS Between Convulsive and Non-Convulsive Seizures. The columns represent the three distinct signal extraction methods. The first row (A) shows the ictal/pre-ictal ratio for Spike Density, and the second row (B) shows the ictal/pre-ictal ratio for RMS. Statistical comparisons between convulsive (C) and non-convulsive (NC) seizures were performed using the Mann–Whitney U test. Non-significant results are indicated as "ns," while statistically significant differences are denoted as ** ($p < 0.01$) and *** ($p < 0.001$).

Motion artifacts and EMG contamination: challenges in vagus nerve recording

VNA has been studied in rodents to extract cardiac or respiratory biomarkers (239, 245, 267, 277) and to explore its role in epilepsy (253, 257, 258, 269, 278, 327). Most studies have been conducted under anesthesia due to the susceptibility of peripheral nerve recordings to movement artifacts. Additionally, the small diameter of the rodent vagus nerve (approximately 100 µm in mice, 250-500 µm in rats) complicates electrode placement and stable recordings (245, 260). Due to its size, achieving precise electrode placement is

challenging, and the recorded signals are susceptible to contamination from movement artifacts and interference.

To date, only Falcone et al. (2020) and Miki et al. (2025) have characterized VNA in awake rodents. Falcone et al. developed a method for chronic VNA recordings in mice using wrappable microwires implanted around the cervical vagus nerve (260, 272). Although movement artifacts were reduced by placing the animals in restraining tubes, contamination remained during active periods. The authors used dual thresholds for CAPs detection and artifact rejection to address this, allowing chronic recordings over extended periods. Miki et al. recorded cervical VNA in freely moving conscious rats, focusing on the interaction between vagal and sympathetic nerve activities. They introduced levobupivacaine via a microcatheter to perfuse the nerve locally, primarily blocking voltage-gated sodium channels and inhibiting both motor A and sensory C fibers to isolate efferent VNA. However, large electrical potentials from neck movements, such as chewing, were identified as movement artifacts, which were distinguished from neural signals by a decrease in spike count. Offline spike sorting using principal component analysis was applied to remove noise and enhance signal quality. Both studies demonstrated the feasibility of chronic VNA recordings in awake rodents using different artifact mitigation strategies, though movement-related contamination persists, warranting further refinement (260, 272).

Given the challenges of minimizing movement artifact contamination, we implemented a dual-electrode approach, allowing identification and removal of in-phase peaks shared by both pairs of electrodes, thereby enhancing the distinction between neural signals and external interference (*Figure 14.A*). Additionally, to further reduce EMG contamination, a bandpass filter with a lower cutoff frequency extended to 500 Hz was applied (328). Our recordings successfully captured neural activity, as demonstrated in *Figures 14.C* and *14.D*. CAPs with similar waveform durations to those reported in the literature, including Falcone et al., were observed (260). Additionally, during sleep, respiratory modulation of VNA was evident, mirroring patterns previously described under anesthesia, further supporting the reliability of our approach (255, 258).

Increased spiking activity during wakefulness: Contributions of fiber type

Evidence from preclinical and clinical studies suggests that ANS reflexes are influenced by behavioral states, particularly during sleep (286, 329). During NREM sleep, parasympathetic activity increases while sympathetic activity

decreases, leading to a reduction in HR and BP, reflecting a shift toward parasympathetic dominance (286). Heart rate variability (HRV), a key indicator of sympathetic-parasympathetic balance, supports these findings by showing heightened parasympathetic activity during NREM sleep (287). In contrast, wakefulness is predominantly characterized by sympathetic activity, while vagus nerve involvement is principally engaged in rapid adjustments, such as baroreflex responses to BP fluctuations (286). Although we expected increased VNA during NREM sleep, our results showed a decreased activity during sleep relative to wakefulness (*Figure 15.A*).

The observed increase in vagal activity during wakefulness may be influenced by the fiber type recorded by our electrode. The vagus nerve consists primarily of unmyelinated C-fibers (70–90% of afferent and efferent fibers), involved in visceral sensory and autonomic functions (330, 331). While the remaining myelinated A- and B-fibers contribute to parasympathetic regulation, A-fibers are particularly involved in mediating rapid reflexes and motor input, while B-fibers convey parasympathetic output (193, 332). Our electrodes record CAPs, which reflect the summed activity of individual fibers, with amplitudes influenced by fiber diameter (333). Consequently, our recordings likely captured activity from large, myelinated fibers, which primarily relay parasympathetic information associated with sudden physiological changes occurring during wakefulness. In contrast, during sleep, homeostasis is maintained with minimal rapid fluctuations, resulting in reduced firing of these fibers. Unmyelinated C-fibers, which predominantly convey visceral sensory and autonomic information, may be more active during sleep. Since our electrodes are less sensitive to these smaller fibers, their contribution to vagal activity could be underestimated, explaining the observed differences between sleep and wakefulness.

This hypothesis is further supported by findings from studies reporting elevated VNA during wakefulness. Smets et al. 2022 observed increased VNA during the light phase, characterized by longer periods of sleep and reduced activity in rodents, using microcuff electrodes (326). Falcone et al. 2020 reported larger VNA during wakefulness compared to anesthesia in mice, using wrappable microwires for chronic recordings (260). Given that myelinated fibers constitute less than 10-30% of total vagal fibers, their selective recruitment during wakefulness, and greater likelihood of being detected by the electrodes likely explain the observed trend.

Finally, a potential limitation of our approach lies in the thresholding method for peak detection. Signal amplitude is lower during sleep than wakefulness; the

fixed detection threshold, based on the mean RMS amplitude over 24 hours, may exclude smaller peaks during sleep, underestimating VNA. However, the chosen fixed threshold over 24 hours allows a fair statistical comparison of awake/sleep-detected peaks.

Increased spiking activity during seizures

Previous studies have demonstrated that VNA is modulated during acute induced seizures, with seizure-related alterations in vagal activity, which were successfully identified as biomarkers for detection (255, 257, 269, 278). Harreby et al. demonstrated that PTZ-induced seizures disrupt both cardiac-related VNA and overall vagal tone, and seizure detection was achieved by extracting the cardiac component of VNA (269). In contrast, more recent methods, such as spike detection and CAP analysis based on template matching, focused on capturing global vagal signals, encompassing both afferent and efferent activity (257). Both approaches successfully identified seizure-related modifications in VNA, achieving 100% sensitivity and specificity in detecting seizures (257, 269). Stump et al induced acute convulsive tonic-clonic seizures through systemic injection of PTZ (257), and these findings were further explored under anesthesia in the intrahippocampal KA model, characterized by non-motor seizures. In this study, the focus lay on respiratory-driven VNA, emphasizing the loss of rhythmicity in the respiratory pattern during seizures (258). This approach achieved 92.9% accuracy. However, 7 out of 20 seizures were undetected, hypothetically explained by possible variations in seizure propagation to the CAN, influencing vagus nerve modulation (258). In line with this interpretation, our findings suggest that non-convulsive seizures might also be associated with a reduced recruitment of central autonomic structures, as indicated by the lower ictal/pre-ictal modulation in spike density and RMS compared to convulsive seizures.

Importantly, none of these studies were conducted in awake animals with spontaneous seizures. Our results suggest a similar trend, with increased vagal activity during spontaneously occurring seizures. However, recordings in freely moving animals introduce additional challenges, as pre-ictal states cannot be strictly controlled, and movement artifacts may impact vagus nerve signal quality, particularly during convulsive seizures. Half of our recorded seizures were Racine stage 1–2 (178), with minimal motor manifestations. In contrast, the remaining seizures exhibited pronounced convulsions, likely amplifying motion-related artifacts and EMG contamination despite using extraneural control electrodes and a band-pass filter (500–8000 Hz). To mitigate this confound, we applied different windowing strategies, including a 10-second

ictal window, minimizing the impact of excessive movement. The consistent modulation of VNA, as evidenced by the increased CAPs density and RMS amplitude across different extraction methods, further supports its potential as a reliable physiological marker of seizure dynamics.

Moreover, Pearson correlation between V1 and V2 did not significantly differ between pre-ictal and ictal windows, indicating that larger contamination or movement artifacts did not drive increased vagal activity.

Nonetheless, the limited number of recorded seizures restricts the robustness of our conclusions. The limited number resulted from different factors: of the 9 initial rats, only 4 completed the entire experiment. Additionally, fewer seizures were observed during the recording periods compared to literature reports (168, 170), highlighting different experimental challenges. Importantly, the observed variability in peak density across seizures appears to reflect the heterogeneous nature of seizure types, as convulsive and non-convulsive events likely induce distinct levels of vagal activation. However, given the small sample size, seizure-type specific analyses were not feasible in the present study.

2.6. Conclusion

In conclusion, this preliminary study establishes the feasibility of recording VNA in freely moving rats. It identifies a trend of increased VNA during spontaneous seizures, suggesting its potential as a biomarker for seizure detection. However, significant challenges related to movement artifacts and the selective recording of specific fiber types were encountered. Further investigations with larger datasets are essential to validate these findings.

2.7. Contribution

Elena Acedo Reina1†, Enrique Germany Morrison†, Javier Chávez Cerda, Elise Collard, Ayse S. Dereli, Anne Vanhoestenberghe, Antoine Nonclercq, Riëm El Tahry, Modulation of Vagus Nerve Activity During Spontaneous Recurrent Seizures in the Kainic Acid Rat Model of Temporal Lobe Epilepsy.

CHAPTER 5 : Discussion

This chapter is organized into three main sections. The first two provide focused discussions on the limitations specific to acute and chronic experimental approaches, respectively, while the final section offers a general discussion relevant to both methodologies. Although the results of the acute and chronic studies conducted within the framework of this thesis have been discussed in their respective chapters, this chapter aims to synthesize the main findings, elaborate on additional limitations, and explore the practical implications of this work, as well as potential future directions.

1. Acute experiments

The primary objective of this acute study was to extend and validate previous findings from the PTZ model using a more physiologically relevant model of epilepsy under anesthetized conditions. A key motivation was to eliminate the confounding effects associated with systemic PTZ administration, particularly the potential early and widespread activation of brainstem structures, which may account for the consistently early VENG modulation observed prior to cortical seizure onset in that model. This led to the central question: Is VNA modulated during KA-induced seizures under anesthesia, and can specific signal features be identified to support reliable seizure detection? Among 20 seizures induced in six anesthetized rats, 13 were successfully detected using the VENG-based algorithm, with a mean detection latency of 25.3 ± 13.5 seconds relative to EEG-defined seizure onset, which is notably longer than the latencies reported in previous studies using the PTZ model. In the remaining 7 seizures, no discernible modulation of the VENG signal was observed, neither visually nor algorithmically, resulting in failed detection. Notably, these undetected events were also associated with weaker cardiac changes, consistent with reduced autonomic engagement.

Although this detection rate may appear lower than what has been reported in the PTZ model, where 100% sensitivity was achieved (e.g., 5/5 seizures in Stumpp et al., 2021; 8/8 in Harreby et al., 2011), direct comparisons must be interpreted cautiously given the fundamental differences between the two models in seizure type, pathophysiological mechanisms, and the neuroanatomical distribution of epileptiform activity. PTZ induces generalized seizures characterized by widespread cortical and subcortical hyperexcitability, including prominent involvement of brainstem autonomic

centers, which are key contributors to the modulation of the VENG signal. In contrast, the intrahippocampal KA model used in our study induces focal seizures, initially confined to limbic structures. Only a subset of these seizures may secondarily generalize and engage central autonomic networks such as the insula, amygdala, or brainstem nuclei. The absence of VENG modulation in some seizures may thus reflect their strictly focal character, with limited recruitment of structures involved in autonomic regulation.

Furthermore, seizures in our KA model were generally mild, remaining below stage 2 of the Racine scale and lacking overt motor signs such as forelimb clonus or rearing. In contrast, PTZ-induced seizures typically present as generalized tonic-clonic episodes (stages 4–5). This difference in severity may suggest more restricted propagation in the KA model, potentially limiting the engagement of circuits involved in autonomic control. Consequently, weaker or absent modulation of vagal activity may reflect a lack of recruitment of downstream autonomic pathways. While this hypothesis is consistent with the lower detection performance observed, it remains speculative in the absence of direct recordings from central autonomic structures. Future investigations targeting brainstem nuclei could clarify how seizure propagation affects vagal output. This approach is feasible, as demonstrated in a recent paper published by Chia-Chu Chiang et al (334). Using simultaneous recordings from the hippocampus, cortex, NA, and vagus nerve, the study showed that seizure-induced bradycardia occurred only when seizures propagated to the NA and was accompanied by increased activity in both the nucleus and the vagus nerve.

Finally, the potential influence of the anesthetic agent on seizure propagation and autonomic reactivity cannot be excluded, as anesthesia may dampen both cortical excitability and downstream autonomic responses. Additionally, the stimulation parameters used to induce seizures (e.g., KA dose and volume) might further influence seizure generalization and VENG modulation. Future studies should aim to incorporate additional readouts from central autonomic structures, such as the NA or NTS, to directly correlate parasympathetic outflow with VNA changes and refine our understanding of autonomic recruitment during focal seizures.

1.1. Sources of seizure-related VNA modulation

1.1.1. Afferent pathway

The vagus nerve is composed predominantly of afferent fibers, which convey sensory information from visceral organs to the brain. These afferents play a central role in conveying sensory information from cardiovascular and respiratory systems to the brain, and are known to drive a substantial portion of VNA. Specific components of the VNA signal have been linked to cardiac, respiratory, and baroreceptive inputs, underscoring the physiological relevance of these afferent pathways. Further supporting this afferent contribution, Miki et al. (2025) showed that pharmacological blockade of afferent conduction using levobupivacaine led to a marked reduction in VNA. Following administration, the VNA signal decreased and stabilized at approximately 84% below the pre-administration level, indicating that the majority of basal VNA is attributable to afferent inputs.

Respiratory afferents constitute a prominent component of the vagal nerve, both in terms of signal contribution and fiber composition. A substantial proportion of vagal fibers are involved in respiratory regulation, particularly through pulmonary baroreceptors capable of relaying mechanical deformation of the lungs during respiration. Given this, the respiratory afferent input likely represents a major contributor to the ictal modulation observed in our VENG recordings. However, as respiratory parameters were not recorded in our experimental design, we were unable to directly correlate respiratory activity with vagal nerve fluctuations. Since our seizure detection algorithm is based on modulation of the respiratory component, this aspect will be addressed in more detail in section 1.2.3: Respiratory Dysfunction During KA-Induced Seizures Under Anesthesia.

Ictal Modulation of VNA in Relation to HR Changes

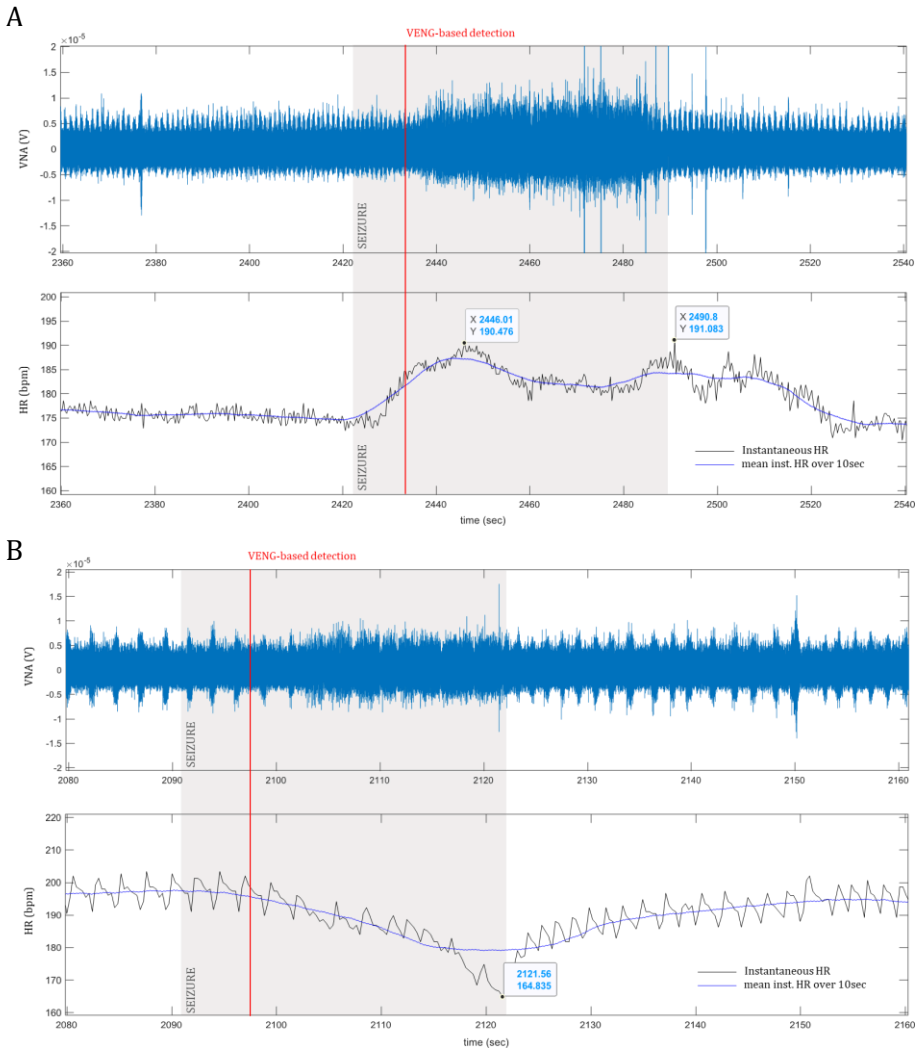

Figure 18. Representative examples from two different rats illustrating ictal autonomic modulation patterns associated with either (A) tachycardia or (B) bradycardia. In each panel, the upper trace shows the VENG signal (vagal nerve activity), expressed in volts (V), and the lower trace shows heart rate dynamics in beats per minute (bpm), including both the instantaneous heart rate (black) and a 10-second sliding window average (blue). The gray shaded area indicates the ictal period, defined by seizure onset and offset based on scalp EEG. The vertical red line marks the time of seizure detection based on VENG activity.

In addition, the cardiac afferent component accounts for a substantial proportion of the vagal signal, particularly through sensory feedback from the heart. This feedback may be a key contributor to seizure-related vagal modulation. Prior studies have reported early heart rate changes at seizure onset, notably ictal tachycardia, further supporting the role of cardiac afferents in vagal-based seizure detection. In our study, one of six rats exhibited seizures exclusively associated with tachycardia (5 seizures), while the remaining animals showed heart rate changes of varying intensity, exclusively in the form of bradycardia. These cardiac fluctuations are likely reflected in the VENG signal. In the case of ictal tachycardia, an increase in firing frequency of vagal afferents may be expected, as baroreceptors detect more frequent cardiac contractions. Notably, in *Figure* 18, VENG modulation and vagal-based detection often coincide with changes in heart rate, whether tachycardia or bradycardia, suggesting a temporally coupled relationship between cardiac dynamics and vagal activity.

This temporal pattern may partly explain the longer detection latencies observed in our study compared to previous work, potentially reflecting delayed recruitment of central autonomic structures and a later onset of autonomic responses relative to seizure onset. However, this remains speculative, as we did not record direct activity from central autonomic nuclei or the sympathetic nervous system. Interestingly, Naggar et al. (2022), using urethane-anesthetized rats and KA-induced seizures of greater severity, showed that sympathetic tone was elevated during all seizures (241). However, during ictal tachycardia, sympathetic activation predominated over total autonomic output (i.e., sympathetic + parasympathetic), whereas during bradycardic seizures, parasympathetic activity was comparatively higher (241).

Finally, we observed that vagal activity tended to return to baseline by the end of the seizure, while heart rate recovery was typically slower. Among the 13 seizures successfully detected by our algorithm, 10 exhibited persistent heart rate fluctuations following seizure offset, with a mean delay of 24 ± 8 seconds to return to baseline values. In the example shown in *Figure* 18.A, heart rate required over 30 additional seconds to normalize, suggesting that cardiac afferent input alone does not fully account for the VENG modulation observed during seizures. This delayed cardiac recovery relative to vagal activity was also reported by Stumpp et al. (2021), where a similar pattern was observed in 4 out of 6 seizures (335).

Depending on the cardiovascular response, seizures could theoretically induce distinct arterial pressure dynamics, which may in turn differentially influence vagal nerve activity, particularly through its afferent component. For instance, in the case of ictal bradycardia, one might expect a decrease in arterial pressure due to reduced cardiac output. This hypotensive response could reduce baroreceptor activation, potentially leading to a decrease in afferent vagal input. Conversely, in the case of ictal tachycardia, increased heart rate and cardiac output could result in elevated arterial pressure, especially if accompanied by peripheral vasoconstriction. Such a hypertensive response could enhance the activation of arterial baroreceptors, potentially resulting in increased afferent signaling through the vagus nerve. A third possibility involves a blood pressure increase independent of heart rate, driven by central sympathetic activation. This scenario could similarly lead to baroreceptor-mediated increases in vagal afferent discharge.

Although speculative in our case, previous studies support such mechanisms. Yambe et al. reported a significant increase in vagal nerve discharges in response to rising blood pressure (243), and Ghazavi et al. observed concurrent increases in CAP frequency and amplitude with hypertensive episodes (248). These findings suggest that ictal hypertension could contribute to increased vagal afferent activity.

Interestingly, prior work has shown that arterial pressure may peak near seizure termination and remain elevated postictally, while vagal activity may have already returned to baseline. This temporal dissociation could imply that multiple afferent sources beyond blood pressure (69, 104) contribute to ictal vagal modulation. However, due to the absence of direct arterial pressure recordings in our protocol, these interpretations remain hypothetical and might be explored in future studies.

Regardless of the nature of the peripheral change, whether respiratory, cardiac, or blood pressure-related, these signals are detected by viscerosensory receptors (e.g., baroreceptors, chemoreceptors, stretch receptors) and transmitted centrally via the afferent fibers of the vagus nerve. These afferents project to the NTS, the primary integrative hub for visceral sensory input. From the NTS, information is relayed to several key structures of the CAN, including the PBN (parabrachial nucleus), PVN, amygdala, IC, PAG, NA, and DMV. This network integrates afferent input and coordinates autonomic output via both parasympathetic (vagal) and sympathetic pathways. During seizures, the extent and nature of this activation likely depend on the specific physiological systems recruited. This bidirectional circuit between peripheral organs and the brain

forms the basis of the VENG signal fluctuations observed during ictal episodes. However, in the absence of direct recordings from CAN structures or sympathetic activity, these mechanisms remain hypothetical and warrant further investigation through combined central and peripheral autonomic monitoring.

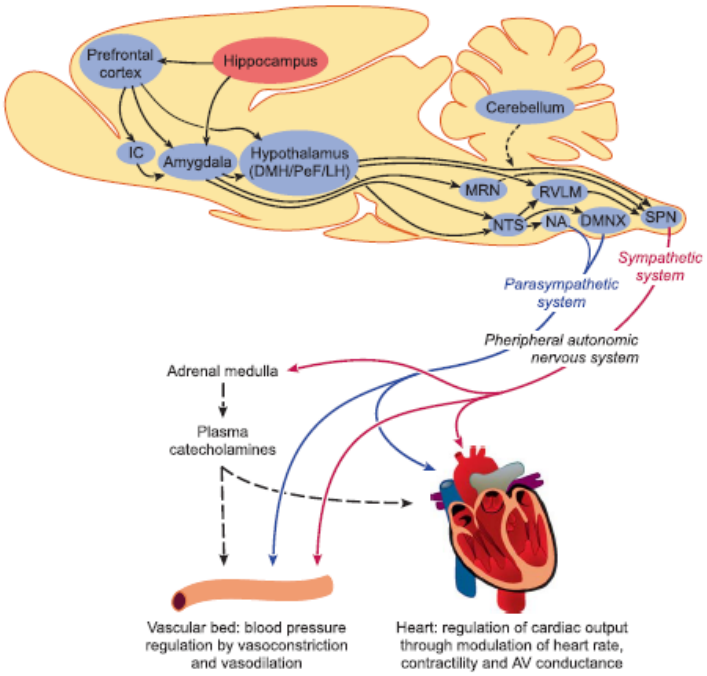

Figure 19. Schematic representation of the central autonomic network (CAN) and its projections to peripheral targets. Blue structures indicate key CAN nodes integrating viscerosensory input and coordinating autonomic output. The hippocampus (red) is shown as a modulatory structure relevant to seizure-induced autonomic changes. Parasympathetic efferents (blue) from the NA and DMNX modulate cardiac, pulmonary, and gastrointestinal function, while sympathetic efferents (red) also target the adrenal medulla, contributing to humoral regulation via catecholamine release. These circuits underlie the autonomic responses observed during seizures, including those reflected in vagus nerve activity (VENG). Figure extracted from: Stiedl, O. and T. Hager (2017). Cardiovascular Conditioning: Neural Substrates (336).

1.1.2. Efferent pathway

In addition to afferent signaling, vagal efferents, originating primarily from the NA and the DMNX, account for approximately 20% of the total vagal fibers and constitute the parasympathetic output to peripheral targets. These fibers exert a broad range of autonomic effects, including modulation of heart rate. During seizures, activation of vagal efferences may result in ictal bradycardia,

hypotension, or gastrointestinal dysregulation, depending on the intensity and anatomical spread of central autonomic recruitment. Parasympathetic outflow is orchestrated through the CAN, which integrates cortical and subcortical inputs, particularly from the hippocampus, amygdala, insula, and hypothalamus, and projects to the NA and DMNX via the NTS and the RVLM (*Figure* 19).

In our model, seizures originate in the hippocampus, a key structure within the CAN, making it plausible that ictal activity could recruit parasympathetic efferent pathways. Consistent with this hypothesis, the majority of recorded seizures in our dataset exhibited ictal bradycardia, supporting vagal efferent engagement. This interpretation is further corroborated by recent findings from Chia-Chu Chiang et al. (334), who demonstrated that seizure-induced bradycardia was contingent on seizure propagation to the NA and was temporally associated with increased activity in both the NA and the vagus nerve.

As illustrated in *Figure* 18.B, even in cases presenting with bradycardia, a temporal delay is consistently observed between seizure onset and the initiation of heart rate deceleration. This delay coincides with the latency in VENG modulation and likely accounts for the reduced sensitivity of early detection algorithms relying on vagal signals. Notably, while vagal activity tends to return to baseline shortly after seizure termination, heart rate recovery is markedly slower, suggesting that VENG dynamics are not solely determined by cardiac efferent control. This temporal dissociation implies that additional physiological signals, beyond direct cardiac modulation, contribute to the observed VENG profile. Moreover, given the anatomical composition of the vagus nerve, where efferent fibers represent only ~20% and are primarily unmyelinated axons, it is unlikely that the overall VENG signal is predominantly driven by efferent activity. Rather, the majority of the recorded signal likely reflects the activity of large-diameter afferent fibers, conveying viscerosensory input from multiple organ systems.

1.2. Major Limitations

1.2.1. Anesthetics

In order to maintain experimental consistency with previous studies using the PTZ model (257, 269), anesthesia in the present work was induced using a combination of ketamine and xylazine. Ketamine, the principal agent in this combination, acts primarily as a dissociative anesthetic via non-competitive inhibition of N-methyl-D-aspartate (NMDA) glutamate receptors. These

receptors are widely distributed throughout the CNS and peripheral tissues, and their **postsynaptic blockade** disrupts ascending sensory transmission from the periphery to the cortex, resulting in profound analgesic and anesthetic effects (337, 338). In addition to NMDA antagonism, ketamine modulates monoaminergic, cholinergic, and opioid neurotransmission, further enhancing its anesthetic and analgesic properties (337, 339).

Significantly, ketamine typically induces cardiovascular activation, characterized by increased blood pressure and heart rate, effects commonly attributed to its sympathoexcitatory properties. Beyond this peripheral activation, growing evidence indicates that ketamine may also modulate central autonomic pathways. In vitro studies have shown that ketamine inhibits nicotinic cholinergic receptor-mediated excitation of cardiac preganglionic parasympathetic neurons in the NA, both by reducing presynaptic neurotransmitter release and by suppressing postsynaptic ligand-gated inward currents. These findings suggest that ketamine may attenuate parasympathetic cardiac output, thereby contributing to its autonomic profile. However, as these effects have been observed primarily under in vitro conditions, their broader physiological relevance within intact autonomic circuits remains to be clarified (312).

Xylazine, an α2-adrenergic receptor agonist, complements ketamine by increasing sedation, analgesia, and muscle relaxation (337). However, xylazine also produces dose-dependent cardiovascular and respiratory depression, with higher doses associated with bradycardia, hypotension, pulmonary edema, and in severe cases, respiratory failure (340). Thus, although the ketamine/xylazine combination offers practical advantages, such as rapid induction and reliable surgical anesthesia, the cardiovascular depressant effects of xylazine may confound autonomic measurements and compromise experimental outcomes that require hemodynamic stability. Moreover, the lipophilic nature of both ketamine and xylazine renders their pharmacokinetics susceptible to physiological variables, such as age-related increases in adiposity, low-grade systemic inflammation, and metabolic alterations, which introduce interindividual variability in anesthetic depth (340).

By contrast, urethane (ethyl carbamate), widely employed in neurophysiological research, including studies involving systemic KA administration, provides stable and long-lasting anesthesia with minimal suppression of cardiorespiratory and spinal reflexes (341). Unlike conventional anesthetics that primarily potentiate GABAergic neurotransmission, urethane exhibits a distinct pharmacodynamic profile, exerting a moderate, nonspecific

modulatory effect across multiple ion channels. Specifically, it enhances the activity of inhibitory GABA_A, glycine, and nicotinic acetylcholine receptors, while concurrently attenuating excitatory currents mediated by NMDA and AMPA receptors (341). In addition to these postsynaptic effects, urethane also exerts **presynaptic actions**, such as the suppression of glutamate release at specific cortical and hippocampal synapses, which may contribute to its anticonvulsant properties (342-344).

Although urethane is often described as preserving autonomic reflex pathways, findings on its cardiovascular effects remain inconsistent. Some investigations have reported reductions in HR and arterial pressure under urethane anesthesia, suggestive of partial autonomic suppression, whereas others have found no significant alterations, indicating preserved reflex integrity (345).

Notably, in models of anaphylactic hypotension, urethane-anesthetized rats exhibit attenuated increases in renal sympathetic nerve activity (RSNA) and HR relative to conscious counterparts, indicating a blunted but not abolished sympathetic response (346). Importantly, this attenuation is substantially less pronounced than that observed under ketamine-xylazine anesthesia, suggesting that urethane affords a higher degree of autonomic preservation (346). Consistently, pharmacological assessments of baroreceptor reflex function have shown that urethane moderately suppresses baroreflex-mediated sympathetic activation during hypotensive challenges. However, this suppression is again milder than that seen with pentobarbital or ketamine-xylazine (346). Collectively, these findings support the view that urethane exerts a more modest inhibitory influence on central autonomic regulatory circuits than other commonly used anesthetic agents.

In contrast, urethane appears to preserve parasympathetic function. Comparative studies have demonstrated its ability to maintain cardiac vagal tone and preserve ventilatory responses to hypoxic and hypercapnic stimuli, particularly at lighter anesthetic depths (341, 347). Remarkably, spontaneous B-fiber activity in the cardiac vagal branch has been reliably recorded only under urethane anesthesia, underscoring its unique capacity to sustain parasympathetic neural integrity (347).

Importantly, it is crucial to note that autonomic effects under urethane may vary considerably across species. In mice, urethane has been reported to exert more pronounced alterations in autonomic reflexes than in rats, suggesting species-specific sensitivity of central autonomic circuits to anesthetic modulation (345). These findings underscore the critical importance of model

selection and highlight substantial variability in anesthetic responses across species, strains, and individual animals. Moreover, the application of urethane in experimental research is severely constrained by its toxicological profile. Its carcinogenic and mutagenic properties, slow metabolic clearance, and poor recovery characteristics render it unsuitable for survival surgeries or studies requiring postoperative recovery and longitudinal follow-up (348).

Direct comparisons between urethane and ketamine/xylazine during KA-induced seizures further underscore the distinct anesthetic profiles previously described. Although both anesthetics allow for the generation of robust electroencephalographic seizure activity, their motor manifestations differ markedly (285). Under urethane anesthesia, animals exhibit minimal or absent motor convulsions. In contrast, ketamine/xylazine anesthesia is associated with prominent motor convulsions, with EMG activity tightly coupled to periodic electrographic discharges.

This divergence may reflect differences in the underlying mechanisms of action of the two anesthetic regimens on excitatory and inhibitory neurotransmission. Urethane's broad-spectrum modulatory profile is thought to include both enhancement of inhibitory GABA_A and glycine receptor function, as well as potential presynaptic suppression of glutamate release, particularly within cortical and hippocampal circuits (342-344). This combination may attenuate the propagation of seizure-related excitation to downstream motor pathways, thereby limiting motor expression. In contrast, ketamine's selective, non-competitive antagonism of NMDA receptors primarily exerts a postsynaptic blockade of excitatory input, while leaving other excitatory and motor circuits relatively unaffected.

Thus, the relative preservation of glutamatergic signaling outside NMDA-dependent pathways under ketamine/xylazine anesthesia may facilitate the propagation of epileptiform activity to spinal and muscular systems, contributing to the more prominent motor convulsions observed (285). In contrast, urethane appears to suppress seizure-related motor activity while still preserving robust electrographic features (285).

In conclusion, while urethane offers substantial advantages for acute neurophysiological investigations, particularly through its preservation of autonomic and respiratory reflexes and minimization of movement artifacts, its toxicological risks and incompatibility with survival studies render it unsuitable for the broader objectives of the present work, which include the transition toward chronic experimental paradigms. The use of

ketamine/xylazine was therefore chosen to maintain consistency with previous PTZ studies (257, 269), ensuring comparable anesthetic biases and physiological conditions. Although ketamine/xylazine introduces some autonomic depression (322) and variability compared to urethane, it remains a widely accepted anesthetic for both acute and chronic procedures. Nevertheless, future investigations comparing urethane and ketamine/xylazine in the modulation of vagal nerve activity during seizures could provide valuable insights into the influence of anesthetic regimens on the detection and characterization of autonomic biomarkers of epilepsy.

1.2.2. Seizure severity

In awake animals, KA is typically administered either systemically (IP) or locally (intracerebral injection), depending on the experimental objective. Systemic administration often follows the protocol described by Hellier et al., where animals receive repeated IP injections of 5 mg/kg KA at hourly intervals until SE is achieved (>10 seizure/h or >4 convulsive seizures/h, during at least 3h) (155, 158, 168). Alternatively, some studies use a single high-dose systemic injection to induce SE, although this approach is associated with high mortality rates (161, 349). In contrast, intracerebral administration is commonly performed at relatively consistent concentrations across studies, typically around 0.4 µg in 0.2 µl, which reliably induces SE with significantly lower mortality (144, 146, 147).

Few studies have systematically examined KA-induced seizures under general anesthesia (120, 241, 284, 285, 350). Existing research in anesthetized models has primarily employed high systemic doses of KA to induce prolonged seizure activity consistent with status epilepticus. For instance, Saito, Sakamoto, and Naggar et al. administered KA intra-arterially at doses ranging from 10 to 12 mg/kg, which elicited severe seizures and frequently resulted in animal mortality, as reported by Naggar et al. (2022) (120, 241, 285). Although such models successfully generate intense epileptiform discharges, they may interfere with the interpretation of subtler neural or autonomic responses due to the extent of neuronal recruitment.

In the present study, we applied the same intracerebral KA dose typically used in awake models (146). Notably, unlike previous studies, anesthesia was induced with ketamine, a non-competitive NMDA receptor antagonist with well-documented antiepileptic properties (299, 338, 351, 352). Given that KA exerts its excitotoxic effects largely through NMDA receptor activation, the use of ketamine may have attenuated seizure severity by limiting excitatory drive and altering seizure dynamics (353, 354). This pharmacological interaction

likely constrained the spread and duration of seizure activity, potentially reducing recruitment of brain regions involved in autonomic regulation.

Supporting this interpretation, a recent study using urethane anesthesia in rats administered a substantially higher KA dose (1–2 µL of a 10 mg/mL solution) into the hippocampus, aiming to induce severe, often fatal seizures to investigate cardiorespiratory disruptions during SUDEP (308). Compared to our approach, which used a lower KA dose under ketamine-xylazine anesthesia, the severity of seizures in that model was markedly greater. However, direct comparisons are limited by differences in anesthetic regimens, as urethane is known to better preserve autonomic and respiratory reflexes than ketamine-xylazine. Still, these findings underscore the importance of both KA concentration and anesthetic choice in shaping seizure severity and associated autonomic outcomes.

Furthermore, it remains possible that the KA dose we used, although standard in awake conditions, was insufficient under ketamine-xylazine anesthesia to induce seizures robust enough to engage central autonomic circuits. Future work may need to adjust KA concentration or consider alternative anesthetic regimens to better balance seizure induction with preservation of autonomic readouts and physiological stability.

1.2.3. Respiratory dysfunction during KA-induced seizures under anesthesia

The first group of 13 seizures was characterized by a noticeable disruption in the rhythmicity of respiration-related VENG bursts during seizures. The majority of this group (10 out of 13 seizures) exhibited a reduction in the mean amplitude during seizures, averaging 5.04 ± 3.44 µV. In contrast, a subset of seizures (3 out of 13) showed an increase in VENG signal amplitude, averaging 56.23 ± 41.17 µV. The algorithm accurately detected all 13 seizures, consistent with these observed amplitude shifts.

The main limitation of our study lies in the absence of direct respiratory recordings, which restricts our ability to validate these findings physiologically. While the algorithm successfully detects rhythmicity changes, we cannot correlate them with actual breathing dynamics or confirm them via respiration extracted from video recordings. However, previous studies have established that respiration-related bursts in the VENG signal are predominantly generated by myelinated vagal efferent fibers (254), particularly pulmonary stretch-sensitive mechanoreceptors. These bursts are closely linked to lung inflation: larger tidal volumes during deep inspirations produce bursts of higher

amplitude and broader width, while increased respiratory frequency results in smaller, narrower bursts due to reduced lung stretch. Thus, the observed amplitude decreases in 10 out of 13 seizures may reflect rapid breathing or hyperventilation, indicative of seizure-induced disruption of respiratory rhythmicity. Conversely, the three seizures showing increased amplitude might correspond to periods of deeper inspiration.

This interpretation aligns with findings by Jefferys et al. (2019), who reported pronounced respiratory alterations, specifically, hyperpnea, in rats receiving intrahippocampal KA injections under urethane anesthesia (308). In that study, the respiratory rate more than doubled during seizures, increasing from 97.5 ± 30.0 to 226.0 ± 91.2 breaths per minute (308). However, it is essential to note that the KA dose used in their protocol was substantially higher (1–2 µL of a 10 mg/mL solution), and urethane anesthesia was employed, which better preserves autonomic function compared to ketamine-xylazine. These methodological differences limit direct comparison but nevertheless support the idea that KA-induced seizures can trigger significant respiratory alterations, including rapid breathing patterns consistent with the reduced VENG burst amplitudes observed in our study.

Notably, the majority of seizures in our study were accompanied by bradycardia rather than tachycardia, suggesting a different profile of autonomic and respiratory dysfunction. In general, seizure-associated bradycardia is more likely to result from apnea or severe hypoventilation. Transient cessation of breathing leads to rapid oxygen desaturation and carbon dioxide accumulation, which in turn activate peripheral chemoreceptors in the carotid and aortic bodies (355). This can trigger powerful vagal reflexes, resulting in a marked slowing of heart rate. Indeed, another plausible explanation for the observed disruption in respiration-related rhythmicity is the occurrence of apnea during seizures. Both central and obstructive apneas have been described in similar models (44, 307, 308). In the same study by Jefferys et al. (2019), transient apneas occurred in nearly all animals, most commonly showing features of airway obstruction (308). Sakamoto et al. further noted that excessive respiratory secretions during seizures can cause respiratory distress resembling asphyxia, which activates both the sympathetic and parasympathetic systems. The resulting increase in arterial CO_2 stimulates vagal outflow, while elevated sympathetic tone and blood pressure may further amplify vagal activity through baroreceptor feedback (120).

This convergence of parasympathetic activation and respiratory dysfunction may contribute to the suppression of spontaneous respiratory rhythmicity

observed in the VENG signal. As general vagal nerve activity increases, driven by chemoreceptor and baroreceptor feedback, the dominance of efferent autonomic signaling may mask or override the more phasic respiration-related bursts originating from pulmonary stretch receptors. This mechanism could explain the loss of distinct respiratory rhythmicity in the signal during bradycardic seizures.

2. Chronic experiments

The primary objective of this chronic study was to assess the feasibility of VNA recordings in awake, freely moving epileptic rats and to examine whether vagal nerve activity is modulated across behavioral states and during spontaneous seizures in the KA model of TLE. This work aimed to address the current lack of data on vagal dynamics in freely behaving epileptic animals, particularly during spontaneous ictal events, by developing a stable neural interface for chronic autonomic monitoring in a preclinical model of epilepsy. Accordingly, the central question was: can VNA be reliably recorded in a chronic, pathological context, and does it show distinct modulation during sleep/wakefulness and seizures?

Our findings provide a positive argument that chronic VNA recordings are feasible in this setting. A dual-electrode configuration, comprising an intraneural linear probe and an extraneural microelectrode placed in parallel, was successfully implemented, enabling longitudinal VNA monitoring with preserved signal fidelity and neural origin. Despite a limited number of spontaneous seizures and a relatively short overall recording duration, we were able to detect state-dependent variations in VNA, with significantly higher CAP density during wakefulness compared to NREM sleep. In contrast, no significant difference in CAP density was observed between pre-ictal and ictal periods. However, RMS values were significantly elevated during seizures, and this effect could not be attributed to movement artifacts, as shown by the stable Pearson correlation between intraneural and extraneural signals across pre-ictal and ictal segments. These results suggest an increase in overall VNA amplitude during seizures, potentially reflecting autonomic disturbances linked to ictal dynamics.

To our knowledge, this study is the first to report chronic VNA recordings in a rodent model of epilepsy with spontaneous recurrent seizures. Although prior studies have demonstrated the feasibility of chronic autonomic recordings in healthy animals, such as in restrained awake mice (Falcone et al., 2020) and

freely moving rats with autonomic recordings (Miki et al., 2025), none have extended this approach to the context of epilepsy. While our results remain preliminary due to the limited sample size and number of recorded seizures, they represent an initial step toward characterizing seizure-related vagal modulation in a physiologically relevant and translational model.

Several methodological and experimental considerations will be addressed, including the choice of the Wistar strain and the high mortality and seizure variability observed. We will also discuss the impact of ictal motor behaviors on chronic recordings, the likely origin of recorded vagal fibers, and the interpretive limits of CAP-based measures. Finally, we will assess our dual-electrode strategy and suggest improvements for future chronic VNA recordings.

2.1. Elevated mortality and inconsistent seizure expression in the Wistar strain

In the present study, epilepsy was successfully induced in all Wistar rats (n = 9) via systemic KA administration. However, high mortality was observed throughout the protocol: only six rats survived the initial induction and stabilization period, and of these, four survived the subsequent electrode implantation procedure, resulting in a final survival rate of 44%. Notably, this was achieved with a relatively low number of KA injections (2.3 ± 0.75), corresponding to a mean cumulative dose of 11.5 ± 3.75 mg/kg, substantially lower than the doses reported in the original Hellier protocol (155). During earlier stages of optimization, mortality reached up to 60% in certain cohorts. Despite the extended latency period of five months following SE induction, the number of seizures recorded during chronic monitoring remained limited. Across all four animals and a total of 14 cumulative days of video-EEG monitoring, only 15 seizures were captured. The average seizure duration was 56.4 ± 23.4 seconds. Among these, 8 seizures were classified as non-convulsive (stage 1–2), and 7 were convulsive (stage 4 tonic-clonic seizures). These findings suggest a relatively low seizure frequency in the chronic phase, which may reflect a combination of strain-dependent sensitivity, KA dosing, and inter-individual variability in epileptogenesis.

Given the extended latency required between SE induction and the chronic recording phase, intrahippocampal KA administration, despite its advantages of reduced systemic toxicity and lower mortality, was not compatible with the constraints of our experimental design. This approach would have required a two-stage surgical protocol: an initial implantation of a hippocampal cannula for KA injection, followed by a second intervention after the epileptogenic

period to place intraneural vagus nerve electrodes and scalp EEG leads. However, the long-term recording stability of intraneural electrodes in this context remains insufficiently validated. Chronic implantation of such interfaces is known to elicit biological responses, including local inflammation, perineural gliosis, and fibrotic encapsulation, which can progressively increase electrode impedance and degrade signal quality. These risks are particularly relevant given the technical sensitivity and low-amplitude nature of vagus nerve signal acquisition. To minimize surgical burden and reduce confounding factors associated with long-term interface degradation, systemic KA administration was selected as the most practical and least disruptive approach for this chronic protocol.

In the literature, systemic KA administration has been associated with a reported mortality rate of approximately 22%, compared to around 5% for intrahippocampal injections (144). However, these figures primarily derive from studies conducted in Sprague Dawley rats, which are the most commonly used strain in the systemic KA model. Wistar rats, by contrast, have consistently been reported to exhibit higher mortality and variability in SE expression following systemic KA administration (158, 356, 357).

Bertoglio et al. (2018) directly compared the effects of the standard Hellier protocol in Sprague Dawley and Wistar rats (158). Among 15 Sprague Dawley rats, all entered SE without mortality during the first four hours, and only one animal died two days post-SE, corresponding to a 7% mortality rate. In contrast, in the Wistar group (n = 6), four rats died within the first four hours following SE induction, and an additional animal died from SE-related complications three days later, yielding an 83% mortality rate. All animals were age-matched and received comparable KA doses under the same protocol, reinforcing the influence of genetic background on KA sensitivity (158).

To reduce mortality in Wistar rats, Bertoglio et al. proposed a modified KA protocol based on an initial injection of 7.5 mg/kg, followed by additional doses of 2.5 mg/kg every 30 minutes after a 45-minute delay (158). This adaptation led to more comparable SE severity between the two strains and reduced early mortality in Wistar rats. Nevertheless, even under this modified protocol, substantial differences remained between strains in the development and expression of chronic epilepsy. Specifically, Sprague Dawley rats exhibited a shorter latent period and a significantly higher frequency of SRS during the chronic phase compared to Wistar rats, with seizure rates of 6.78 SRS/day versus 0.46 SRS/day, respectively (158).

Despite the widespread use of the KA model in preclinical epilepsy research, a high degree of variability persists in reported outcomes, including mortality rates, KA dosing requirements, latency to SRS onset, and seizure frequency. These inconsistencies are shaped not only by strain-dependent factors but also by experimental design and seizure detection methods. For instance, many studies restrict quantification to convulsive seizures (Racine stage 4–5), while early or focal seizures of lower severity (stage 1–2) often go unreported in the absence of intracranial EEG monitoring.

Van Nieuwenhuyse et al. (2015) evaluated the progression of epileptogenesis in Sprague Dawley rats over 30 weeks following systemic KA-induced SE, observing a sigmoid increase in seizure frequency from 1.0 ± 0.2/day (week 2) to a plateau of 24.4 ± 6.4/day by week 30, reached around 122 ± 9 days post-SE, with considerable interindividual variability (168). In contrast, Bertoglio et al. (2017) reported lower seizure rates: 6.78 seizures/day in Sprague Dawley rats and 0.46 seizures/day in Wistar rats, recorded between weeks 8 and 10 post-SE using epidural electrodes, which reflects earlier stages of seizure progression and highlights strain-dependent differences in chronic seizure burden (158).

Altogether, these findings reinforce the observation that inter-strain and intra-strain differences significantly influence the expression of SE and the trajectory of chronic epilepsy development in the KA model. Wistar and Sprague Dawley rats, as outbred strains, exhibit high genetic heterogeneity, which may partially explain the variability in KA sensitivity, seizure severity, and chronic seizure frequency (158, 358-360). Environmental and epigenetic factors, including vendor origin, housing conditions, handling, and stress exposure, are additional contributors to the heterogeneity observed within and between experimental cohorts (158, 358-360).

2.2. Major limitation: How to deal with movement artefact?

The KA model of temporal lobe epilepsy was used in both acute and chronic experiments of this thesis. While acute experiments are typically conducted under anesthesia, thereby minimizing movement and enabling stable recordings, chronic protocols introduce significant differences and substantial experimental challenges, particularly the presence of severe motor manifestations during seizures, which generate significant motion artifacts. Peripheral nerve recordings, including the vagus nerve, are especially sensitive to such perturbations due to their inherently low-amplitude signals and high impedance interfaces (260, 272). Achieving an adequate signal-to-noise ratio under chronic, awake conditions remains technically demanding. To date, only

a limited number of studies have attempted long-term peripheral nerve recordings in awake animals (260, 272).

The KA model was selected for its translational relevance. It reproduces key neuropathological features of human TLE, is associated with autonomic dysfunction, and models one of the most pharmacoresistant epilepsy subtypes (140). However, seizures induced by systemic KA typically originate focally and often secondarily generalize to produce convulsive tonic-clonic seizures. These seizures involve pronounced motor activity, which presents a major limitation for stable peripheral nerve recording due to movement artifacts as well as EMG artifacts produced by muscle contraction during tonic phases.

To mitigate these constraints, several strategies can be considered. Technical refinements, including optimization of the electrode design, improved mechanical stability at the nerve-electrode interface or recording setup, and enhanced artifact rejection through advanced signal processing, may significantly improve recording fidelity and signal-to-noise ratio. The choice of animal model may also warrant reconsideration. Since convulsive motor seizures generate considerable movement artifacts, models characterized by non-convulsive seizure phenotypes could provide a more stable behavioral context for high-fidelity peripheral nerve electrophysiological recordings.

2.2.1. Model reconsideration

Although most chronic epilepsy models, such as those based on chemoconvulsants or electrical kindling, are associated with convulsive motor seizures, genetic models of absence epilepsy represent a compelling alternative. The Wistar Albino Glaxo from Rijswijk (WAG/Rij) and GAERS strains exhibit frequent, spontaneous, and stereotyped generalized non-convulsive seizures. These seizures are characterized behaviorally by brief episodes of behavioral arrest and electrographically by bilateral spike-and-wave discharges on cortical EEG. The minimal somatic movement during these events significantly reduces motion-induced artifacts, thereby facilitating high-fidelity recordings of seizure-related modulation of VNA and other peripheral signals.

The GAERS model, extensively characterized since 1982, has been shown to closely recapitulate key features of idiopathic generalized epilepsy (IGE), including childhood absence epilepsy (CAE). This common pediatric epilepsy syndrome is typically not eligible for surgical treatment (361). Absence seizures are also a defining feature of other IGE syndromes such as juvenile absence epilepsy, juvenile myoclonic epilepsy, and myoclonic absence epilepsy

(362, 363). Importantly, evidence from human studies indicates that autonomic dysregulation is also present in IGE. Shaker et al. (2021) reported that both TLE and IGE patients exhibit signs of disrupted autonomic regulation, including interictal abnormalities in HRV, BP response, and sympathetic skin conductance. Furthermore, episodes of ictal tachypnea and bradypnea have been observed in children with CAE, supporting the hypothesis that absence seizures can transiently impair central autonomic control (364). However, Shaker et al. (2021) also demonstrated that the frequency and severity of autonomic dysfunction are significantly greater in patients with TLE compared to those with IGE (361). This is likely due to the central role of the temporal lobe in regulating the CAN. Experimental data indicate that epileptogenic activity originating in the temporal lobe can propagate to subcortical and brainstem structures involved in autonomic regulation. Chronic TLE is also associated with structural pathology, including neuronal loss and sclerosis in regions such as the hippocampus and amygdala, which are integral to CAN function. Consistent with these findings, multiple studies have reported a higher proportion of seizures accompanied by autonomic changes in TLE relative to extra-temporal seizure types (82, 85, 87, 361). Although genetic absence epilepsy models provide a favorable framework for minimizing motion artifacts in peripheral nerve recordings, the more robust association between TLE and autonomic dysregulation underscores the clinical relevance of TLE models for investigating seizure-related autonomic disturbances and evaluating neuromodulation strategies.

2.2.2. Detection of focal seizure in the KA model of TLE

Importantly, seizures in the KA model of TLE are typically focal in origin and may subsequently generalize across broader brain regions. As a result, a proportion of seizures may remain confined to limbic structures and thus only be detectable using intracerebral electrodes, particularly within the hippocampus as performed by Raedt et al (2009) or Van Nieuwenhuyse et al (2015) (146, 168). This highlights a key limitation of the present study, namely the absence of usable intrahippocampal recordings to reliably identify focal seizures of lower severity and reduced motor expression. Therefore, rather than necessitating a change in the animal model, future work should prioritize the integration of high-quality depth electrode recordings within the existing setup to enhance seizure detection sensitivity. Although all animals were initially implanted with intrahippocampal electrodes, signal quality was insufficient for inclusion in the final analyses. This was evidenced by signal amplitudes that did not align with the expected values from the literature, minimal modulation in relation to behavioral state or scalp-detected seizure

activity, and the absence of ictal discharges characteristic of hippocampal recordings. Notably, such hippocampal-restricted ictal activity had been previously observed in the representative animal described in Chapter 5, further suggesting a technical limitation rather than a biological absence of focal seizures.

Importantly, implementing functional depth electrodes would not only improve the detection of focal seizures but could substantially increase the overall seizure count captured during chronic recordings. This may help explain the low seizure incidence observed in our animals after 5 to 6 months of latency following SE induction. Moreover, the ability to detect focal, non-generalized events would provide a critical benefit for the analysis of VNA by substantially increasing the number of analyzable ictal events per animal. Specifically, it would allow for comparisons of VNA modulation across a broader spectrum of ictal phenotypes, including focal seizures and secondary generalized convulsive seizures. Such an approach would greatly enhance the physiological and translational relevance of peripheral nerve recordings in epilepsy research.

2.2.3. Optimization of the recording setup for motion artifact reduction

An additional perspective for technical improvement concerns the placement of the preamplifier in the recording setup. In the current configuration, the preamplifier is positioned at the level of the slippering, and the signal is transmitted from the electrode through a cable of approximately 30 cm plug to the headcap connector. This relatively long distance between the signal source and the first stage of amplification may increase the vulnerability of the recorded signal to several sources of degradation. These include mechanical artifacts induced by the animal's movement, electronic interference from the surrounding environment, and possible impedance mismatches along the transmission path. This is particularly problematic when recording low-amplitude signals such as those generated by the vagus nerve, which are especially sensitive to noise and distortion.

Repositioning the preamplifier directly onto the animal's head, close to the electrode, could help mitigate these issues. Amplifying the signal as early as possible in the acquisition chain may reduce the impact of noise and improve the SNR, thereby enhancing the reliability and interpretability of the recordings.

However, implementing this solution in our setup would raise several engineering challenges, including how to power the preamplifier, how to

Method	Metric	Total seizure (n=15)				Convulsive seizure (n=7)			
		Pearson's r	dz	Required sample size	Achieved power	Pearson's r	dz	Required sample size	Achieved power
M1	Spike Density	-0,35	0,437	61	0,471	0,21	1,832	6	0,993
	RMS	0,49	0,729	23	0,83	0,543	1,148	11	0,828
M2	Spike Density	-0,42	0,45	58	0,488	0,383	1,809	6	0,992
	RMS	0,46	0,701	25	0,808	0,496	1,126	11	0,816
M3	Spike Density	-0,22	0,492	49	0,548	-0,086	1,687	6	0,984
	RMS	0,49	0,432	63	0,463	0,858	1,234	10	0,873

Table 4. Summary of statistical analyses for three extraction methods (M1–M3) and two signal metrics (Spike Density, RMS), assessed on total seizures (n = 15) and convulsive seizures (n = 7). For each condition, Pearson's correlation coefficient (r), the standardized effect size for matched pairs (dz), the required sample size to achieve 80% statistical power, and the achieved post hoc power are reported. All analyses were conducted in GPower 3.1.9.7 using the t-test family (means: Wilcoxon signed-rank test for matched pairs).

minimize its weight to avoid affecting the animal's behavior, and how to ensure the mechanical stability of the headstage. I believe that these aspects could be effectively addressed in collaboration with biomedical engineers and that such refinements represent a valuable direction for improving signal quality in future experiments.

2.3. Post Hoc Analysis and Power Estimation

Given the limited sample size and the heterogeneity of seizure types, our findings should be interpreted as preliminary. To evaluate whether our dataset was adequately powered to detect reliable effects and to assess the robustness of our results, we performed post hoc power analyses on two signal metrics, root mean square (RMS) amplitude and spike density, extracted using three different segmentation methods. Analyses were conducted across all seizures (n = 15), including both convulsive and non-convulsive events, as well as separately for convulsive seizures only (n = 7), which typically exhibited more pronounced fluctuations in vagus nerve activity.

For each metric, we report Pearson's correlation coefficient (r), the standardized effect size for paired data (dz), the estimated sample size required to achieve 80% statistical power, and the achieved post hoc power. All analyses were performed in G*Power (version 3.1.9.7) using the t-test family with the Wilcoxon signed-rank test for matched pairs. A complete summary of these results is presented in *Table 4*.

Effect sizes and post hoc power estimates provide useful benchmarks for evaluating the robustness of our findings. For paired-sample effect sizes (dz), which represent a version of Cohen's d adapted for within-subject designs, values around 0.2 are typically considered small, 0.5 medium, and 0.8 or higher large (365). Correlation coefficients (r), which range from 0 to ±1, can be interpreted similarly: values <0.20 are generally considered poor, 0.30–0.49 moderate, 0.50–0.79 strong, and >0.80 excellent, with values near ±1 indicating a perfect linear relationship (366). Statistical power, defined as $1 - \beta$, represents the probability of correctly detecting a true effect; low power increases the risk of a Type II error, i.e., failing to detect an effect that actually exists.

2.3.1. All seizure together

Across all seizures (n = 15), RMS consistently outperformed spike density in terms of effect size and post hoc power across all three extraction methods, although the limited sample size prevented reaching the estimated number of seizures required for 80% power:

- Method 1 RMS: Moderate-to-large effect (dz = 0.73, r = 0.49), post hoc power 83%; estimated 23 seizures required for 80% power, which exceeds the available 15 seizures.
- Method 2 RMS: Comparable effect (dz = 0.70, r = 0.46), post hoc power 80.8%; estimated 25 seizures needed, again above the current sample.
- Method 3 RMS: Weakest performance (dz = 0.43, r = 0.49), post hoc power 46%; 63 seizures would be required for sufficient sensitivity.
- Spike density (all methods): Small-to-moderate effect sizes (dz = 0.45–0.49), low power (47–55%), large estimated sample size requirements (49–61 seizures), indicating that the current dataset was underpowered to reliably detect these effects.

2.3.2. Convulsive seizures

For convulsive seizures only (n = 7), RMS again generally outperformed spike density, though the very small sample limited the achievable power:

- Method 1 RMS: Moderate effect (dz = 1.15, r = 0.54), post hoc power 82.8%; estimated 11 seizures required for 80% power, slightly above the available 7 seizures.
- Method 2 RMS: Similar effect (dz = 1.13, r = 0.50), post hoc power 81.6%; estimated 11 seizures needed, above the current sample.
- Method 3 RMS: Strong effect (dz = 1.23, r = 0.86), post hoc power 87.3%; estimated 10 seizures required, still exceeding the 7 available.
- Spike density (all methods): Small-to-moderate effects (dz = 1.69–1.83, r = −0.09–0.38), very high effect size values but limited reliability due to low sample size; estimated seizures required ranged 6–7, highlighting that although effect sizes were large, power estimates may be unstable with this small n.

2.3.3. Interpretation

When considering all seizures together (n = 15), including both convulsive and less severe events, RMS generally outperformed spike density in terms of effect size and post hoc power. However, the overall power remained limited, likely due to the inclusion of less severe seizures (n = 8) that manifested primarily as brief behavioral arrests. These milder events probably recruit the central autonomic network to a lesser extent, resulting in smaller ictal vagus nerve modulation, which is consistent with our prior hypotheses from the acute phase performed under anesthesia.

Focusing exclusively on convulsive seizures (n = 7), which are more severe, both RMS and spike density exhibited increased sensitivity and statistical power. For RMS, the number of available seizures was sufficient to reach near-optimal power, whereas spike density required only a few additional events to achieve comparable levels (~95% power). These results suggest that pooling only the more severe seizures can enhance the robustness of VENG-based metrics, particularly for RMS.

Despite these advantages, RMS remains inherently more susceptible to contamination from movement artifacts or background noise due to its reliance on signal amplitude. In contrast, spike density provides a temporally discrete and more artifact-resistant measure, though it may fail to capture subtle or distributed neural events. Consequently, while RMS offers increased statistical sensitivity, its physiological specificity must be interpreted with caution. A combined approach using both metrics may therefore provide a more balanced assessment of ictal autonomic dynamics, optimizing both sensitivity and specificity depending on the analytic context.

CHAPTER 6 : Conclusion

In this thesis, two complementary studies were conducted to characterize genuine VNA modulation during epileptic seizures. The ability to reliably detect and quantify VNA changes in this context holds significant translational potential, particularly for the development of more precise and adaptive closed-loop VNS systems. Current closed-loop paradigms, which primarily rely on abrupt cardiac changes, often suffer from limitations in sensitivity and specificity, thereby constraining their clinical efficacy.

By investigating VNA dynamics in relation to seizure onset and propagation, this work supports the emerging notion that peripheral autonomic signatures, specifically efferent vagal output, may serve as valuable complementary or alternative biomarkers for seizure detection. Unlike cardiac-based metrics, which are often confounded by non-epileptic influences such as physical activity or emotional stress, direct recordings from the vagus nerve may provide a more robust and seizure-specific correlate of ictal events.

Furthermore, given the vagus nerve's integrative role in relaying signals across multiple organ systems, it offers a unique vantage point for capturing widespread autonomic alterations associated with seizures. These features position VNA as a promising physiological biomarker for enhancing both sensitivity and specificity of closed-loop neuromodulation strategies.

The primary goal of the *First Study* was to evaluate the feasibility of detecting seizure-related autonomic changes by analyzing VNA in an acute, anesthetized rat model of intrahippocampal KA-induced seizures. This work aimed to determine whether VNA modulation could serve as a physiologically relevant signal for seizure detection, thereby informing future closed-loop VNS strategies.

Two main hypotheses were tested:

(1) That non-convulsive seizures induced by focal KA injection would propagate to CAN structures and lead to measurable changes in VNA.
(2) That specific features of VNA, particularly respiratory-modulated components of the VENG signal, could be extracted and used to detect seizures with high accuracy.

Our findings support both hypotheses. First, we demonstrated that hippocampal seizures, even under anesthesia and in the absence of motor manifestations, were associated with transient but detectable modulations of VNA, confirming the recruitment of central autonomic pathways. Second, we showed that respiratory-derived features of the VENG signal allowed for automated seizure detection, achieving a detection accuracy of 92.9% with a mean delay of approximately 25 seconds. This delay may reflect the temporally coupled relationship between vagal activity and seizure-related autonomic changes; while we demonstrated such temporal association with heart rate fluctuations, other physiological parameters were not recorded, preventing a broader assessment of this coupling. Moreover, a subset of seizures was not detected, likely due to differences in their seizure spreading pattern and autonomic centers recruitment, which the anesthetic administration might influence.

Moreover, the choice of anesthetic was carefully addressed in the discussion, as ketamine/xylazine exerts multiple effects on the autonomic nervous system that may influence vagus nerve activity and introduce potential bias in the interpretation of VNA during seizures. These pharmacological influences necessitated caution in extrapolating findings to the awake state.

Building on the first study, the *Second Study* aimed to translate these initial observations into a chronic model by recording vagus nerve activity during spontaneous recurrent seizures in awake, freely moving rats. This transition introduced considerable technical challenges due to the low-amplitude nature of VNA signals, the presence of motion artifacts, and variability in physiological state. Nevertheless, the study provides important preliminary insights into the modulation of VNA across behavioral and ictal states.

Two main hypotheses were tested:

(3) VNA exhibits state-dependent modulation, with greater activity observed during sleep compared to wakefulness.
(4) VNA undergoes dynamic modulation during spontaneous focal seizures in the KA model of TLE, reflecting seizure-related autonomic disturbances.

Contrary to our initial hypothesis, CAPs density was significantly higher during wakefulness than NREM sleep. This unexpected result may be attributed to the type of fibers primarily captured by our recordings. The intraneural electrodes may likely record large, myelinated fibers, which are more active during wake-related physiological fluctuations. In contrast, unmyelinated C-fibers, more

involved in slow, homeostatic autonomic regulation during sleep, may have been underrepresented due to their lower amplitude signals. Furthermore, the application of a fixed spike detection threshold, chosen using a 24-hour RMS baseline, may have introduced systematic bias, potentially resulting in the underdetection of lower-amplitude events that predominate during sleep. This is consistent with the observation that global signal amplitude is reduced during sleep epochs relative to wakefulness, attributable in part to diminished movement-related artifacts. These factors likely contribute to the observed state-dependent variations in detected events and underscore the necessity for further refinement of both detection algorithms and recording setups.

The fourth hypothesis proposed that spontaneous focal seizures might induce detectable VNA modulation, potentially reflecting autonomic perturbations mediated by seizure propagation to CAN structures. Although no significant difference in CAPs density was observed between pre-ictal and ictal periods, RMS analysis indicated an increase during seizures. Notably, envelope Pearson correlation analyses suggested that this increase was unlikely to be explained by movement artifacts. While these findings do not conclusively confirm the hypothesis across all measured features, they offer preliminary evidence for dynamic VNA modulation during spontaneous seizures.

Several methodological refinements are warranted further to enhance the chronic electrophysiological recording component of this study. Firstly, optimization of the recording interface, particularly electrode design, remains critical. The long-term stability of the current electrode configuration requires systematic evaluation under chronic implantation conditions. Design modification, such as reducing the exposed non-insulated electrode surface area, may enhance the SNR by increasing neural signal amplitude and improving the detection fidelity of CAPs. Concurrently, refinement of the surgical implantation technique may further mitigate tissue response and mechanical instability as well as optimize electrode-to-nerve fiber proximity, thereby improving recording reliability and signal stability over prolonged recording periods.

Furthermore, rigorous validation of the recorded signals as physiological ANS activity is imperative. This can be addressed by employing controlled experimental manipulations that selectively modulate autonomic output. For instance, the application of a hypercapnic challenge via a CO_2 exposure chamber could induce reproducible autonomic reflexes, thereby serving as a physiological reference to confirm the specificity and origin of the recorded vagal nerve signals.

Lastly, the incorporation of intrahippocampal electrodes represents a promising strategy to expand the range of seizure phenotypes captured, including both focal and secondary generalized seizures. This integrative recording approach is expected to increase both the number and heterogeneity of ictal events recorded, thereby enriching the dataset and enabling a more comprehensive characterization of seizure-associated autonomic network dynamics. This setup would also facilitate comparative analyses of VNA across seizures of varying severity.

APPENDIX 1 :

From acute to chronic: Methodological optimization

1. Preface

This chapter presents the methodological transition from acute, anesthetized recordings to chronic recordings in awake animals. This transition was prompted by the observation that neural signals recorded chronically using the same extraneural cuff electrodes, previously validated under anesthesia, exhibited reduced physiological clarity and increased susceptibility to movement artifacts. Specifically, characteristic features such as respiration-related bursting and cardiac modulation became less consistently detectable in the chronic setting.

The central question addressed is whether modifying the electrode design, specifically transitioning from extraneural cuff electrodes to intraneural implantation, could improve the quality of the recorded signal under chronic conditions. We hypothesized that intraneural electrodes, due to their closer proximity to active neural fibers, would enable recordings with a higher signal-to-noise ratio compared to epineural configurations used in acute experiments.

This hypothesis was motivated by both the degradation of signal quality observed postoperatively in chronic recordings and by discrepancies with previously published findings reporting robust neural activity during early recovery phases. As a result, we developed and tested a new intraneural electrode configuration, designed not only to enhance neural selectivity but also to reduce contamination from movement artifacts and external sources.

The present chapter outlines the rationale behind this methodological shift, the experimental and technical constraints associated with chronic peripheral nerve recordings, and the preliminary results that informed the redesign. These data, although currently unpublished, formed the empirical basis for the selection of intraneural electrodes in subsequent experimental phases.

2. Introduction

Previous studies have recorded VNA in both acute and chronic settings, across

various experimental contexts, including but not limited to epilepsy models (239, 241, 242, 244-247, 249, 251-258, 260-262, 264-267, 269, 272, 273, 277, 278, 326, 367-371). A wide range of electrode types have been employed, including extraneural configurations (hook and cuff electrodes) and intraneural approaches (e.g., linear arrays or carbon nanotube yarns) (120, 241, 243-247, 277, 334). These technologies have enabled the extraction of multiple signal components from the vagus nerve, such as CAPs, respiratory-related modulations, and cardiac-synchronous bursts, each reflecting distinct physiological processes.

In the specific context of epilepsy, all VENG recordings to date have been performed in acute, anesthetized conditions, primarily using extraneural electrodes in rats or pigs to detect seizure-related changes in VNA following PTZ or KA administration. While intraneural approaches have shown promise in other fields, their use in epilepsy models remains limited, with the recent exception of the study by Chia-Chu Chiang et al. (2024), which employed CNT yarn electrodes under urethane anesthesia (334).

In our laboratory, we previously established and validated an acute recording setup in rats using epineural cuff electrodes placed around the cervical vagus nerve under ketamine/xylazine anesthesia (Stumpp et al., (255, 257)). This configuration reliably captured PTZ-induced seizure responses and distinct physiological modulations, including rhythmic bursts phase-locked to respiration and smaller events synchronized with cardiac cycles. Application of lidocaine to the nerve abolished both components, confirming their physiological origin.

However, translating this methodology to chronic recordings in awake animals proved challenging. Despite maintaining identical surgical procedures and electrode configurations, signal quality degraded rapidly after implantation. Respiratory and cardiac signatures became inconsistent or undetectable, and action potentials were no longer distinguishable from background noise. As shown in *Figure 20.A*, acute intraoperative recordings exhibited clear respiration-related bursts. In contrast, by postoperative day 2, during a segment of NREM sleep, devoid of voluntary movement, these features had disappeared, and signal amplitude was markedly reduced (*Figure 20.B*). Amplitude increases were observed only during movement (*Figure 20.C*), consistent with motion artifacts. These findings highlighted the limitations of extraneural cuff electrodes for stable long-term VENG acquisition.

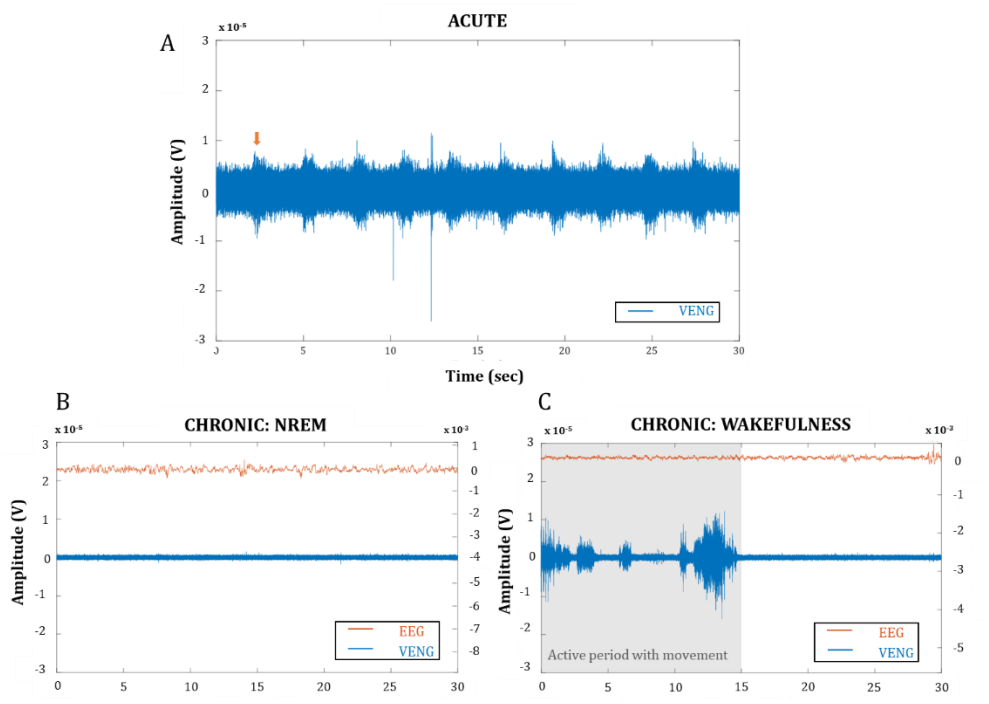

Figure 20: Comparison of acute and chronic VENG recordings in the rat. (A) Representative acute VENG trace obtained intraoperatively under anesthesia, showing pronounced respiration-related bursting activity indicated by the orange arrow. (B) Chronic VENG trace recorded on postoperative day 2 during an NREM sleep episode. At this stage, the signal exhibits markedly reduced amplitude, and respiration-related bursts are no longer distinguishable from background noise. The EEG trace is shown in red, and its corresponding scale is displayed on the right y-axis. (C) Chronic VENG trace recorded on postoperative day 2 during an awake period. During the first 15 seconds, the animal is actively moving; this time window is highlighted in grey. The y-axis scale for the VENG signal is kept consistent across all panels to allow direct amplitude comparison.

In contrast, other studies have reported successful detection of vagus nerve signals during early recovery from anesthesia, suggesting that electrode type and configuration may critically influence signal integrity. For instance, Falcone et al. (2020) reported clear CAPs and increased signal amplitude and frequency in rats emerging from isoflurane anesthesia (*Figure 21*), using tightly wrapped extraneural wires (260).

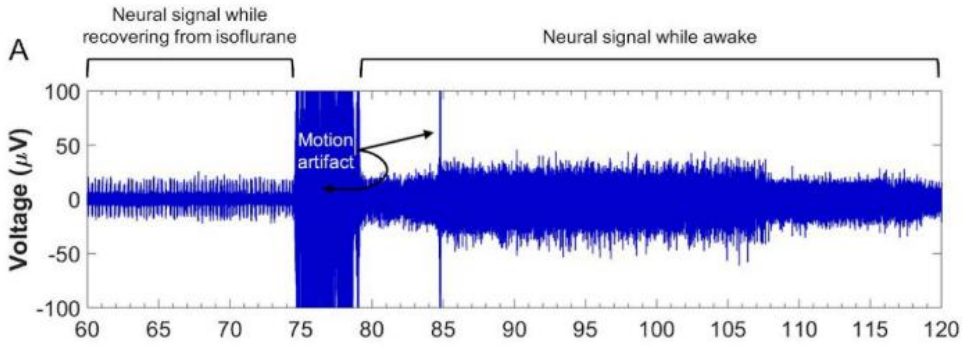

Figure 21 illustrates the impact of anesthesia on neural activity by presenting an example of neural recordings from an animal during the recovery phase following isoflurane induction. During the initial period of recovery (60 to 75 seconds), the predominant neural signal corresponds to respiratory activity. As the animal begins to regain consciousness (75 to 80 seconds), motion artifacts emerge. Subsequently, a distinct alteration in the neural signal is observed (260). Figure extracted from: Falcone, J. D., et al. (2020). "A novel microwire interface for small diameter peripheral nerves in a chronic, awake murine model."

These inconsistencies led us to explore alternative electrode strategies for chronic recordings. In this intermediate study, we evaluated the performance of multiple designs: modified extraneural cuffs with tighter nerve contact (similar to Falcone et al.)(260), sling electrodes as described by Silverman et al. (2018)(266), and intraneural platinum/iridium microelectrodes. To address limitations related to movement artifacts and external contamination, we ultimately adopted a bipolar configuration, with one electrode inserted intraneurally and the reference placed outside the nerve, extraneurally. This configuration, also implemented in a recent study by Rodríguez et al. (2025), facilitates common-mode artifact rejection and improves signal specificity in freely moving animals (372).

Only the results obtained with the intraneural configuration are presented in this section, as this approach provided superior signal quality and was selected for subsequent chronic experiments focused on vagus nerve dynamics in epilepsy.

3. Methods

3.1. Acute validation

3.1.1. Surgical procedure

Anesthesia was induced in a healthy adult Wistar rat (n = 1) using a combination of ketamine and xylazine. The animal was positioned supine, and both cervical vagus nerves were exposed via a midline neck incision. For the right cervical vagus nerve, a tripolar micro-cuff electrode (Microprobes, Gaithersburg, USA) was carefully implanted around the nerve for vagus nerve recordings. For the left cervical vagus nerve, a custom intraneural electrode was implanted by inserting two electrode contacts transversely into the nerve, spaced 4 mm apart, with non-insulated tips and a small hook at each end to ensure stable positioning. The electrode was fabricated from a 10 cm, 76.2 µm diameter PFA-coated platinum wire (AM-systems, USA), with insulation removed from both ends. This configuration enabled direct comparison of neural recordings obtained with a tripolar micro-cuff and a custom intraneural electrode (see schematic in *Figure 22).*

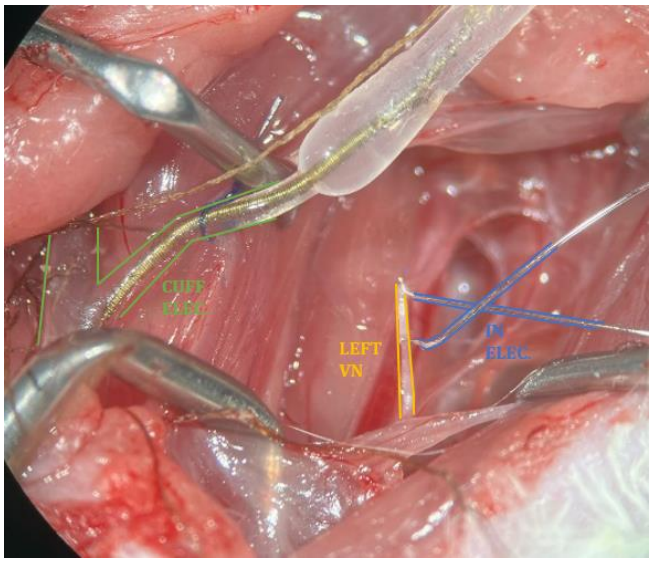

Figure 22 illustrates the surgical implantation of a cuff electrode on the right cervical vagus nerve, performed concurrently with the implantation of a bipolar intraneural linear microelectrode on the left cervical vagus nerve.

In a separate configuration, a monopolar stainless-steel electrode was inserted into the sternomastoid muscle, adjacent to the left cervical vagus nerve, to assess potential contamination of neural recordings by EMG activity.

In all configurations, a stainless-steel ground electrode was affixed to the skull using a small screw to complete the recording setup.

3.1.2. Signal acquisition

The acute recording setup enabled the simultaneous acquisition of two VENG channels. Multiple recordings were conducted under the following conditions:

1. Cuff and linear electrode comparison: Simultaneous recordings from the right and left cervical vagus nerves using the cuff and intraneural electrodes, respectively, to allow direct comparison of signal morphology between electrode types.
2. Intraneural linear Electrode and EMG Signal Recording: Assessment of Signal Contamination and Evaluation of VENG Signal Quality.

During this recording, both vagus nerve and EMG signals were acquired for several minutes under baseline conditions. Subsequently, the vagus nerve was transected caudal to the electrode to eliminate afferent neural input, and signal acquisition continued for several minutes post-transection, up to the point of the animal's death.

3.1.3. Chronic validation

Chronic recordings refer here to neural recordings performed in awake, conscious rats, freely moving without restriction. To validate the acute findings, chronic implantation of bipolar intraneural linear microelectrodes was performed in four epileptic rats under sevoflurane anesthesia.

In each animal, the left vagus nerve was exposed at the cervical segment. A custom-made bipolar intraneural electrode, with non-insulated tips and spaced 4 mm apart, was inserted transversely into the nerve. A small hook was formed to secure each electrode in position, and the external portions were covered with medical-grade silicone to ensure stability and insulation. Control extraneural electrodes, made from the same materials and with identical spacing and orientation as the intraneural electrodes, were positioned near the nerve (*Figure* 14.B).

Following surgery, the animals were placed in lab-made chronic cages, allowing continuous monitoring in freely moving conditions. Signals were acquired immediately after recovery from anesthesia and recorded for 2 to 5 consecutive days. All results from these experiments concern the modulation of vagus nerve activity during epileptic seizures. In this section, only data related to the quality and validity of the recorded signal are presented. The complete analysis of vagus nerve modulation during spontaneous recurrent seizures is provided **in**

CHAPTER 4: Modulation of VNA during spontaneous recurrent seizures in the KA model of temporal lobe epilepsy.

4. Results

4.1. Cuff and needle electrode comparison – bilateral vagus nerve implantation

Both recordings exhibited respiration-related bursting activity and comparable background noise amplitudes (*Figure 23*). Notably, ECG artifacts were clearly visible in the cuff electrode recordings, whereas such contamination was less pronounced in the intraneural electrode recordings. Additionally, the intraneural signal displayed a higher density of discrete, spike-like events, suggesting the presence of more CAPs between respiration-related modulations. The average frequency of these CAPs was approximately 7 Hz, with individual CAPs exhibiting a width between 1 and 1.5 milliseconds. However, these spiky events should be interpreted with caution, as they appear to exhibit a certain rhythmicity, although their frequency differs from that typically observed in HR-related artifacts seen in the cuff electrode recordings.

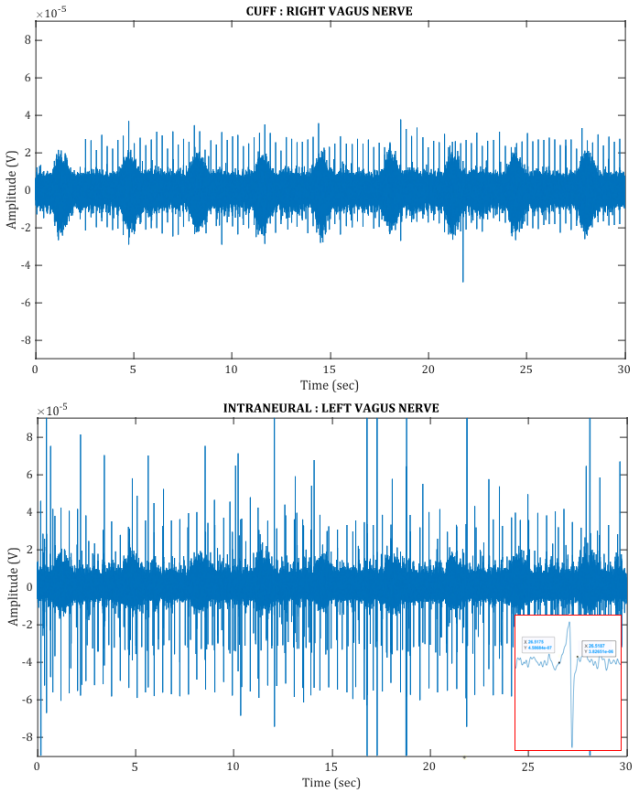

Figure 23. Simultaneous recordings from the right and left cervical vagus nerves under anesthesia, using a cuff electrode (upper panel) and an intraneural electrode (lower panel), respectively. Upper panel: VENG signals recorded from the cuff electrode exhibit distinct respiration-related bursts, accompanied by ECG artifacts that emerge a few seconds after the start of the recording. Lower panel: Intraneural recordings reveal clear respiration-related bursts as well as CAPs, characterized by their typical triphasic morphology. An enlarged view of a representative CAP is shown in the bottom right corner (highlighted in red).

4.2. Intraneural needle electrode and EMG signal recording from the left vagus nerve and sternomastoid muscle

During baseline recordings, the intraneural signal exhibited respiration-related modulation, accompanied by numerous spike-like events (*Figure 24*). These events were less repetitive and did not exhibit a clear temporal correlation with the ECG artifacts observed in the EMG signal. This lack of association with cardiac-related activity provides further evidence supporting the neural origin of these spike-like events.

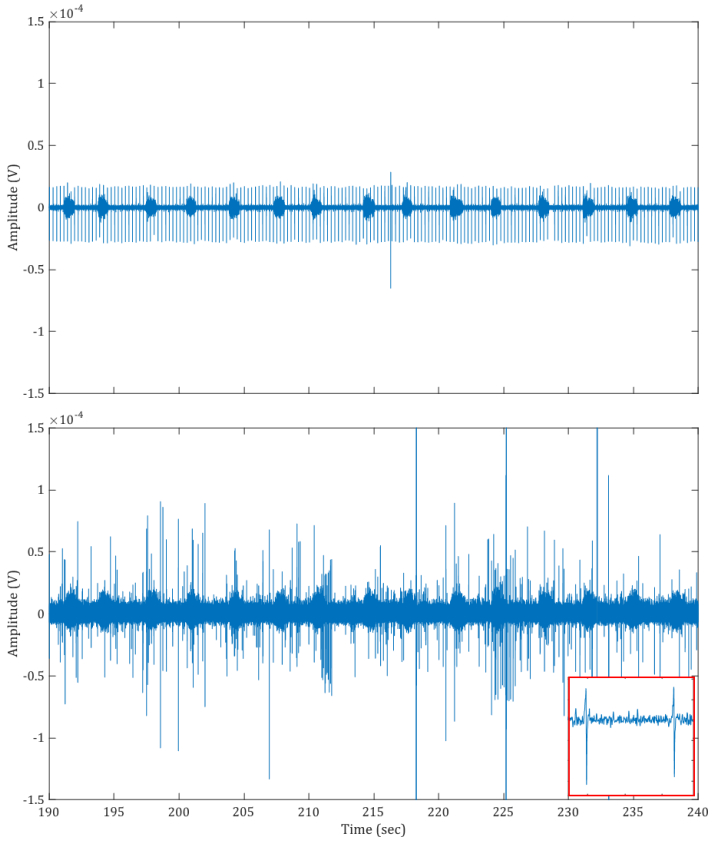

Figure 24. Simultaneous recordings of EMG activity (top panel) and intraneural VENG signals using a needle electrode (bottom panel) in a healthy anesthetized rat. Top panel: EMG recording during the baseline period under anesthesia. Respiratory and cardiac modulations are clearly observed at frequencies of approximately 24 breaths per minute and 300 beats per minute (bpm), respectively. Bottom panel: Intraneural VENG recording during the same baseline period under deep anesthesia. Respiration-related bursts are visible, along with CAPs. The CAPs exhibited a typical width of approximately 1.5 ms. An enlarged view of a representative CAP is shown in the bottom right corner(highlighted in red).

Following the 6-minute baseline recording, the vagus nerve was ligated caudal to the electrode. As expected, the EMG signal remained unaffected by the ligation (*Figure 25*). In contrast, the vagus nerve recording demonstrated a clear but progressive loss of respiration-related bursts, indicating the disruption of afferent signal propagation. Notably, the frequency and pattern of spike-like events in the intraneural recording appeared unchanged.

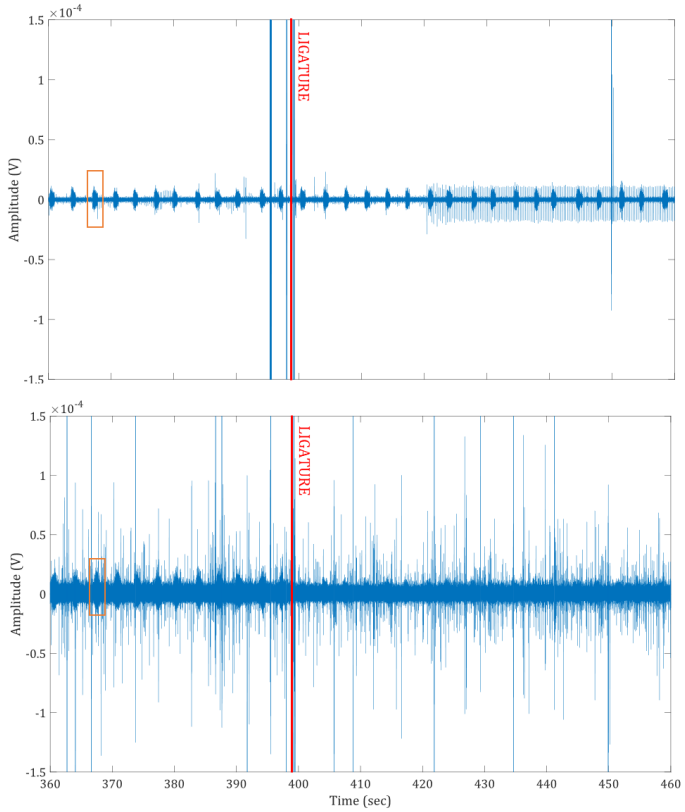

Figure 25. Simultaneous recordings of EMG activity (top panel) and intraneural VENG signals using a needle electrode (bottom panel) in a healthy anesthetized rat, following ligation of the left cervical vagus nerve caudal to the electrode (ligature time indicated by the red line). Top panel: Respiratory modulation (highlighted by the orange box) remains visible throughout the recording. Cardiac modulation becomes apparent around 420 seconds. Following ligation, respiratory rhythmicity is maintained. Bottom panel: Respiratory-related modulation is visible prior to ligation but disappears progressively afterward. In contrast, CAPs persist following ligation, indicating that descending fiber activity remains detectable at the recording site.

At 28 minutes post-ligation, the rat exhibited respiratory arrest, as indicated by the disappearance of respiration-related modulation in the EMG signal shown in the left panel (*Figure 26)*. Cardiac activity remained visible, suggesting that breathing cessation occurred prior to cardiac arrest. In comparison to baseline and immediate post-ligation recordings, the frequency of spike-like events in the intraneural VENG signal was reduced during this period of respiratory arrest.

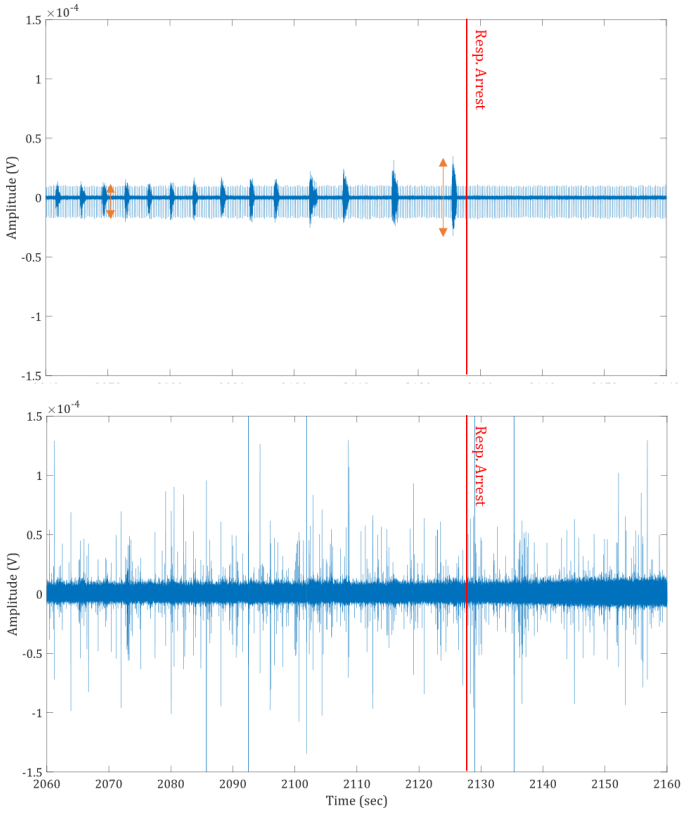

Figure 26. Simultaneous recordings of EMG activity (top panel) and intraneural VENG signals using a needle electrode (bottom panel) in an anesthetized rat during a period of respiratory arrest (highlighted by the red bar). Top panel: Respiratory modulation decreases in frequency and increases in amplitude (highlighted by orange arrows), indicating a progressive slowing of respiration accompanied by increased tidal volume. This pattern evolves into complete respiratory arrest. Cardiac modulation remains visible throughout the recording, indicating that respiratory arrest occurred prior to cardiac arrest. Bottom panel: Neural activity remains stable after the onset of respiratory arrest suggesting persistent nerve firing despite the absence of respiratory drive.

4.3. Chronic validation: Intraneural and extraneural vagus nerve recording in conscious rat

Acute findings were further validated under chronic conditions, where VENG recordings consistently exhibited distinct spike-like events during periods of non-movement NREM sleep (*Figure 27*). In recordings obtained immediately following surgery, clear respiration-related modulations were observed during NREM sleep, alongside frequent spike events. Although respiration-related modulations became less prominent two days post-surgery, the presence of spike events persisted, indicating stability of the neural signal over time.

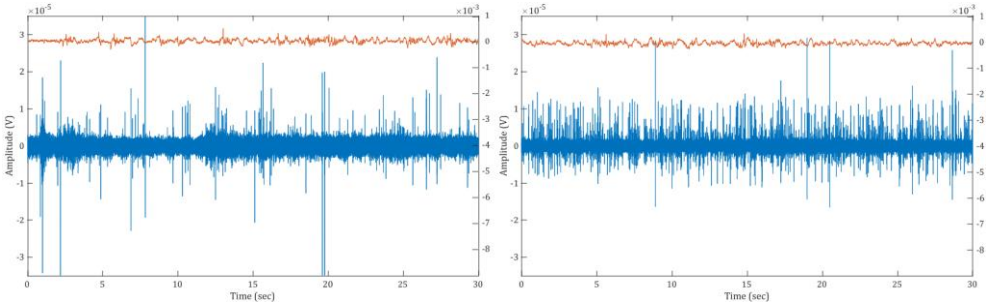

Figure 27. Chronic intraneural recordings in a conscious rat during non-rapid eye movement (NREM) sleep on Day 1 (left panel) and Day 2 (right panel) post-surgery. Respiration-related bursts are faintly distinguishable, along with identifiable CAPs. The EEG trace is shown in red, with its corresponding scale indicated on the right y-axis.

These spike-like events were typically characterized by a triphasic waveform, with an average peak-to-peak amplitude of approximately 20 μV and a duration of around 2 ms, consistent with the expected profile of CAPs.

5. Discussion

Our results demonstrate that intraneural electrode recordings provide higher-quality neural signals compared to extraneural cuff electrodes under both acute and chronic conditions. In acute experiments, both electrode types captured respiration-related modulations; however, intraneural recordings revealed a higher density of spike-like events consistent with CAP morphology and exhibited reduced contamination from external sources. Respiration-related bursts progressively disappeared following caudal vagus nerve ligation, although spike-like events persisted.

Importantly, chronic recordings using intraneural electrodes confirmed the long-term stability of these spike-like signals during low-movement states such as non-REM sleep. CAPs maintained consistent morphology and amplitude, and although respiration-related modulation faded two days post-implantation, the

persistence of neural spiking suggests that the signal remained of neural origin and did not degrade substantially over time.

5.1. Persistent Neural Activity After Vagal Nerve Ligation

Following caudal ligation and transection of the vagus nerve, we consistently observed the persistence of spike-like events in the neural recordings, even in the absence of respiration-related modulation. This observation is particularly intriguing, as the sectioning of the nerve eliminates all ascending afferent input, which should normally suppress activity if driven solely by peripheral sensory feedback. While one might hypothesize an efferent origin, given that vagal efferents comprise approximately 20% of the fiber population, this is unlikely to fully account for the sustained and intense spiking patterns observed, due to the small diameter and limited number of such fibers in rodents (272).

Instead, we propose that the persistent neural activity may reflect acute electrophysiological responses triggered by the injury itself, particularly ion flux–driven ectopic firing within axons (373). Peripheral nerve injury, including tight ligature, is known to disrupt axonal membranes, leading to a rapid influx of sodium (Na^+) and calcium (Ca^{2+}) ions (373). This ion dysregulation can trigger membrane depolarization, even in severed or isolated axon segments, thus enabling local generation of action potentials independently of synaptic or somatic inputs (373).

This mechanism has been well described in models of sciatic nerve ligation, where spontaneous activity is detected in both large and small caliber fibers shortly after injury (373). Although this has often been interpreted in the context of chronic neuropathic pain, similar ionic processes are activated within minutes to hours post-injury (373). The initial depolarization is driven by increased sodium permeability and reduced potassium conductance, further amplified by calcium-mediated second-messenger cascades (373). Calcium influx, in particular, can also enhance neurotransmitter vesicle mobilization (even in damaged terminals), activate phospholipases and kinases, and modulate ion channel sensitivity, resulting in a heightened excitability state of the damaged axon (373).

Importantly, these ectopic discharges do not require the presence of a cell body or an intact synapse and can occur locally within the nerve trunk, including in intraneural compartments far from both the periphery and the central nervous system (373, 374). Thus, in the context of our intraneural recordings, the persistence of spike-like events after vagal ligation may reflect this local hyperexcitability of damaged fibers, rather than genuine ongoing physiological

signaling (373, 374). Taken together, these findings suggest that injury-induced ionic dysregulation and axonal membrane destabilization can transiently give rise to spontaneous nerve activity, which is neural in origin but pathophysiological in nature. This has critical implications for interpreting post-injury neural signals and underscores the need for caution when attributing such activity to intact physiological processes.

From a methodological standpoint, complete nerve ligation may not represent the most physiologically appropriate strategy to abolish afferent input, as it induces acute structural disruption and profound ionic imbalance that can give rise to non-physiological, injury-related neural activity. An alternative approach, as described by Stumpp et al., involves the local application of lidocaine, a voltage-gated sodium channel blocker, which transiently and reversibly inhibits action potential propagation along both afferent and efferent fibers without causing mechanical damage (257). This pharmacological silencing preserves the structural integrity of the nerve and prevents the emergence of ectopic discharges associated with axonal injury, thereby offering a more controlled means of assessing the functional contribution of vagal signaling.

5.2. Optimizing Electrode Configuration for Chronic VENG Recordings in Rodents

Within the framework of our chronic recording paradigm, extraneural cuff electrodes failed to provide the signal fidelity required for reliable long-term analysis. While their minimally invasive nature and translational relevance are well recognized, their performance in the rodent model is limited, likely due to the small diameter of the vagus nerve, which compromises electrode-nerve coupling and reduces SNR.

To overcome these limitations, we adopted intraneural electrodes. Although more invasive and less clinically translatable, this configuration provided substantially higher SNR and improved spatiotemporal resolution, enabling the detection of neural events that were indistinguishable with cuff electrodes. In particular, spike-like events emerged above baseline noise and between respiration-related modulations, indicating enhanced sensitivity to fast neural dynamics.

These events were consistently recorded under chronic conditions in awake animals, suggesting physiological relevance and temporal stability. Furthermore, the improved resolution allowed for the dissociation of distinct components within the VENG signal, including those not phase-locked to

respiration, which were previously obscured by low SNR in cuff-based recordings.

To confirm the neural origin of the recorded signals and control for non-neuronal contamination such as motion artifacts, EMG, or ambient electrical noise, a control electrode was introduced. This electrode, matched in geometry and material, was positioned adjacent to the nerve but external to the fascicle. Its comparative use enabled the differentiation between true intraneural activity and extrinsic sources, strengthening the validity of the recorded neural signals. This configuration, also implemented in a recent study by Rodríguez et al. (2025), facilitates common-mode artifact rejection and improves signal specificity in freely moving animals (372).

Chronic intraneural implantation was successfully replicated across animals (n=4), supporting the robustness of the method and enabling its application to pathological models. In particular, it facilitated the recording of VNA during spontaneous seizures in awake animals, a key step toward identifying peripheral neural biomarkers of epileptic activity and informing the development of closed-loop neuromodulation strategies. However, while the current intraneural design proved effective over the timescale of our experiments, further optimization is warranted to improve long-term biocompatibility, mechanical stability, and signal consistency. Future studies should systematically assess both the chronic integrity of the electrode-tissue interface and the temporal stability of the recorded signals to validate the suitability of this approach for extended experimental paradigms.

Taken together, these findings demonstrate that intraneural electrodes offer a significant advantage over extraneural configurations for chronic VENG acquisition in rodents, providing the resolution and fidelity required to detect subtle and physiologically meaningful neural dynamics.

6. Conclusion

These results represent an important step toward transitioning from acute to chronic recording, with the ultimate goal of recording VNA during spontaneous seizures in awake, freely moving rats.

APPENDIX 2 :

Comprehensive Summary of Vagus Nerve Recording Research

To facilitate the identification of the different studies involving vagus nerve recordings, we compiled the following tables, originally sourced from the thesis of Lars Stumpp (defended in 2022), and updated them with the most recent studies. *Table 5* provides a summary of studies on vagus nerve recordings in the context of epilepsy. *Table 6* presents an overview of studies focused on vagus nerve recordings related to cardiovascular function, while *Table 7* highlights research on vagus nerve recordings for respiratory function. *Table 8* outlines methodological approaches for performing vagus nerve recordings. *Table 9* reviews studies investigating vagus nerve recordings in other contexts. *Table 10* details studies on vagus nerve recordings in the context of VNS. Finally, *Table 11* illustrates studies that have recorded vagus nerve activity (VNA) in humans.

Study	Species	Anesthesia	Acute/ Chronic	Electrode type	Signal type	Purpose
Sakamoto et al 2008 (120)	Rats	Urethane	acute	Linear array electrode (intraneural)	CAPs	Autonomic consequences of KA–induced seizures in rats
Harreby et al 2011 (278)	Rats	Ketamine/ xylazine	acute	Hook (extraneural)	Signal power Spectral power	Investigation of ictal and peri-ictal VNA changes during PTZ-induced seizures.
Harreby et al 2011 (269)	Rats	Ketamine/ xylazine	acute	Hook (extraneural)	crVENG	VENG-based seizure detection
Nielsen et al 2013 (251)	Pigs	Ketamine/ xylazine	acute	Cuff (extraneural)	CrVENG	Evaluation of VENG signals for detecting PTZ-induced seizures.

Table 5. Summary of studies reporting spontaneous vagus nerve electroneurogram (VENG) recordings in the context of epilepsy. crVENG: cardiac-related vagus nerve electroneurogram.

Study	Species	Anesthesia	Acute/ Chronic	Electrode type	Signal type	Purpose
Sevcencu et al 2016 (253)	Pigs	Ketamine/ xylazine	acute	Cuff (extraneural)	CrVENG	Investigation of VNA changes during ictal tachycardia in PTZ-induced seizures.
Stumpp et al 2020 (255)	Rats	Ketamine/ xylazine	acute	Cuff/Hook (extraneural)	CAP	Acute extraneural vagus nerve recording setup in rats for PTZ-induced seizures: Description and validation.
Stumpp et al 2021 (257)	Rats	Ketamine/ xylazine	acute	Cuff (extraneural)	CAP	Evaluation of VENG signals for detecting PTZ-induced seizures.
Naggar et al 2022 (241)	Rats	Urethane	acute	Linear array (intraneural)	Filtered and rectified time-averaged activity	Investigation of autonomic changes and symp./parasymp. imbalance during KA-induced seizures.

Study	Species	Anesthesia	Acute/ Chronic	Electrode type	Signal type	Purpose
Acedo Reina et al 2024 (258)	Rats	Ketamine/ xylazine	acute	Cuff (extraneural)	Respiratory-related components of global signal	VENG-based seizure detection of acute KA-induced seizures
Chia-Chu Chiang et al 2025 (334)	Rats	Urethane	acute	CNT yarn (intraneural)	SUA	Investigation of the relationship between brainstem seizures, VNA, and cardiac function during seizures.

Vagus nerve recording in cardiovascular-related functions

Study	Species	Anesthesia	Acute/ Chronic	Electrode type	Signal type	Purpose
Yambe et al 2003 (243)	Goat	None	Chronic	Needle electrode (intraneural)	CAP	Vagus nerve cardiovascular signals for potential use in artificial heart systems.
Rozman & Ribaric 2007 (259)	Dogs	Isoflurane	Chronic	Cuff (extraneural)	Spectral power	Detection of respiratory and BP related fibers in selective recording of vagus nerve for selective VNS
Plachta et al 2012 (267)	Rats	Isoflurane	acute	Cuff (extraneural)	Coherent avereging	Detection of baroreceptor fibers in the vagus nerve for optimization of selective VNS therapy of hypertension.
Sevcencu et al 2014 (252)	Pigs	Ketamine/ xylazine	acute	Cuff (extraneural)	crVENG	Investigation of changes in VNA related to BP changes.

Table 6. Summary of studies reporting spontaneous vagus nerve electroneurogram (VENG) recordings focus on cardiovascular function.

Study	Species	Anesthesia	Acute/ Chronic	Electrode type	Signal type	Purpose
Sevcencu et al 2016 (253)	Pigs	Ketamine/ xylazine	Acute	Cuff (extraneural)	crVENG	Investigation of changes in VNA in response to ictal tachycardia during PTZ-induced seizures
Marmerstein et al 2021 (245)	Rats	Isoflurane	Acute/ Chronic	CNT yarn (intraneural)	SUA	Detection of respiratory and BP related fibers in selective recording of vagus nerve for selective VNA

Vagus nerve recording in respiration-related functions.

Study	Species	Anesthesia	Acute/ Chronic	Electrode type	Signal type	Purpose
Rozman & Ribaric 2007 (259)	Dogs	Isoflurane	Chronic	Cuff (extraneural)	Spectral power	Detection of respiratory and BP related fibers in selective recording of vagus nerve for selective VNS
Sevcencu et al 2018 (254)	Pigs	Ketamine/ xylazine	Acute	Cuff (extraneural)	Spectral power	Investigation of VNA related to varied mechanical ventilation
Tavares et al 2019 (271)	Dogs	Alpha-chloralose	acute	Hook (extraneural)	Raw signal	Investigation of VNA related to apnea
Jiman et al 2020 (277)	Rats	Isoflurane	acute	Micro needle electrode array (intraneural)	SUA	Investigation of VNA related to blood glucose and respiration changes.

Table 7. Summary of studies reporting spontaneous vagus nerve electroneurogram (VENG) recordings focus on respiratory-related function.

Table 8. Summary of studies reporting spontaneous vagus nerve electroneurogram (VENG) recordings focus on proofing a methodology.

Methodological aspects						
Study	**Species**	**Anesthesia**	**Acute/ Chronic**	**Electrode type**	**Signal type**	**Purpose**
McCallum et al 2017 (244)	Rats	Isoflurane	Acute/ Chronic	CNT Yarn (intraneural)	SUA	Description of VNA recorded in chronic setup with CNT yarn electrodes
Silverman et al 2018 (266)	Mice	Isoflurane	Chronic	Cuff/Hook (extraneural)	CAP	Description and confirmation of an acute extra neural vagus nerve recording in mice
Stumpp et al 2020 (255)	Rats	Ketamine/ xylazine	acute	Cuff/Hook (extraneural)	CAP	Acute extraneural vagus nerve recording setup in rats for PTZ-induced seizures: Description and validation.
Jiman et al 2020 (277)	Rats	Isoflurane	acute	Micro needle electrode array (intraneural)	SUA	Description and confirmation of an acute intraneural vagus nerve recording setting.

Study	Species	Anesthesia	Acute/ Chronic	Electrode type	Signal type	Purpose
Ghazavi et al 2020 (248)	Rats	Isoflurane	acute	Micro needle electrode array (intraneural)	SUA	Investigation of VNA related to blood glucose and respiration changes.
Falcone et al 2020	Mice	None/isoflurane	Chronic	Cuff-like (extraneural)	CAP	Detection of respiratory and BP-related fibers in selective recording of vagus nerve for selective VNS
Marmerstein et al 2022 (247)	Rats	None	Chronic	CNT Yarn (intraneural)	SUA	Description of spontaneous spikes recorded in freely moving animals.
Miki et al 2025 (272)	Rats	None	Chronic	Hook (extraneural)	CAP	Direct Measurement and Selective Afferent Blockade of Cervical Vagal Nerve Activity in Conscious Rats

Table 9. Summary of studies reporting spontaneous vagus nerve electroneurogram (VENG) recordings in other context.

Vagus nerve recording in other contexts.

Study	Species	Anesthesia	Acute/ Chronic	Electrode type	Signal type	Purpose
Miyashita & Williams 2005 (268)	Mice	Urethane	acute	Hook (extraneural)	CAP	Investigation of vagus nerve response to arousal induced by systemic administration of epinephrine
Caravaca et al 2017 (371)	Mice	Isoflurane	acute	16-channel microelectrode (extraneural)	CAP	Recording and stimulation of the mouse vagus nerve to investigate neuroimmune regulation.
Zanos et al 2018 (273)	Mice	Isoflurane	acute	Cuff/Hook (extraneural)	CAP	Investigation of VNA changes to inflammatory reflexes provoked by cytokine injectionverifier
Shikano et al 2018 (262)	Rats	None	chronic	Cuff (extraneural)	CAP	Investigation of VNA related to different stages of locomotion and cortical arousal.

Study	Species	Anesthesia	Acute/ Chronic	Electrode type	Signal type	Purpose
Nishimura et al 2020 (263)	Mice	Urethane	acute	Cuff (extraneural)	CAP	Investigation of VNA related to capsaicin application to small intestines
Marmerstein et al 2022 (247)	Rats	None	Chronic	CNT Yarn (intraneural)	SUA	Decoding VNA during food intake: linking neural patterns to feeding behavior
Smets et al 2022 (326)	Rats	None	Chronic	Cuff (extraneural)	CAP	Circadian modulation of VNA in healthy rats

Vagus nerve recording in VNS animal studies

Study	Species	Anesthesia	Acute/ Chronic	Electrode type	Signal type	Purpose
Qing et al 2018 (264)	Rats	Isoflurane	acute	Cuff (extraneural)	CAP	Vagal fiber activation as a consistent measure of stimulation dose and a predictor of cardiac effect.
Chang et al 2020 (261)	Rats	Isoflurane	acute	Cuff (extraneural)	CAP	Investigation of vagal nerve fibers engagement by VNS.
Castel et al 2021 (265)	Sheep	None	chronic	Cuff (extraneural)	CAP	Effect of VNS in utero on various organ systems, such as immunity and inflammation
Okonogi et al 2024 (256)	Mice	None	acute	Cuff (extraneural)	CAP	VNS influence on anxiety-related behavior.

Table 10. Summary of studies reporting spontaneous vagus nerve electroneurogram (VENG) recordings in VNS animal studies.

Table 11. Summary of studies reporting acute vagus nerve electroneurogram (VENG) recordings in humans.

Vagus nerve recording in human

Study	Species	Anesthesia	Acute/ Chronic	Electrode type	Signal type	Purpose
Ottaviani et al 2020 (249)	Human	None	acute	Tungsten microelectrode (intraneural)	SUA	First recordings from the human vagus nerve using ultrasound-guided microneurography.
Patros et al 2024 (250)	Human	None	acute	Tungsten microelectrode (intraneural)	SUA	First microelectrode recordings from the cervical vagus nerve in two awake DRE patients with chronically implanted VNS systems.

REFERENCES

1. Fiest KM, Sauro KM, Wiebe S, Patten SB, Kwon C-S, Dykeman J, et al. Prevalence and incidence of epilepsy. Neurology. 2017;88(3):296-303.
2. Fisher RS, Acevedo C, Arzimanoglou A, Bogacz A, Cross JH, Elger CE, et al. ILAE Official Report: A practical clinical definition of epilepsy. Epilepsia. 2014;55(4):475-82.
3. Fisher RS, Cross JH, French JA, Higurashi N, Hirsch E, Jansen FE, et al. Operational classification of seizure types by the International League Against Epilepsy: Position Paper of the ILAE Commission for Classification and Terminology. Epilepsia. 2017;58(4):522-30.
4. Blumenfeld H. What Is a Seizure Network? Long-Range Network Consequences of Focal Seizures. In: Scharfman HE, Buckmaster PS, editors. Issues in Clinical Epileptology: A View from the Bench: Springer Netherlands; 2014. p. 63-70.
5. Beniczky S, Trinka E, Wirrell E, Abdulla F, Al Baradie R, Alonso Vanegas M, et al. Updated classification of epileptic seizures: Position paper of the International League Against Epilepsy. Epilepsia. 2025.
6. Beniczky S, Trinka E, Wirrell E, Abdulla F, Al Baradie R, Alonso Vanegas M, et al. Updated classification of epileptic seizures: Position paper of the International League Against Epilepsy. Epilepsia. 2025;66(6):1804-23.
7. Wu S, Nordli DR. Motor seizure semiology. Handbook of Clinical Neurology: Elsevier; 2023. p. 295-304.
8. Kwan P, Brodie MJ. Early identification of refractory epilepsy. N Engl J Med. 2000;342(5):314-9.
9. Gaitatzis A. Life expectancy in people with newly diagnosed epilepsy. Brain. 2004;127(11):2427-32.
10. Kwan P, Arzimanoglou A, Berg AT, Brodie MJ, Allen Hauser W, Mathern G, et al. Definition of drug resistant epilepsy: Consensus proposal by the ad hoc Task Force of the ILAE Commission on Therapeutic Strategies. Epilepsia. 2010;51(6):1069-77.
11. Perucca E, Perucca P, White HS, Wirrell EC. Drug resistance in epilepsy. Lancet Neurol. 2023;22(8):723-34.
12. Engel J, Jr. Surgery for seizures. N Engl J Med. 1996;334(10):647-52.
13. Téllez-Zenteno JF, Dhar R, Wiebe S. Long-term seizure outcomes following epilepsy surgery: a systematic review and meta-analysis. Brain. 2005;128(5):1188-98.
14. Jette N, Wiebe S. Update on the surgical treatment of epilepsy. Curr Opin Neurol. 2013;26(2):201-7.

15. De Tisi J, Bell GS, Peacock JL, McEvoy AW, Harkness WF, Sander JW, et al. The long-term outcome of adult epilepsy surgery, patterns of seizure remission, and relapse: a cohort study. The Lancet. 2011;378(9800):1388-95.
16. Georgiadis I, Kapsalaki EZ, Fountas KN. Temporal Lobe Resective Surgery for Medically Intractable Epilepsy: A Review of Complications and Side Effects. Epilepsy Research and Treatment. 2013;2013:1-12.
17. Young GB, McLachlan RS, Seshia SS. Wilder Penfield and Herbert Jasper: Epilepsy and the Functional Anatomy of the Human Brain. Can J Neurol Sci. 2024:1-2.
18. Nair DR, Laxer KD, Weber PB, Murro AM, Park YD, Barkley GL, et al. Nine-year prospective efficacy and safety of brain-responsive neurostimulation for focal epilepsy. Neurology. 2020;95(9):e1244-e56.
19. Fetzer S, Dibué M, Nagel AM, Trollmann R. A systematic review of magnetic resonance imaging in patients with an implanted vagus nerve stimulation system. Neuroradiology. 2021;63(9):1407-17.
20. Toffa DH, Touma L, El Meskine T, Bouthillier A, Nguyen DK. Learnings from 30 years of reported efficacy and safety of vagus nerve stimulation (VNS) for epilepsy treatment: A critical review. Seizure. 2020;83:104-23.
21. Hamilton P, Soryal I, Dhahri P, Wimalachandra W, Leat A, Hughes D, et al. Clinical outcomes of VNS therapy with AspireSR® (including cardiac-based seizure detection) at a large complex epilepsy and surgery centre. Seizure. 2018;58:120-6.
22. Elliott RE, Morsi A, Kalhorn SP, Marcus J, Sellin J, Kang M, et al. Vagus nerve stimulation in 436 consecutive patients with treatment-resistant epilepsy: long-term outcomes and predictors of response. Epilepsy Behav. 2011;20(1):57-63.
23. Boon P, Vonck K, Van Walleghem P, D'Have M, Goossens L, Vandekerckhove T, et al. Programmed and magnet-induced vagus nerve stimulation for refractory epilepsy. J Clin Neurophysiol. 2001;18(5):402-7.
24. Morris GL, 3rd. A retrospective analysis of the effects of magnet-activated stimulation in conjunction with vagus nerve stimulation therapy. Epilepsy Behav. 2003;4(6):740-5.
25. Zabara J. Inhibition of experimental seizures in canines by repetitive vagal stimulation. Epilepsia. 1992;33(6):1005-12.
26. Afra P, Adamolekun B, Aydemir S, Watson GDR. Evolution of the Vagus Nerve Stimulation (VNS) Therapy System Technology for Drug-Resistant Epilepsy. Front Med Technol. 2021;3:696543.
27. Datta P, Galla KM, Sajja K, Wichman C, Wang H, Madhavan D. Vagus nerve stimulation with tachycardia detection provides additional seizure reduction compared to traditional vagus nerve stimulation. Epilepsy Behav. 2020;111:107280.

28. Cukiert A, Cukiert CM, Mariani PP, Burattini JA. Impact of Cardiac-Based Vagus Nerve Stimulation Closed-Loop Stimulation on the Seizure Outcome of Patients With Generalized Epilepsy: A Prospective, Individual-Control Study. Neuromodulation. 2021;24(6):1018-23.
29. Boon P, Vonck K, van Rijckevorsel K, El Tahry R, Elger CE, Mullatti N, et al. A prospective, multicenter study of cardiac-based seizure detection to activate vagus nerve stimulation. Seizure. 2015;32:52-61.
30. Fisher RS, Afra P, Macken M, Minecan DN, Bagic A, Benbadis SR, et al. Automatic Vagus Nerve Stimulation Triggered by Ictal Tachycardia: Clinical Outcomes and Device Performance--The U.S. E-37 Trial. Neuromodulation. 2016;19(2):188-95.
31. Hampel KG, Vatter H, Elger CE, Surges R. Cardiac-based vagus nerve stimulation reduced seizure duration in a patient with refractory epilepsy. Seizure. 2015;26:81-5.
32. Bauer S, Baier H, Baumgartner C, Bohlmann K, Fauser S, Graf W, et al. Transcutaneous Vagus Nerve Stimulation (tVNS) for Treatment of Drug-Resistant Epilepsy: A Randomized, Double-Blind Clinical Trial (cMPsE02). Brain Stimul. 2016;9(3):356-63.
33. Butt MF, Albusoda A, Farmer AD, Aziz Q. The anatomical basis for transcutaneous auricular vagus nerve stimulation. Journal of Anatomy. 2019;236(4):588-611.
34. Devinsky O. Effects of Seizures on Autonomic and Cardiovascular Function. Epilepsy Curr. 2004;4(2):43-6.
35. Lamotte G, Shouman K, Benarroch EE. Stress and central autonomic network. Auton Neurosci. 2021;235:102870.
36. Benarroch EE. The Central Autonomic Network: Functional Organization, Dysfunction, and Perspective. Mayo Clinic Proceedings. 1993;68(10):988-1001.
37. Ghali MGZ. Role of the medullary lateral tegmental field in sympathetic control. J Integr Neurosci. 2017;16(2):189-208.
38. You S-M, Cho B-H, Bae H-E, Kim Y-K, Kim J-R, Park S-R, et al. Exploring Autonomic Alterations during Seizures in Temporal Lobe Epilepsy: Insights from a Heart-Rate Variability Analysis. Journal of Clinical Medicine. 2023;12(13):4284.
39. Oppenheimer S. Cerebrogenic cardiac arrhythmias. Clinical Autonomic Research. 2006;16(1):6-11.
40. Oppenheimer SM, Gelb A, Girvin JP, Hachinski VC. Cardiovascular effects of human insular cortex stimulation. Neurology. 1992;42(9):1727-.
41. Ghchime R, Benjelloun H, Kiai H, Belaidi H, Lahjouji F, Ouazzani R. Cerebral Hemispheric Lateralization Associated with Hippocampal Sclerosis May Affect Interictal Cardiovascular Autonomic Functions in Temporal Lobe Epilepsy. Epilepsy Research and Treatment. 2016;2016:1-7.

42. Koseoglu E, Kucuk S, Arman F, Ersoy AO. Factors that affect interictal cardiovascular autonomic dysfunction in temporal lobe epilepsy: role of hippocampal sclerosis. Epilepsy Behav. 2009;16(4):617-21.
43. Tomson T, Ericson M, Ihrman C, Lindblad LE. Heart rate variability in patients with epilepsy. Epilepsy Research. 1998;30(1):77-83.
44. Stewart M. An explanation for sudden death in epilepsy (SUDEP). J Physiol Sci. 2018;68(4):307-20.
45. Khan MA, Dev S, Kumari M, Mahak F, Umair A, Rasool M, et al. Respiratory Dysfunction in Epileptic Encephalopathies: Insights and Challenges. Cureus. 2023.
46. Blum AS. Respiratory physiology of seizures. J Clin Neurophysiol. 2009;26(5):309-15.
47. Micalizzi E, Vaudano AE, Ballerini A, Talami F, Giovannini G, Turchi G, et al. Ictal apnea: A prospective monocentric study in patients with epilepsy. European Journal of Neurology. 2022;29(12):3701-10.
48. Vilella L, Lacuey N, Hampson JP, Rani MRS, Loparo K, Sainju RK, et al. Incidence, Recurrence, and Risk Factors for Peri-ictal Central Apnea and Sudden Unexpected Death in Epilepsy. Front Neurol. 2019;10:166.
49. So EL, Sam MC, Lagerlund TL. Postictal Central Apnea as a Cause of SUDEP: Evidence From Near-SUDEP Incident. Epilepsia. 2000;41(11):1494-7.
50. Teran FA, Bravo E, Richerson GB. Sudden unexpected death in epilepsy: Respiratory mechanisms. Handb Clin Neurol. 2022;189:153-76.
51. Scharf MT, Greenberg P, Wong S, Mani R. Obstructive sleep apnea risk in patients with focal versus generalized epilepsy. Epilepsy Behav. 2020;111:107190.
52. Fitzgerald S. Patients with Generalized Epilepsy May Be at Higher Risk for Obstructive Sleep Apnea. Neurology Today. 2020;20(21):1,21-2.
53. Nakase K, Kollmar R, Lazar J, Arjomandi H, Sundaram K, Silverman J, et al. Laryngospasm, central and obstructive apnea during seizures: Defining pathophysiology for sudden death in a rat model. Epilepsy Res. 2016;128:126-39.
54. Stewart M, Silverman JB, Sundaram K, Kollmar R. Causes and Effects Contributing to Sudden Death in Epilepsy and the Rationale for Prevention and Intervention. Front Neurol. 2020;11:765.
55. Ravindran M. Temporal lobe seizure presenting as "laryngospasm". Clin Electroencephalogr. 1981;12(3):139-40.
56. Lacuey N, Vilella L, Hampson JP, Sahadevan J, Lhatoo SD. Ictal laryngospasm monitored by video-EEG and polygraphy: a potential SUDEP mechanism. Epileptic Disorders. 2018;20(2):146-50.
57. Tavee J, Morris Iii H. Severe postictal laryngospasm as a potential mechanism for sudden unexpected death in epilepsy: a near-miss in an EMU. Epilepsia. 2008;49(12):2113-7.

58. Antoniuk SA, Oliva LV, Bruck I, Malucelli M, Yabumoto S, Castellano JL. Sudden unexpected, unexplained death in epilepsy autopsied patients. Arquivos de Neuro-Psiquiatria. 2001;59(1):40-5.
59. Morentin Campillo B, Alcaraz Manzano R. Muerte súbita inesperada en epilepsia en niños y jóvenes. Revista de Neurología. 2002;34(05):462.
60. Salmo EN, Connolly CE. Mortality in epilepsy in the West of Ireland: a 10-year review. Irish Journal of Medical Science. 2002;171(4):199-201.
61. Murray-Calderon P, Connolly MA. Laryngospasm and noncardiogenic pulmonary edema. J Perianesth Nurs. 1997;12(2):89-94.
62. Umbrain V, Camu F. Acute pulmonary edema after laryngospasm. Acta Anaesthesiol Belg. 1993.
63. Geerling JC, Shin JW, Chimenti PC, Loewy AD. Paraventricular hypothalamic nucleus: Axonal projections to the brainstem. Journal of Comparative Neurology. 2010;518(9):1460-99.
64. Tio E, Culler GW, Bachman EM, Schuele S. Ictal central apneas in temporal lobe epilepsies. Epilepsy & Behavior. 2020;112:107434.
65. Lacuey N, Hupp NJ, Hampson J, Lhatoo S. Ictal Central Apnea (ICA) may be a useful semiological sign in invasive epilepsy surgery evaluations. Epilepsy Research. 2019;156:106164.
66. Nashef L, Walker F, Allen P, Sander JW, Shorvon SD, Fish DR. Apnoea and bradycardia during epileptic seizures: relation to sudden death in epilepsy. J Neurol Neurosurg Psychiatry. 1996;60(3):297-300.
67. Lacuey N, Hampson JP, Harper RM, Miller JP, Lhatoo S. Limbic and paralimbic structures driving ictal central apnea. Neurology. 2019;92(7):e655-e69.
68. Lacuey N, Zonjy B, Londono L, Lhatoo SD. Amygdala and hippocampus are symptomatogenic zones for central apneic seizures. Neurology. 2017;88(7):701-5.
69. Magnaes B, Nornes H. Circulatory and Respiratory Changes in Spontaneous Epileptic Seizures in Man. European Neurology. 1974;12(2):104-15.
70. Freeman R. Cardiovascular manifestations of autonomic epilepsy. Clinical Autonomic Research. 2006;16(1):12-7.
71. Jansen K, Lagae L. Cardiac changes in epilepsy. Seizure. 2010;19(8):455-60.
72. Adjei P, Surges R, Scott CA, Kallis C, Shorvon S, Walker MC. Do subclinical electrographic seizure patterns affect heart rate and its variability? Epilepsy Research. 2009;87(2-3):281-5.
73. Keilson MJ, Hauser WA, Magrill JP. Electrocardiographic Changes During Electrographic Seizures. Archives of Neurology. 1989;46(11):1169-70.
74. Nei M, Ho RT, Sperling MR. EKG Abnormalities During Partial Seizures in Refractory Epilepsy. Epilepsia. 2000;41(5):542-8.

75. Opherk C, Coromilas J, Hirsch LJ. Heart rate and EKG changes in 102 seizures: analysis of influencing factors. Epilepsy Research. 2002;52(2):117-27.
76. Zijlmans M, Flanagan D, Gotman J. Heart Rate Changes and ECG Abnormalities During Epileptic Seizures: Prevalence and Definition of an Objective Clinical Sign. Epilepsia. 2002;43(8):847-54.
77. Mayer H, Benninger F, Urak L, Plattner B, Geldner J, Feucht M. EKG abnormalities in children and adolescents with symptomatic temporal lobe epilepsy. Neurology. 2004;63(2):324-8.
78. Wilder-Smith E, Lim SH. Heart rate changes during partial seizures: a study amongst Singaporean patients. BMC Neurol. 2001;1(1):5.
79. Blumhardt L. ELECTROCARDIOGRAPHIC ACCOMPANIMENTS OF TEMPORAL LOBE EPILEPTIC SEIZURES. The Lancet. 1986;327(8489):1051-6.
80. Britton JW, Ghearing GR, Benarroch EE, Cascino GD. The Ictal Bradycardia Syndrome: Localization and Lateralization. Epilepsia. 2006;47(4):737-44.
81. Li LM, Roche J, Sander JWAS. Ictal ECG changes in temporal lobe epilepsy. Arquivos de Neuro-Psiquiatria. 1995;53(3b):619-24.
82. Eggleston KS, Olin BD, Fisher RS. Ictal tachycardia: the head-heart connection. Seizure. 2014;23(7):496-505.
83. Mazzola L, Rheims S. Ictal and Interictal Cardiac Manifestations in Epilepsy. A Review of Their Relation With an Altered Central Control of Autonomic Functions and With the Risk of SUDEP. Frontiers in Neurology. 2021;12.
84. Garcia M, D'Giano C, Estellés S, Leiguarda R, Rabinowicz A. Ictal tachycardia: its discriminating potential between temporal and extratemporal seizure foci. Seizure. 2001;10(6):415-9.
85. Weil S, Arnold S, Eisensehr I, Noachtar S. Heart rate increase in otherwise subclinical seizures is different in temporal versus extratemporal seizure onset: support for temporal lobe autonomic influence. Epileptic Disord. 2005;7(3):199-204.
86. Sevcencu C, Struijk JJ. Autonomic alterations and cardiac changes in epilepsy. Epilepsia. 2010;51(5):725-37.
87. Leutmezer F, Schernthaner C, Lurger S, Pötzelberger K, Baumgartner C. Electrocardiographic Changes at the Onset of Epileptic Seizures. Epilepsia. 2003;44(3):348-54.
88. Reeves AL, Nollet KE, Klass DW, Sharbrough FW, So EL. The ictal bradycardia syndrome. Epilepsia. 1996;37(10):983-7.
89. Di Gennaro G, Quarato PP, Sebastiano F, Esposito V, Onorati P, Grammaldo LG, et al. Ictal heart rate increase precedes EEG discharge in drug-resistant mesial temporal lobe seizures. Clinical Neurophysiology. 2004;115(5):1169-77.

90. Galimberti CA, Marchioni E, Barzizza F, Manni R, Sartori I, Tartara A. Partial Epileptic Seizures of Different Origin Variably Affect Cardiac Rhythm. Epilepsia. 1996;37(8):742-7.
91. Casale MJ, Marcuse LV, Young JJ, Jette N, Panov FE, Bender HA, et al. The Sensitivity of Scalp EEG at Detecting Seizures-A Simultaneous Scalp and Stereo EEG Study. J Clin Neurophysiol. 2022;39(1):78-84.
92. Benarroch EE. The central autonomic network: functional organization, dysfunction, and perspective. Mayo Clin Proc. 1993;68(10):988-1001.
93. Jeppesen J, Fuglsang-Frederiksen A, Brugada R, Pedersen B, Rubboli G, Johansen P, et al. Heart rate variability analysis indicates preictal parasympathetic overdrive preceding seizure-induced cardiac dysrhythmias leading to sudden unexpected death in a patient with epilepsy. Epilepsia. 2014;55(7):e67-e71.
94. Jeppesen J, Beniczky S, Fuglsang-Frederiksen A, Sidenius P, Jasemian Y. Detection of epileptic-seizures by means of power spectrum analysis of heart rate variability: a pilot study. Technol Health Care. 2010;18(6):417-26.
95. Tinuper P, Bisulli F, Cerullo A, Carcangiu R, Marini C, Pierangeli G, et al. Ictal bradycardia in partial epileptic seizures: Autonomic investigation in three cases and literature review. Brain. 2001;124(Pt 12):2361-71.
96. Smith PEM, Howell SJL, Owen L, Blumhardt LD. Profiles of instant heart rate during partial seizures. Electroencephalography and Clinical Neurophysiology. 1989;72(3):207-17.
97. Rugg-Gunn FJ, Simister RJ, Squirrell M, Holdright DR, Duncan JS. Cardiac arrhythmias in focal epilepsy: a prospective long-term study. Lancet. 2004;364(9452):2212-9.
98. Hampel KG, Jahanbekam A, Elger CE, Surges R. Seizure-related modulation of systemic arterial blood pressure in focal epilepsy. Epilepsia. 2016;57(10):1709-18.
99. Schuele SU, Bermeo AC, Locatelli E, Burgess RC, Luders HO. Ictal asystole: a benign condition? Epilepsia. 2008;49(1):168-71.
100. Shlobin NA, Thijs RD, Benditt DG, Zeppenfeld K, Sander JW. Sudden death in epilepsy: the overlap between cardiac and neurological factors. Brain Commun. 2024;6(5):fcae309.
101. Shmuely S, Van Der Lende M, Lamberts RJ, Sander JW, Thijs RD. The heart of epilepsy: Current views and future concepts. Seizure. 2017;44:176-83.
102. Magder SA. The highs and lows of blood pressure: toward meaningful clinical targets in patients with shock. Crit Care Med. 2014;42(5):1241-51.
103. Mayet J. Cardiac and vascular pathophysiology in hypertension. Heart. 2003;89(9):1104-9.
104. Nass RD, Hampel KG, Elger CE, Surges R. Blood Pressure in Seizures and Epilepsy. Frontiers in Neurology. 2019;10.

105. Jaychandran R, Chaitanya G, Satishchandra P, Bharath RD, Thennarasu K, Sinha S. Monitoring peri-ictal changes in heart rate variability, oxygen saturation and blood pressure in epilepsy monitoring unit. Epilepsy Res. 2016;125:10-8.
106. Jardine DL, Crozier IG, Ikram H, Anderson TJ. Paroxysmal hypertension during a complex partial seizure. J Neurol Neurosurg Psychiatry. 2001;71(1):132-3.
107. Bozorgi A, Chung S, Kaffashi F, Loparo KA, Sahoo S, Zhang GQ, et al. Significant postictal hypotension: Expanding the spectrum of seizure-induced autonomic dysregulation. Epilepsia. 2013;54(9):e127-e30.
108. Simon RP, Aminoff MJ, Benowitz NL. Changes in plasma catecholamines after tonic-clonic seizures. Neurology. 1984;34(2):255-.
109. Geersing PGKB, Bulte CSE, Viersen VA, Stek ML, Bouwman RA, Boer C, et al. Beat-to-Beat Hemodynamic Monitoring During Electroconvulsive Therapy. The Journal of ECT. 2011;27(3):189-91.
110. Hampel KG, Elger CE, Surges R. Impaired Baroreflex Sensitivity after Bilateral Convulsive Seizures in Patients with Focal Epilepsy. Front Neurol. 2017;8:210.
111. Esmaeili B, Kaffashi F, Theeranaew W, Dabir A, Lhatoo SD, Loparo KA. Post-ictal Modulation of Baroreflex Sensitivity in Patients With Intractable Epilepsy. Front Neurol. 2018;9:793.
112. Benarroch EE. The arterial baroreflex. Neurology. 2008;71(21):1733-8.
113. Shorvon S, Tomson T. Sudden unexpected death in epilepsy. The Lancet. 2011;378(9808):2028-38.
114. Tomson T, Walczak T, Sillanpaa M, Sander JW. Sudden unexpected death in epilepsy: a review of incidence and risk factors. Epilepsia. 2005;46 Suppl 11:54-61.
115. Mostacci B, Bisulli F, Vignatelli L, Licchetta L, Di Vito L, Rinaldi C, et al. Incidence of sudden unexpected death in nocturnal frontal lobe epilepsy: a cohort study. Sleep Medicine. 2015;16(2):232-6.
116. Ryvlin P, Nashef L, Lhatoo SD, Bateman LM, Bird J, Bleasel A, et al. Incidence and mechanisms of cardiorespiratory arrests in epilepsy monitoring units (MORTEMUS): a retrospective study. Lancet Neurol. 2013;12(10):966-77.
117. Bateman LM, Li CS, Seyal M. Ictal hypoxemia in localization-related epilepsy: analysis of incidence, severity and risk factors. Brain. 2008;131(Pt 12):3239-45.
118. Seyal M, Bateman LM. Ictal apnea linked to contralateral spread of temporal lobe seizures: Intracranial EEG recordings in refractory temporal lobe epilepsy. Epilepsia. 2009;50(12):2557-62.
119. Johnston SC, Horn JK, Valente J, Simon RP. The role of hypoventilation in a sheep model of epileptic sudden death. Ann Neurol. 1995;37(4):531-7.

120. Sakamoto K, Saito T, Orman R, Koizumi K, Lazar J, Salciccioli L, et al. Autonomic consequences of kainic acid-induced limbic cortical seizures in rats: peripheral autonomic nerve activity, acute cardiovascular changes, and death. Epilepsia. 2008;49(6):982-96.
121. Paydarfar D, Eldridge FL, Scott SC, Dowell RT, Wagner PG. Respiratory responses to focal and generalized seizures in cats. American Journal of Physiology-Regulatory, Integrative and Comparative Physiology. 1991;260(5):R934-R40.
122. Devinsky O. Sudden, unexpected death in epilepsy. N Engl J Med. 2011;365(19):1801-11.
123. Athira SB, Pal P, Nair PP, Nanda N, Aghoram R. Cardiovascular autonomic function and baroreflex sensitivity in drug-resistant temporal lobe epilepsy. Epilepsy & Behavior. 2023;138:109013.
124. Mueller SG, Bateman LM, Laxer KD. Evidence for brainstem network disruption in temporal lobe epilepsy and sudden unexplained death in epilepsy. Neuroimage Clin. 2014;5:208-16.
125. Mueller SG, Nei M, Bateman LM, Knowlton R, Laxer KD, Friedman D, et al. Brainstem network disruption: A pathway to sudden unexplained death in epilepsy? Human Brain Mapping. 2018;39(12):4820-30.
126. Wang Y, Wei P, Yan F, Luo Y, Zhao G. Animal Models of Epilepsy: A Phenotype-oriented Review. Aging and disease. 2022;13(1):215.
127. Howbert JJ, Patterson EE, Stead SM, Brinkmann B, Vasoli V, Crepeau D, et al. Forecasting seizures in dogs with naturally occurring epilepsy. PLoS One. 2014;9(1):e81920.
128. Löscher W. Critical review of current animal models of seizures and epilepsy used in the discovery and development of new antiepileptic drugs. Seizure. 2011;20(5):359-68.
129. Gawel K, Langlois M, Martins T, Van Der Ent W, Tiraboschi E, Jacmin M, et al. Seizing the moment: Zebrafish epilepsy models. Neuroscience & Biobehavioral Reviews. 2020;116:1-20.
130. Gorter JA, van Vliet EA, Lopes da Silva FH. Which insights have we gained from the kindling and post-status epilepticus models? J Neurosci Methods. 2016;260:96-108.
131. Fan J, Shan W, Yang H, Zhu F, Liu X, Wang Q. Neural Activities in Multiple Rat Brain Regions in Lithium-Pilocarpine-Induced Status Epilepticus Model. Frontiers in Molecular Neuroscience. 2020;12.
132. Jefferys J, Steinhäuser C, Bedner P. Chemically-induced TLE models: Topical application. Journal of Neuroscience Methods. 2016;260:53-61.
133. Nascimento FA, Friedman D, Peters JM, Meriem, Cendes F, Rampp S, et al. Focal epilepsies: Update on diagnosis and classification. Epileptic Disorders. 2023;25(1):1-17.

134. Téllez-Zenteno JF, Hernández-Ronquillo L. A Review of the Epidemiology of Temporal Lobe Epilepsy. Epilepsy Research and Treatment. 2012;2012:1-5.
135. Blümcke I, Thom M, Aronica E, Armstrong DD, Bartolomei F, Bernasconi A, et al. International consensus classification of hippocampal sclerosis in temporal lobe epilepsy: A Task Force report from the<scp>ILAE</scp>Commission on Diagnostic Methods. Epilepsia. 2013;54(7):1315-29.
136. Roy A, Millen KJ, Kapur RP. Hippocampal granule cell dispersion: a non-specific finding in pediatric patients with no history of seizures. Acta Neuropathologica Communications. 2020;8(1).
137. Thom M. Epilepsy Pathology. Elsevier; 2014. p. 136-41.
138. Ben-Ari Y, Lagowska J. Epileptogenic action of intra-amygdaloid injection of kainic acid. C R Acad Hebd Seances Acad Sci D. 1978;287:813-6.
139. Ben-Ari Y, Lagowska J, Tremblay E, Le Gal La Salle G. A new model of focal status epilepticus: intra-amygdaloid application of kainic acid elicits repetitive secondarily generalized convulsive seizures. Brain Research. 1979;163(1):176-9.
140. Levesque M, Avoli M. The kainic acid model of temporal lobe epilepsy. Neurosci Biobehav Rev. 2013;37(10 Pt 2):2887-99.
141. Murakami S, Takemoto T, Shimizu Z. Studies on the Effective Principles of Digenea simplex Aq. I. Yakugaku Zasshi. 1953;73(9):1026-8.
142. Zhang X-M, Zhu J. Kainic Acid-Induced Neurotoxicity: Targeting Glial Responses and Glia-Derived Cytokines. Current Neuropharmacology. 2011;9(2):388-98.
143. Behan WMH, Stone TW. Role of kynurenines in the neurotoxic actions of kainic acid. British Journal of Pharmacology. 2000;129(8):1764-70.
144. Rusina E, Bernard C, Williamson A. The Kainic Acid Models of Temporal Lobe Epilepsy. eNeuro. 2021;8(2).
145. Bragin A, Engel J, Jr., Wilson CL, Vizentin E, Mathern GW. Electrophysiologic analysis of a chronic seizure model after unilateral hippocampal KA injection. Epilepsia. 1999;40(9):1210-21.
146. Raedt R, Van Dycke A, Van Melkebeke D, De Smedt T, Claeys P, Wyckhuys T, et al. Seizures in the intrahippocampal kainic acid epilepsy model: characterization using long-term video-EEG monitoring in the rat. Acta Neurol Scand. 2009;119(5):293-303.
147. Rattka M, Brandt C, Loscher W. The intrahippocampal kainate model of temporal lobe epilepsy revisited: epileptogenesis, behavioral and cognitive alterations, pharmacological response, and hippoccampal damage in epileptic rats. Epilepsy Res. 2013;103(2-3):135-52.

148. French ED, Aldinio C, Schwarcz R. Intrahippocampal kainic acid, seizures and local neuronal degeneration: Relationships assessed in unanesthetized rats. Neuroscience. 1982;7(10):2525-36.
149. Bouilleret V, Ridoux V, Depaulis A, Marescaux C, Nehlig A, Le Gal La Salle G. Recurrent seizures and hippocampal sclerosis following intrahippocampal kainate injection in adult mice: electroencephalography, histopathology and synaptic reorganization similar to mesial temporal lobe epilepsy. Neuroscience. 1999;89(3):717-29.
150. Twele F, Bankstahl M, Klein S, Römermann K, Löscher W. The AMPA receptor antagonist NBQX exerts anti-seizure but not antiepileptogenic effects in the intrahippocampal kainate mouse model of mesial temporal lobe epilepsy. Neuropharmacology. 2015;95:234-42.
151. Gurbanova AA, Aker RG, Sirvanci S, Demiralp T, Onat FY. Intra-Amygdaloid Injection of Kainic Acid in Rats with Genetic Absence Epilepsy: The Relationship of Typical Absence Epilepsy and Temporal Lobe Epilepsy. The Journal of Neuroscience. 2008;28(31):7828-36.
152. Mouri G, Jimenez-Mateos E, Engel T, Dunleavy M, Hatazaki S, Paucard A, et al. Unilateral hippocampal CA3-predominant damage and short latency epileptogenesis after intra-amygdala microinjection of kainic acid in mice. Brain Research. 2008;1213:140-51.
153. Zeidler Z, Brandt-Fontaine M, Leintz C, Krook-Magnuson C, Netoff T, Krook-Magnuson E. Targeting the Mouse Ventral Hippocampus in the Intrahippocampal Kainic Acid Model of Temporal Lobe Epilepsy. eneuro. 2018;5(4):ENEURO.0158-18.
154. Dudek FE, Clark S, Williams PA, Grabenstatter HL. Kainate-Induced Status Epilepticus: A Chronic Model of Acquired Epilepsy. Models of Seizures and Epilepsy: Elsevier; 2006. p. 415-32.
155. Hellier JL, Patrylo PR, Buckmaster PS, Dudek FE. Recurrent spontaneous motor seizures after repeated low-dose systemic treatment with kainate: assessment of a rat model of temporal lobe epilepsy. Epilepsy Res. 1998;31(1):73-84.
156. Williams PA, White AM, Clark S, Ferraro DJ, Swiercz W, Staley KJ, et al. Development of spontaneous recurrent seizures after kainate-induced status epilepticus. J Neurosci. 2009;29(7):2103-12.
157. Drexel M, Preidt AP, Sperk G. Sequel of spontaneous seizures after kainic acid-induced status epilepticus and associated neuropathological changes in the subiculum and entorhinal cortex. Neuropharmacology. 2012;63(5):806-17.
158. Bertoglio D, Amhaoul H, Van Eetveldt A, Houbrechts R, Van De Vijver S, Ali I, et al. Kainic Acid-Induced Post-Status Epilepticus Models of Temporal Lobe Epilepsy with Diverging Seizure Phenotype and Neuropathology. Front Neurol. 2017;8:588.

159. Lado FA. Chronic Bilateral Stimulation of the Anterior Thalamus of Kainate-treated Rats Increases Seizure Frequency. Epilepsia. 2006;47(1):27-32.
160. Hellier JL, Dudek FE. Chemoconvulsant Model of Chronic Spontaneous Seizures. Current Protocols in Neuroscience. 2005;31(1).
161. Sperk G, Lassmann H, Baran H, Kish SJ, Seitelberger F, Hornykiewicz O. Kainic acid induced seizures: Neurochemical and histopathological changes. Neuroscience. 1983;10(4):1301-15.
162. Haas KZ, Sperber EF, Opanashuk LA, Stanton PK, Moshé SL. Resistance of immature hippocampus to morphologic and physiologic alterations following status epilepticus or kindling. Hippocampus. 2001;11(6):615-25.
163. Tauck D, Nadler J. Evidence of functional mossy fiber sprouting in hippocampal formation of kainic acid-treated rats. The Journal of Neuroscience. 1985;5(4):1016-22.
164. Fritsch B, Qashu F, Figueiredo TH, Aroniadou-Anderjaska V, Rogawski MA, Braga MFM. Pathological alterations in GABAergic interneurons and reduced tonic inhibition in the basolateral amygdala during epileptogenesis. Neuroscience. 2009;163(1):415-29.
165. Covolan L, Mello LEAM. Temporal profile of neuronal injury following pilocarpine or kainic acid-induced status epilepticus. Epilepsy Research. 2000;39(2):133-52.
166. Loscher W, Brandt C. Prevention or modification of epileptogenesis after brain insults: experimental approaches and translational research. Pharmacol Rev. 2010;62(4):668-700.
167. Curia G, Lucchi C, Vinet J, Gualtieri F, Marinelli C, Torsello A, et al. Pathophysiogenesis of Mesial Temporal Lobe Epilepsy: Is Prevention of Damage Antiepileptogenic? Current Medicinal Chemistry. 2014;21(6):663-88.
168. Van Nieuwenhuyse B, Raedt R, Sprengers M, Dauwe I, Gadeyne S, Carrette E, et al. The systemic kainic acid rat model of temporal lobe epilepsy: Long-term EEG monitoring. Brain Res. 2015;1627:1-11.
169. Lee M, Choi BY, Suh SW. Unexpected Effects of Acetylcholine Precursors on Pilocarpine Seizure- Induced Neuronal Death. Current Neuropharmacology. 2017;16(1).
170. Levesque M, Avoli M, Bernard C. Animal models of temporal lobe epilepsy following systemic chemoconvulsant administration. J Neurosci Methods. 2016;260:45-52.
171. Groticke I, Hoffmann K, Loscher W. Behavioral alterations in the pilocarpine model of temporal lobe epilepsy in mice. Exp Neurol. 2007;207(2):329-49.
172. Cavalheiro EA, Leite JP, Bortolotto ZA, Turski WA, Ikonomidou C, Turski L. Long-term effects of pilocarpine in rats: structural damage of the brain

triggers kindling and spontaneous recurrent seizures. Epilepsia. 1991;32(6):778-82.
173. Turski WA, Cavalheiro EA, Schwarz M, Czuczwar SJ, Kleinrok Z, Turski L. Limbic seizures produced by pilocarpine in rats: Behavioural, electroencephalographic and neuropathological study. Behavioural Brain Research. 1983;9(3):315-35.
174. Turski L, Ikonomidou C, Turski WA, Bortolotto ZA, Cavalheiro EA. Review: cholinergic mechanisms and epileptogenesis. The seizures induced by pilocarpine: a novel experimental model of intractable epilepsy. Synapse. 1989;3(2):154-71.
175. Covolan L, Ribeiro LTC, Longo BM, Mello LEAM. Cell damage and neurogenesis in the dentate granule cell layer of adult rats after pilocarpine- or kainate-induced status epilepticus. Hippocampus. 2000;10(2):169-80.
176. Browning RA, Nelson DK. Variation in threshold and pattern of electroshock-induced seizures in rats depending on site of stimulation. Life Sciences. 1985;37(23):2205-11.
177. Sakkaki S, Gangarossa G, Lerat B, Francon D, Forichon L, Chemin J, et al. Blockade of T-type calcium channels prevents tonic-clonic seizures in a maximal electroshock seizure model. Neuropharmacology. 2016;101:320-9.
178. Luttjohann A, Fabene PF, van Luijtelaar G. A revised Racine's scale for PTZ-induced seizures in rats. Physiol Behav. 2009;98(5):579-86.
179. Shimada T, Yamagata K. Pentylenetetrazole-Induced Kindling Mouse Model. Journal of Visualized Experiments. 2018(136).
180. Kandratavicius L, Balista P, Lopes-Aguiar C, Ruggiero R, Umeoka E, Garcia-Cairasco N, et al. Animal models of epilepsy: use and limitations. Neuropsychiatric Disease and Treatment. 2014:1693.
181. Dorofeeva NA, Grigorieva YS, Nikitina LS, Lavrova EA, Nasluzova EV, Glazova MV, et al. Effects of ERK1/2 kinases inactivation on the nigrostriatal system of Krushinsky-Molodkina rats genetically prone to audiogenic seizures. Neurological Research. 2017;39(10):918-25.
182. De Sarro G, Russo E, Citraro R, Meldrum BS. Genetically epilepsy-prone rats (GEPRs) and DBA/2 mice: Two animal models of audiogenic reflex epilepsy for the evaluation of new generation AEDs. Epilepsy Behav. 2017;71(Pt B):165-73.
183. Damasceno S, Menezes NB, Rocha CS, Matos AHB, Vieira AS, Moraes MFD, et al. Transcriptome of the Wistar audiogenic rat (WAR) strain following audiogenic seizures. Epilepsy Res. 2018;147:22-31.
184. Garcia-Cairasco N, Umeoka EHL, Cortes de Oliveira JA. The Wistar Audiogenic Rat (WAR) strain and its contributions to epileptology and related comorbidities: History and perspectives. Epilepsy Behav. 2017;71(Pt B):250-73.

185. Depaulis A, David O, Charpier S. The genetic absence epilepsy rat from Strasbourg as a model to decipher the neuronal and network mechanisms of generalized idiopathic epilepsies. J Neurosci Methods. 2016;260:159-74.
186. Danober L, Deransart C, Depaulis A, Vergnes M, Marescaux C. Pathophysiological mechanisms of genetic absence epilepsy in the rat. Prog Neurobiol. 1998;55(1):27-57.
187. Marescaux C, Vergnes M, Depaulis A. Genetic absence epilepsy in rats from Strasbourg — A review. Generalized Non-Convulsive Epilepsy: Focus on GABA-B Receptors. Journal of Neural Transmission (NEURAL SUPPL,volume 35): Springer Vienna; 1992. p. 37-69.
188. Sarkisova K, Van Luijtelaar G. The WAG/Rij strain: A genetic animal model of absence epilepsy with comorbidity of depressiony. Progress in Neuro-Psychopharmacology and Biological Psychiatry. 2011;35(4):854-76.
189. Vergnes M, Marescaux C, Micheletti G, Reis J, Depaulis A, Rumbach L, et al. Spontaneous paroxysmal electroclinical patterns in rat: A model of generalized non-convulsive epilepsy. Neuroscience Letters. 1982;33(1):97-101.
190. Gower AT, Hirsch E, Boehrer A, Noyer M, Marescaux C. Effects of levetiracetam, a novel antiepileptic drug, on convulsant activity in two genetic rat models of epilepsy. Epilepsy Research. 1995;22(3):207-13.
191. O'Regan ME, Brown JK. Abnormalities in cardiac and respiratory function observed during seizures in childhood. Dev Med Child Neurol. 2005;47(1):4-9.
192. Clancy JA, Deuchars SA, Deuchars J. The wonders of the Wanderer. Exp Physiol. 2013;98(1):38-45.
193. Ruffoli R, Giorgi FS, Pizzanelli C, Murri L, Paparelli A, Fornai F. The chemical neuroanatomy of vagus nerve stimulation. Journal of Chemical Neuroanatomy. 2011;42(4):288-96.
194. Camara R, Griessenauer CJ. Anatomy of the Vagus Nerve. Nerves and Nerve Injuries2015. p. 385-97.
195. Akgul Caglar T, Durdu ZB, Turhan MU, Gunal MY, Aydın MS, Ozturk G, et al. Evaluation of the bilateral cardiac afferent distribution at the spinal and vagal ganglia by retrograde labeling. Brain Research. 2021;1751:147201.
196. Van Weperen VYH, Vaseghi M. Cardiac vagal afferent neurotransmission in health and disease: review and knowledge gaps. Frontiers in Neuroscience. 2023;17.
197. Armour JA. Cardiac neuronal hierarchy in health and disease. American Journal of Physiology-Regulatory, Integrative and Comparative Physiology. 2004;287(2):R262-R71.
198. Hainsworth R. Reflexes from the heart. Physiological Reviews. 1991;71(3):617-58.

199. Quigg M. Distribution of vagal afferent fibers of the guinea pig heart labeled by anterograde transport of conjugated horseradish peroxidase. Journal of the Autonomic Nervous System. 1991;36(1):13-24.
200. Shenton FC, Campbell T, Jones JFX, Pyner S. Distribution and morphology of sensory and autonomic fibres in the subendocardial plexus of the rat heart. Journal of Anatomy. 2021;238(1):36-52.
201. Beaumont E, Salavatian S, Southerland EM, Vinet A, Jacquemet V, Armour JA, et al. Network interactions within the canine intrinsic cardiac nervous system: implications for reflex control of regional cardiac function. The Journal of Physiology. 2013;591(18):4515-33.
202. Salavatian S, Hoang JD, Yamaguchi N, Lokhandwala ZA, Swid MA, Armour JA, et al. Myocardial infarction reduces cardiac nociceptive neurotransmission through the vagal ganglia. JCI Insight. 2022;7(4).
203. Lawrence AJ, Jarrott B. Neurochemical modulation of cardiovascular control in the nucleus tractus solitarius. Progress in Neurobiology. 1996;48(1):21-53.
204. Standish A, Enquist LW, Schwaber JS. Innervation of the Heart and Its Central Medullary Origin Defined by Viral Tracing. Science. 1994;263(5144):232-4.
205. Neff RA, Mihalevich M, Mendelowitz D. Stimulation of NTS activates NMDA and non-NMDA receptors in rat cardiac vagal neurons in the nucleus ambiguus. Brain Research. 1998;792(2):277-82.
206. Mazzone SB, Undem BJ. Vagal Afferent Innervation of the Airways in Health and Disease. Physiological Reviews. 2016;96(3):975-1024.
207. Mazzone SB, Mori N, Canning BJ. Synergistic interactions between airway afferent nerve subtypes regulating the cough reflex in guinea-pigs. The Journal of Physiology. 2005;569(2):559-73.
208. Kollarik M, Undem BJ. Mechanisms of acid-induced activation of airway afferent nerve fibres in guinea-pig. The Journal of Physiology. 2002;543(2):591-600.
209. Undem BJ, Chuaychoo B, Lee MG, Weinreich D, Myers AC, Kollarik M. Subtypes of vagal afferent C-fibres in guinea-pig lungs. The Journal of Physiology. 2004;556(3):905-17.
210. Mazzone SB, Canning BJ. Evidence for Differential Reflex Regulation of Cholinergic and Noncholinergic Parasympathetic Nerves Innervating the Airways. American Journal of Respiratory and Critical Care Medicine. 2002;165(8):1076-83.
211. Kubin L, Alheid GF, Zuperku EJ, McCrimmon DR. Central pathways of pulmonary and lower airway vagal afferents. Journal of Applied Physiology. 2006;101(2):618-27.

212. Berthoud HR, Powley TL. Vagal afferent innervation of the rat fundic stomach: Morphological characterization of the gastric tension receptor. Journal of Comparative Neurology. 1992;319(2):261-76.
213. Berthoud H-R, Neuhuber WL. Functional and chemical anatomy of the afferent vagal system. Autonomic Neuroscience. 2000;85(1-3):1-17.
214. Powley TL, Phillips RJ. Musings on the wanderer: what's new in our understanding of vago-vagal reflexes? I. Morphology and topography of vagal afferents innervating the GI tract. Am J Physiol Gastrointest Liver Physiol. 2002;283(6):G1217-25.
215. Phillips RJ, Baronowsky EA, Powley TL. Afferent innervation of gastrointestinal tract smooth muscle by the hepatic branch of the vagus. The Journal of Comparative Neurology. 1997;384(2):248-70.
216. Bellono NW, Bayrer JR, Leitch DB, Castro J, Zhang C, O'Donnell TA, et al. Enterochromaffin Cells Are Gut Chemosensors that Couple to Sensory Neural Pathways. Cell. 2017;170(1):185-98.e16.
217. Norgren R, Smith GP. A method for selective section of vagal afferent or efferent axons in the rat. American Journal of Physiology-Regulatory, Integrative and Comparative Physiology. 1994;267(4):R1136-R41.
218. Rinaman L, Schwartz G. Anterograde Transneuronal Viral Tracing of Central Viscerosensory Pathways in Rats. The Journal of Neuroscience. 2004;24(11):2782-6.
219. Jayaprakash N, Song W, Toth V, Vardhan A, Levy T, Tomaio J, et al. Organ- and function-specific anatomical organization of vagal fibers supports fascicular vagus nerve stimulation. Brain Stimulation. 2023;16(2):484-506.
220. Ben-Menachem E. Vagus-nerve stimulation for the treatment of epilepsy. Lancet Neurol. 2002;1(8):477-82.
221. The Vagus Nerve Stimulation Study Group. A randomized controlled trial of chronic vagus nerve stimulation for treatment of medically intractable seizures. The Vagus Nerve Stimulation Study Group. Neurology. 1995;45(2):224-30.
222. Handforth A, DeGiorgio CM, Schachter SC, Uthman BM, Naritoku DK, Tecoma ES, et al. Vagus nerve stimulation therapy for partial-onset seizures: a randomized active-control trial. Neurology. 1998;51(1):48-55.
223. Chavel SM, Westerveld M, Spencer S. Long-term outcome of vagus nerve stimulation for refractory partial epilepsy. Epilepsy & Behavior. 2003;4(3):302-9.
224. Kimberley TJ, Pierce D, Prudente CN, Francisco GE, Yozbatiran N, Smith P, et al. Vagus Nerve Stimulation Paired With Upper Limb Rehabilitation After Chronic Stroke. Stroke. 2018;49(11):2789-92.
225. Dawson J, Pierce D, Dixit A, Kimberley TJ, Robertson M, Tarver B, et al. Safety, Feasibility, and Efficacy of Vagus Nerve Stimulation Paired With Upper-Limb Rehabilitation After Ischemic Stroke. Stroke. 2016;47(1):143-50.

226. Dawson J, Liu CY, Francisco GE, Cramer SC, Wolf SL, Dixit A, et al. Vagus nerve stimulation paired with rehabilitation for upper limb motor function after ischaemic stroke (VNS-REHAB): a randomised, blinded, pivotal, device trial. Lancet. 2021;397(10284):1545-53.
227. Spindler P, Bohlmann K, Straub H-B, Vajkoczy P, Schneider UC. Effects of vagus nerve stimulation on symptoms of depression in patients with difficult-to-treat epilepsy. Seizure. 2019;69:77-9.
228. Conway CR, Olin B, Aaronson ST, Sackeim HA, Bunker M, Kriedt C, et al. A prospective, multi-center randomized, controlled, blinded trial of vagus nerve stimulation for difficult to treat depression: A novel design for a novel treatment. Contemporary Clinical Trials. 2020;95:106066.
229. Shikora SA, Toouli J, Herrera MF, Kulseng B, Brancatisano R, Kow L, et al. Intermittent Vagal Nerve Block for Improvements in Obesity, Cardiovascular Risk Factors, and Glycemic Control in Patients with Type 2 Diabetes Mellitus: 2-Year Results of the VBLOC DM2 Study. Obesity Surgery. 2016;26(5):1021-8.
230. Fadel MG, Fehervari M, Das B, Soleimani-Nouri P, Ashrafian H. Vagal Nerve Therapy in the Management of Obesity: A Systematic Review and Meta-Analysis. European Surgical Research. 2023;64(4):365-75.
231. Ben-Menachem E. Vagus nerve stimulation, side effects, and long-term safety. J Clin Neurophysiol. 2001;18(5):415-8.
232. Ramsay RE, Uthman BM, Augustinsson LE, Upton ARM, Naritoku D, Willis J, et al. Vagus Nerve Stimulation for Treatment of Partial Seizures: 2. Safety, Side Effects, and Tolerability. Epilepsia. 1994;35(3):627-36.
233. Ciotti F, John R, Katic Secerovic N, Gozzi N, Cimolato A, Jayaprakash N, et al. Towards enhanced functionality of vagus neuroprostheses through in silico optimized stimulation. Nature Communications. 2024;15(1).
234. Thompson N, Ravagli E, Mastitskaya S, Iacoviello F, Stathopoulou TR, Perkins J, et al. Organotopic organization of the porcine mid-cervical vagus nerve. Front Neurosci. 2023;17:963503.
235. Upadhye AR, Kolluru C, Druschel L, Al Lababidi L, Ahmad SS, Menendez DM, et al. Fascicles split or merge every ∼560 microns within the human cervical vagus nerve. Journal of Neural Engineering. 2022;19(5):054001.
236. Settell ML, Pelot NA, Knudsen BE, Dingle AM, McConico AL, Nicolai EN, et al. Functional vagotopy in the cervical vagus nerve of the domestic pig: implications for the study of vagus nerve stimulation. Journal of Neural Engineering. 2020;17(2).
237. Pelot NA, Goldhagen GB, Cariello JE, Musselman ED, Clissold KA, Ezzell JA, et al. Quantified Morphology of the Cervical and Subdiaphragmatic Vagus Nerves of Human, Pig, and Rat. Front Neurosci. 2020;14:601479.
238. Settell ML, Skubal AC, Chen RCH, Kasole M, Knudsen BE, Nicolai EN, et al. In vivo Visualization of Pig Vagus Nerve "Vagotopy" Using Ultrasound. Frontiers in Neuroscience. 2021;15.

239. Plachta DT, Gierthmuehlen M, Cota O, Espinosa N, Boeser F, Herrera TC, et al. Blood pressure control with selective vagal nerve stimulation and minimal side effects. J Neural Eng. 2014;11(3):036011.
240. Aristovich K, Donega M, Fjordbakk C, Tarotin I, Chapman CAR, Viscasillas J, et al. Model-based geometrical optimisation and in vivo validation of a spatially selective multielectrode cuff array for vagus nerve neuromodulation. Journal of Neuroscience Methods. 2021;352:109079.
241. Naggar I, Sakamoto K, Jones S, Stewart M. Autonomic nerve activity and cardiovascular changes during discrete seizures in rats. Auton Neurosci. 2022;240:102971.
242. Chiang C-C, Durand D, editors. Bradycardia Is Induced by Hyperactivity of the Vagus Nerve and Nucleus Ambiguus During Propagating Seizure Attack in the Brainstem. American Epilepsy Society 2024 Annual Meeting; 2024; Los Angeles, USA.
243. Yambe T, Nanka SS, Shiraishi Y, Tanaka A, Yoshizawa M, Abe K, et al. Recording vagal nerve activity for the control of an artificial heart system. ASAIO J. 2003;49(6):698-700.
244. McCallum GA, Sui X, Qiu C, Marmerstein J, Zheng Y, Eggers TE, et al. Chronic interfacing with the autonomic nervous system using carbon nanotube (CNT) yarn electrodes. Scientific Reports. 2017;7(1).
245. Marmerstein JT, McCallum GA, Durand DM. Direct measurement of vagal tone in rats does not show correlation to HRV. Scientific Reports. 2021;11(1).
246. Chronic Vagus-Nerve Activity with Carbon Nanotube Sensors in Freely Moving Rodents [Internet]. 2022.
247. Marmerstein JT, McCallum GA, Durand DM. Decoding Vagus-Nerve Activity with Carbon Nanotube Sensors in Freely Moving Rodents. Biosensors. 2022;12(2).
248. Ghazavi A, Gonzalez-Gonzalez MA, Romero-Ortega MI, Cogan SF. Intraneural ultramicroelectrode arrays for function-specific interfacing to the vagus nerve. Biosens Bioelectron. 2020;170:112608.
249. Ottaviani MM, Wright L, Dawood T, Macefield VG. In vivo recordings from the human vagus nerve using ultrasound-guided microneurography. The Journal of Physiology. 2020;598(17):3569-76.
250. Patros M, Farmer DGS, Moneghetti K, Ottaviani MM, Sivathamboo S, Simpson HD, et al. First-in-human microelectrode recordings from the vagus nerve during clinical vagus nerve stimulation. Epilepsia Open. 2024;9(6):2522-7.
251. Nielsen TN, Struijk JJ, Harreby KR, Sevcencu C. Early Detection of Epileptic Seizures in Pigs Based on Vagus Nerve Activity. Converging Clinical and Engineering Research on Neurorehabilitation. Biosystems & Biorobotics2013. p. 43-7.

252. Sevcencu C, Nielsen TN, Struijk JJ. A Blood Pressure-Related Profile Extracted from Pig Left Vagus Nerves Using Cuff Electrodes. Replace, Repair, Restore, Relieve – Bridging Clinical and Engineering Solutions in Neurorehabilitation. Biosystems & Biorobotics2014. p. 717-23.
253. Sevcencu C, Nielsen TN, Struijk JJ. Changes in vagus nerve activity associated with ictal tachycardia in pigs. Epilepsy Research. 2016;128:52-60.
254. Sevcencu C, Nielsen TN, Kjaergaard B, Struijk JJ. A Respiratory Marker Derived From Left Vagus Nerve Signals Recorded With Implantable Cuff Electrodes. Neuromodulation. 2018;21(3):269-75.
255. Stumpp L, Smets H, Vespa S, Cury J, Doguet P, Delbeke J, et al. Recording of spontaneous vagus nerve activity during Pentylenetetrazol-induced seizures in rats. Journal of Neuroscience Methods. 2020;343.
256. Okonogi T, Kuga N, Yamakawa M, Kayama T, Ikegaya Y, Sasaki T. Stress-induced vagal activity influences anxiety-relevant prefrontal and amygdala neuronal oscillations in male mice. Nature Communications. 2024;15(1).
257. Stumpp L, Smets H, Vespa S, Cury J, Doguet P, Delbeke J, et al. Vagus Nerve Electroneurogram-Based Detection of Acute Pentylenetetrazol Induced Seizures in Rats. Int J Neural Syst. 2021;31(7):2150024.
258. Acedo Reina E, Germany Morrison E, Dereli AS, Collard E, Raffoul R, Nonclercq A, et al. Vagus nerve electroneurogram-based detection of acute kainic acid induced seizures. Frontiers in Neuroscience. 2024;18.
259. Rozman J, Ribaric S. Selective recording of electroneurograms from the left vagus nerve of a dog during stimulation of cardiovascular or respiratory systems. Chin J Physiol. 2007;50(5):240-50.
260. Falcone JD, Liu T, Goldman L, David DP, Rieth L, Bouton CE, et al. A novel microwire interface for small diameter peripheral nerves in a chronic, awake murine model. J Neural Eng. 2020;17(4):046003.
261. Chang Y-C, Cracchiolo M, Ahmed U, Mughrabi I, Gabalski A, Daytz A, et al. Quantitative estimation of nerve fiber engagement by vagus nerve stimulation using physiological markers. Brain Stimulation. 2020;13(6):1617-30.
262. Shikano Y, Nishimura Y, Okonogi T, Ikegaya Y, Sasaki T. Vagus nerve spiking activity associated with locomotion and cortical arousal states in a freely moving rat. European Journal of Neuroscience. 2018;49(10):1298-312.
263. Nishimura Y, Fukuda Y, Okonogi T, Yoshikawa S, Karasuyama H, Osakabe N, et al. Dual real-time in vivo monitoring system of the brain-gut axis. Biochemical and Biophysical Research Communications. 2020;524(2):340-5.
264. Qing KY, Wasilczuk KM, Ward MP, Phillips EH, Vlachos PP, Goergen CJ, et al. B fibers are the best predictors of cardiac activity during Vagus nerve stimulation. Bioelectronic Medicine. 2018;4(1).
265. Castel A, Burns PM, Benito J, Liu HL, Kuthiala S, Durosier LD, et al. Recording and manipulation of vagus nerve electrical activity in chronically

instrumented unanesthetized near term fetal sheep. Journal of Neuroscience Methods. 2021;360.
266. Silverman HA, Stiegler A, Tsaava T, Newman J, Steinberg BE, Masi EB, et al. Standardization of methods to record Vagus nerve activity in mice. Bioelectronic Medicine. 2018;4(1).
267. Plachta DT, Espinosa N, Gierthmuehlen M, Cota O, Herrera TC, Stieglitz T. Detection of baroreceptor activity in rat vagal nerve recording using a multi-channel cuff-electrode and real-time coherent averaging. Annu Int Conf IEEE Eng Med Biol Soc2012. p. 3416-9.
268. Miyashita T, Williams CL. Epinephrine administration increases neural impulses propagated along the vagus nerve: Role of peripheral beta-adrenergic receptors. Neurobiol Learn Mem. 2006;85(2):116-24.
269. Harreby KR, Sevcencu C, Struijk JJ. Early seizure detection in rats based on vagus nerve activity. Med Biol Eng Comput. 2011;49(2):143-51.
270. Harreby KR, Sevcencu C, Struijk JJ. The effect of spinal cord stimulation on seizure susceptibility in rats. Neuromodulation. 2011;14(2):111-6; discussion 6.
271. Tavares L, Rodríguez-Mañero M, Kreidieh B, Ibarra-Cortez SH, Chen J, Wang S, et al. Cardiac Afferent Denervation Abolishes Ganglionated Plexi and Sympathetic Responses to Apnea. Circulation: Arrhythmia and Electrophysiology. 2019;12(6).
272. Miki K, Miyaura W, Ikegame S, Yoshimoto M. Method for measuring cervical vagal nerve activity in conscious rats. American Journal of Physiology-Endocrinology and Metabolism. 2025;328(2):E230-E41.
273. Zanos TP, Silverman HA, Levy T, Tsaava T, Battinelli E, Lorraine PW, et al. Identification of cytokine-specific sensory neural signals by decoding murine vagus nerve activity. Proceedings of the National Academy of Sciences. 2018;115(21):E4843-E52.
274. Zanos TP. Recording and Decoding of Vagal Neural Signals Related to Changes in Physiological Parameters and Biomarkers of Disease. Cold Spring Harbor Perspectives in Medicine. 2019;9(12).
275. Rijnbeek EH, Eleveld N, Olthuis W. Update on Peripheral Nerve Electrodes for Closed-Loop Neuroprosthetics. Frontiers in Neuroscience. 2018;12.
276. Christie BP, Freeberg M, Memberg WD, Pinault GJC, Hoyen HA, Tyler DJ, et al. "Long-term stability of stimulating spiral nerve cuff electrodes on human peripheral nerves". Journal of NeuroEngineering and Rehabilitation. 2017;14(1).
277. Jiman AA, Ratze DC, Welle EJ, Patel PR, Richie JM, Bottorff EC, et al. Multi-channel intraneural vagus nerve recordings with a novel high-density carbon fiber microelectrode array. Scientific Reports. 2020;10(1).

278. Harreby KR, Sevcencu C, Struijk JJ. Ictal and peri-ictal changes in cervical vagus nerve activity associated with cardiac effects. Medical & Biological Engineering & Computing. 2011;49(9):1025-33.
279. Huang R-Q, Bell-Horner CL, Dibas MI, Covey DF, Drewe JA, Dillon GH. Pentylenetetrazole-Induced Inhibition of Recombinant γ-Aminobutyric Acid Type A (GABAA) Receptors: Mechanism and Site of Action. The Journal of Pharmacology and Experimental Therapeutics. 2001;298(3):986-95.
280. Faingold CL. Brainstem reticular formation mechanisms subserving generalized seizures: Effects of convulsants and anticonvulsants on sensory-evoked responses. Progress in Neuro-Psychopharmacology. 1978;2(4):401-22.
281. Faingold CL. Pentylenetetrazol-induced enhancement of responses of mesencephalic reticular neurons to visual stimuli. Brain Research. 1978;150(2):418-23.
282. Mirski MA, Rossell LA, Terry JB, Fisher RS. Anticonvulsant effect of anterior thalamic high frequency electrical stimulation in the rat. Epilepsy Research. 1997;28(2):89-100.
283. Mirski MA, Ferrendelli JA. Anterior thalamic mediation of generalized pentylenetetrazol seizures. Brain Research. 1986;399(2):212-23.
284. Hotta H, Koizumi K, Stewart M. Cardiac sympathetic nerve activity during kainic acid–induced limbic cortical seizures in rats. Epilepsia. 2009;50(4):923-7.
285. Saito T, Sakamoto K, Koizumi K, Stewart M. Repeatable focal seizure suppression: a rat preparation to study consequences of seizure activity based on urethane anesthesia and reversible carotid artery occlusion. J Neurosci Methods. 2006;155(2):241-50.
286. Fink AM, Bronas UG, Calik MW. Autonomic regulation during sleep and wakefulness: a review with implications for defining the pathophysiology of neurological disorders. Clinical Autonomic Research. 2018;28(6):509-18.
287. Cabiddu R, Cerutti S, Viardot G, Werner S, Bianchi AM. Modulation of the Sympatho-Vagal Balance during Sleep: Frequency Domain Study of Heart Rate Variability and Respiration. Frontiers in Physiology. 2012;3.
288. Boon P, Vonck K, Reuck JD, Caemaert J. Vagus nerve stimulation for refractory epilepsy. Seizure. 2001;10(6):448-55.
289. Sucholeiki R, Alsaadi TM, Morris GL, 3rd, Ulmer JL, Biswal B, Mueller WM. fMRI in patients implanted with a vagal nerve stimulator. Seizure. 2002;11(3):157-62.
290. Kawaji H, Yamamoto T, Fujimoto A, Uchida D, Ichikawa N, Yamazoe T, et al. Additional seizure reduction by replacement with Vagus Nerve Stimulation Model 106 (AspireSR). Neuroscience Letters. 2020;716:134636.
291. Tzadok M, Harush A, Nissenkorn A, Zauberman Y, Feldman Z, Ben-zeev B. Clinical outcomes of closed-loop vagal nerve stimulation in patients with refractory epilepsy. Seizure. 2019;71:140-4.

292. Wannamaker BB. Autonomic nervous system and epilepsy. Epilepsia. 1985;26 Suppl 1:S31-9.
293. Devinsky O, Hesdorffer DC, Thurman DJ, Lhatoo S, Richerson G. Sudden unexpected death in epilepsy: epidemiology, mechanisms, and prevention. Lancet Neurol. 2016;15(10):1075-88.
294. Sivathamboo S, Constantino TN, Chen Z, Sparks PB, Goldin J, Velakoulis D, et al. Cardiorespiratory and autonomic function in epileptic seizures: A video-EEG monitoring study. Epilepsy Behav. 2020;111:107271.
295. Faingold CL, Feng HJ. A unified hypothesis of SUDEP: Seizure-induced respiratory depression induced by adenosine may lead to SUDEP but can be prevented by autoresuscitation and other restorative respiratory response mechanisms mediated by the action of serotonin on the periaqueductal gray. Epilepsia. 2023;64(4):779-96.
296. Sowers LP, Massey CA, Gehlbach BK, Granner MA, Richerson GB. Sudden unexpected death in epilepsy: fatal post-ictal respiratory and arousal mechanisms. Respir Physiol Neurobiol. 2013;189(2):315-23.
297. Medlej Y, Asdikian R, Wadi L, Salah H, Dosh L, Hashash R, et al. Enhanced setup for wired continuous long-term EEG monitoring in juvenile and adult rats: application for epilepsy and other disorders. BMC Neurosci. 2019;20(1):8.
298. Smets H, Stumpp L, Julémont N, Cury J, Debelle A, Innocenti B, et al. Analysing vagus nerve spontaneous activity using finite element modelling. Journal of Neural Engineering. 2021.
299. Martin BS, Kapur J. A combination of ketamine and diazepam synergistically controls refractory status epilepticus induced by cholinergic stimulation. Epilepsia. 2008;49(2):248-55.
300. Vermoesen K, Smolders I, Massie A, Michotte Y, Clinckers R. The control of kainic acid-induced status epilepticus. Epilepsy Res. 2010;90(1-2):164-6.
301. Mollet L, Raedt R, Delbeke J, El Tahry R, Grimonprez A, Dauwe I, et al. Electrophysiological responses from vagus nerve stimulation in rats. Int J Neural Syst. 2013;23(6):1350027.
302. Lee L-Y. Respiratory sensations evoked by activation of bronchopulmonary C-fibers. Respiratory Physiology & Neurobiology. 2009;167(1):26-35.
303. Charlton PH, Birrenkott DA, Bonnici T, Pimentel MAF, Johnson AEW, Alastruey J, et al. Breathing Rate Estimation From the Electrocardiogram and Photoplethysmogram: A Review. IEEE Rev Biomed Eng. 2018;11:2-20.
304. Patros M, Ottaviani MM, Wright L, Dawood T, Macefield VG. Quantification of cardiac and respiratory modulation of axonal activity in the human vagus nerve. The Journal of Physiology. 2022;600(13):3113-26.
305. Schober P, Vetter TR. Logistic Regression in Medical Research. Anesthesia & Analgesia. 2021;132(2):365-6.

306. Ashraf O, Huynh T, Purnell BS, Murugan M, Fedele DE, Chitravanshi V, et al. Suppression of phrenic nerve activity as a potential predictor of imminent sudden unexpected death in epilepsy (SUDEP). Neuropharmacology. 2021;184:108405.
307. Stewart M, Kollmar R, Nakase K, Silverman J, Sundaram K, Orman R, et al. Obstructive apnea due to laryngospasm links ictal to postictal events in <scp>SUDEP</scp> cases and offers practical biomarkers for review of past cases and prevention of new ones. Epilepsia. 2017;58(6):e87-e90.
308. Jefferys JGR, Arafat MA, Irazoqui PP, Lovick TA. Brainstem activity, apnea, and death during seizures induced by intrahippocampal kainic acid in anaesthetized rats. Epilepsia. 2019;60(12):2346-58.
309. Budde RB, Arafat MA, Pederson DJ, Lovick TA, Jefferys JGR, Irazoqui PP. Acid reflux induced laryngospasm as a potential mechanism of sudden death in epilepsy. Epilepsy Research. 2018;148:23-31.
310. Racine RJ. Modification of seizure activity by electrical stimulation: II. Motor seizure. Electroencephalography and Clinical Neurophysiology. 1972;32(3):281-94.
311. Englot DJ, Blumenfeld H. Consciousness and epilepsy: why are complex-partial seizures complex? In: Laureys S, Schiff ND, Owen AM, editors. Coma Science: Clinical and Ethical Implications. Progress in Brain Research. 177: Elsevier; 2009. p. 147-70.
312. Irnaten M, Wang J, Chang KS, Andresen MC, Mendelowitz D. Ketamine inhibits sodium currents in identified cardiac parasympathetic neurons in nucleus ambiguus. Anesthesiology. 2002;96(3):659-66.
313. Ruíz-López P, Morgaz J, Quirós-Carmona S, Navarrete-Calvo R, Domínguez JM, Gómez-Villamandos RJ, et al. Parasympathetic Tone Changes in Anesthetized Horses after Surgical Stimulation, and Morphine, Ketamine, and Dobutamine Administration. Animals. 2022;12(8):1038.
314. Zhao Y, Zhao J, Li Q. Derivation of Respiratory Signals from Single-Lead ECG. 2008 International Seminar on Future BioMedical Information Engineering; 2008: IEEE; 2008. p. 15-8.
315. Klinkenberg S, Majoie HJM, van der Heijden MMAA, Rijkers K, Leenen L, Aldenkamp AP. Vagus nerve stimulation has a positive effect on mood in patients with refractory epilepsy. Clinical Neurology and Neurosurgery. 2012;114(4):336-40.
316. Grote V, Levnajic Z, Puff H, Ohland T, Goswami N, Fruhwirth M, et al. Dynamics of Vagal Activity Due to Surgery and Subsequent Rehabilitation. Front Neurosci. 2019;13:1116.
317. Waise TMZ, Dranse HJ, Lam TKT. The metabolic role of vagal afferent innervation. Nature Reviews Gastroenterology & Hepatology. 2018;15(10):625-36.

318. Berthoud H-R. The vagus nerve, food intake and obesity. Regulatory Peptides. 2008;149(1-3):15-25.
319. Browning KN, Verheijden S, Boeckxstaens GE. The Vagus Nerve in Appetite Regulation, Mood, and Intestinal Inflammation. Gastroenterology. 2017;152(4):730-44.
320. Borovikova LV, Ivanova S, Zhang M, Yang H, Botchkina GI, Watkins LR, et al. Vagus nerve stimulation attenuates the systemic inflammatory response to endotoxin. Nature. 2000;405(6785):458-62.
321. Hoffman HH, Schnitzlein HN. The numbers of nerve fibers in the vagus nerve of man. Anat Rec. 1961;139:429-35.
322. Mei N, Condamin M, Boyer A. The composition of the vagus nerve of the cat. Cell and Tissue Research. 1980;209(3).
323. Zhang K, Tolstykh GP, Sanchez RM, Cavazos JE. Chronic Cellular Hyperexcitability in Elderly Epileptic Rats with Spontaneous Seizures Induced by Kainic Acid Status Epilepticus while Young Adults. Aging Dis. 2011;2(4):332-8.
324. Tolstykh GP, Cavazos JE. Potential mechanisms of sudden unexpected death in epilepsy. Epilepsy & Behavior. 2013;26(3):410-4.
325. Chavez Cerda J, Acedo Reina E, Smets H, Verstraeten M, Vande Perre L, Diaz Cortes M, et al. Chronic Setup System for Continuous Monitoring of Epileptic Rats. 2022 IEEE Biomedical Circuits and Systems Conference (BioCAS); 13-15 Oct. 20222022. p. 591-4.
326. Smets H, Stumpp L, Chavez J, Cury J, Vande Perre L, Doguet P, et al. Chronic recording of the vagus nerve to analyze modulations by the light-dark cycle. J Neural Eng. 2022;19(4).
327. Stumpp L, Smets H, Cury J, Doguet P, Delbeke J, Nonclercq A, et al., editors. Characterization of Single Unit Activity of the Vagus Nerve Electroneurogram During Acute Pentylenetetrazol-Induced Seizures in Rats. American Epilepsy Society 2019 Annual Meeting; 2019.
328. Shaw L, Bagha S. Online EMG signal analysis for diagnosis of neuromuscular diseases by using PCA and PNN. International Journal of Engineering Science and Technology (IJEST). 2012;4(10):4453-9.
329. De Zambotti M, Trinder J, Silvani A, Colrain IM, Baker FC. Dynamic coupling between the central and autonomic nervous systems during sleep: A review. Neuroscience & Biobehavioral Reviews. 2018;90:84-103.
330. Asala SA, Bower AJ. An electron microscope study of vagus nerve composition in the ferret. Anatomy and Embryology. 1986;175(2):247-53.
331. Czura CJ, Rosas-Ballina M, Tracey KJ. Cholinergic Regulation of Inflammation. Psychoneuroimmunology (Fourth Edition). I: Elsevier; 2007. p. 85-96.
332. Paintal AS. Vagal sensory receptors and their reflex effects. Physiological Reviews. 1973;53(1):159-227.

333. Krarup C. Compound sensory action potential in normal and pathological human nerves. Muscle & Nerve. 2004;29(4):465-83.
334. Chia-Chu Chiang BPK, Dominique M. Durand. Bradycardia is induced by hyperactivity of the vagus nerve and nucleus ambiguus during seizures propagating into the brainstem. Epilepsia Open. 2025.
335. Stumpp L, Smets H, Vespa S, Cury J, Doguet P, Delbeke J, et al., editors. Vagus nerve electroneurogram-based detection of acute pentylenetetrazol induced seizures in rats. International Brain Stimulation; 2021.
336. Stiedl O, Hager T. Cardiovascular Conditioning: Neural Substrates☆. Elsevier; 2017.
337. Irwin MR, Curay CM, Choi S, Kiyatkin EA. Basic physiological effects of ketamine-xylazine mixture as a general anesthetic preparation for rodent surgeries. Brain Research. 2023;1804:148251.
338. Sleigh J, Harvey M, Voss L, Denny B. Ketamine – More mechanisms of action than just NMDA blockade. Trends in Anaesthesia and Critical Care. 2014;4(2-3):76-81.
339. Smith D, Bouchal R, Desanctis C, Monroe P, Amedro J, Perrotti J, et al. Properties of the interaction between ketamine and opiate binding sites in vivo and in vitro. Neuropharmacology. 1987;26(9):1253-60.
340. Sotoudeh N, Namavar MR. Optimisation of ketamine-xylazine anaesthetic dose and its association with changes in the dendritic spine of CA1 hippocampus in the young and old male and female Wistar rats. Veterinary Medicine and Science. 2022;8(6):2545-52.
341. Teppema LJ, Baby S. Anesthetics and control of breathing. Respiratory Physiology & Neurobiology. 2011;177(2):80-92.
342. Beitchman JA, Krishna G, Bromberg CE, Thomas TC. Effects of isoflurane and urethane anesthetics on glutamate neurotransmission in rat brain usingin vivoamperometry. bioRxiv2023.
343. Kurz C, Baranowska U, Łupiński S, Göthert M, Malinowska B, Schlicker E. Urethane, but not pentobarbitone, attenuates presynaptic receptor function in rats: a contribution to the choice of anaesthetic. British Journal of Pharmacology. 2009;157(8):1474-82.
344. Tian Y, Lei T, Yang Z, Zhang T. Urethane suppresses hippocampal CA1 neuron excitability via changes in presynaptic glutamate release and in potassium channel activity. Brain Res Bull. 2012;87(4-5):420-6.
345. Vasileva A, Flores LDM, Vasilyev M, Buckman MA, Deruisseau LR, Tomasson MH, et al. Cardiovascular function and autonomic regulation in urethane-anesthetized and conscious mice. American Journal of Physiology-Regulatory, Integrative and Comparative Physiology. 2025;328(1):R133-R44.
346. Sun L, Tanida M, Wang M, Kuda Y, Kurata Y, Shibamoto T. Effects of Anesthetics on the Renal Sympathetic Response to Anaphylactic Hypotension in Rats. PLoS ONE. 2014;9(11):e113945.

347. O'Leary DM, Jones JFX. Discharge Patterns of Preganglionic Neurones with Axons in a Cardiac Vagal Branch in the Rat. Experimental Physiology. 2003;88(6):711-23.
348. Vogler GA. Anesthesia and Analgesia. The Laboratory Rat (Second Edition): Elsevier; 2006. p. 627-64.
349. Stafstrom CE, Thompson JL, Holmes GL. Kainic acid seizures in the developing brain: status epilepticus and spontaneous recurrent seizures. Brain Res Dev Brain Res. 1992;65(2):227-36.
350. Naggar I, Lazar J, Kamran H, Orman R, Stewart M. Relation of autonomic and cardiac abnormalities to ventricular fibrillation in a rat model of epilepsy. Epilepsy Res. 2014;108(1):44-56.
351. Green CJ, Knight J, Precious S, Simpkin S. Ketamine alone and combined with diazepam or xylazine in laboratory animals: a 10 year experience. Lab Anim. 1981;15(2):163-70.
352. Flecknell PA, Mitchell M. Midazolam and fentanyl-fluanisone: assessment of anaesthetic effects in laboratory rodents and rabbits. Lab Anim. 1984;18(2):143-6.
353. Rice AC, Floyd CL, Lyeth BG, Hamm RJ, Delorenzo RJ. Status Epilepticus Causes Long-Term NMDA Receptor-Dependent Behavioral Changes and Cognitive Deficits. Epilepsia. 1998;39(11):1148-57.
354. Sombati S, Delorenzo RJ. Recurrent spontaneous seizure activity in hippocampal neuronal networks in culture. Journal of Neurophysiology. 1995;73(4):1706-11.
355. Dereli AS, Apaire A, El Tahry R. Sudden Unexpected Death in Epilepsy: Central Respiratory Chemoreception. Int J Mol Sci. 2025;26(4).
356. Golden GT, Smith GG, Ferraro TN, Reyes PF, Kulp JK, Fariello RG. Strain differences in convulsive response to the excitotoxin kainic acid. NeuroReport. 1991;2(3):141-4.
357. Golden GT, Smith GG, Ferraro TN, Reyes PF. Rat strain and age differences in kainic acid induced seizures. Epilepsy Res. 1995;20(2):151-9.
358. Langer M, Brandt C, Löscher W. Marked strain and substrain differences in induction of status epilepticus and subsequent development of neurodegeneration, epilepsy, and behavioral alterations in rats. Epilepsy Research. 2011;96(3):207-24.
359. Löscher W, Ferland RJ, Ferraro TN. The relevance of inter- and intrastrain differences in mice and rats and their implications for models of seizures and epilepsy. Epilepsy & Behavior. 2017;73:214-35.
360. Portelli J, Aourz N, De Bundel D, Meurs A, Smolders I, Michotte Y, et al. Intrastrain differences in seizure susceptibility, pharmacological response and basal neurochemistry of Wistar rats. Epilepsy Research. 2009;87(2-3):234-46.

361. Shaker KK, Al Mahdawi AM, Hamdan FB. Interictal autonomic dysfunction in patients with epilepsy. The Egyptian Journal of Neurology, Psychiatry and Neurosurgery. 2021;57(1):165-.
362. Crunelli V, Leresche N. Childhood absence epilepsy: Genes, channels, neurons and networks. Nature Reviews Neuroscience. 2002;3(5):371-82.
363. Smyk MK, Van Luijtelaar G. Circadian Rhythms and Epilepsy: A Suitable Case for Absence Epilepsy. Frontiers in Neurology. 2020;11.
364. Jansen K, Varon C, Van Huffel S, Lagae L. Ictal and interictal respiratory changes in temporal lobe and absence epilepsy in childhood. Epilepsy Res. 2013;106(3):410-6.
365. Lakens D. Calculating and reporting effect sizes to facilitate cumulative science: a practical primer for t-tests and ANOVAs. Frontiers in Psychology. 2013;4.
366. Akoglu H. User's guide to correlation coefficients. Turkish Journal of Emergency Medicine. 2018;18(3):91-3.
367. Kotamraju BP, Eggers TE, McCallum GA, Durand DM. Selective chronic recording in small nerve fascicles of sciatic nerve with carbon nanotube yarns in rats. Journal of Neural Engineering. 2024;20(6).
368. Ribeiro M, Koh RGL, Donnelly T, Lutteroth C, Proulx MJ, Rocha PRF, et al. Denoising and decoding spontaneous vagus nerve recordings with machine learning. 2023 45th Annual International Conference of the IEEE Engineering in Medicine & Biology Society (EMBC)2023. p. 1-4.
369. Guemes Gonzalez A, Carnicer-Lombarte A, Hilton S, Malliaras G. A multivariate physiological model of vagus nerve signalling during metabolic challenges in anaesthetised rats for diabetes treatment. J Neural Eng. 2023;20(5).
370. Durand DM. Recording and decoding neural signals from the vagus nerve. Open Access Government. 2023;39(1):36-7.
371. Caravaca AS, Tsaava T, Goldman L, Silverman H, Riggott G, Chavan SS, et al. A novel flexible cuff-like microelectrode for dual purpose, acute and chronic electrical interfacing with the mouse cervical vagus nerve. Journal of Neural Engineering. 2017;14(6):066005.
372. Rodrigues AJ, Marmerstein JT, Kotamraju BP, McCallum GA, Durand DM. Effect of Anesthesia and Diurnal Variation on Chronic Vagus Nerve Activity in Rats. Journal of Neuroscience Research. 2025;103(5).
373. Yaksh TL. Calcium Channels As Therapeutic Targets in Neuropathic Pain. The Journal of Pain. 2006;7(1):S13-S30.
374. Dorrego-Rivas A, Grubb MS. The axon initial segment as a source of neuropathic pain. Brain. 2022;145(5):1574-5.